

Modification of rhodamine-based fluorescence probe for specific cation detection

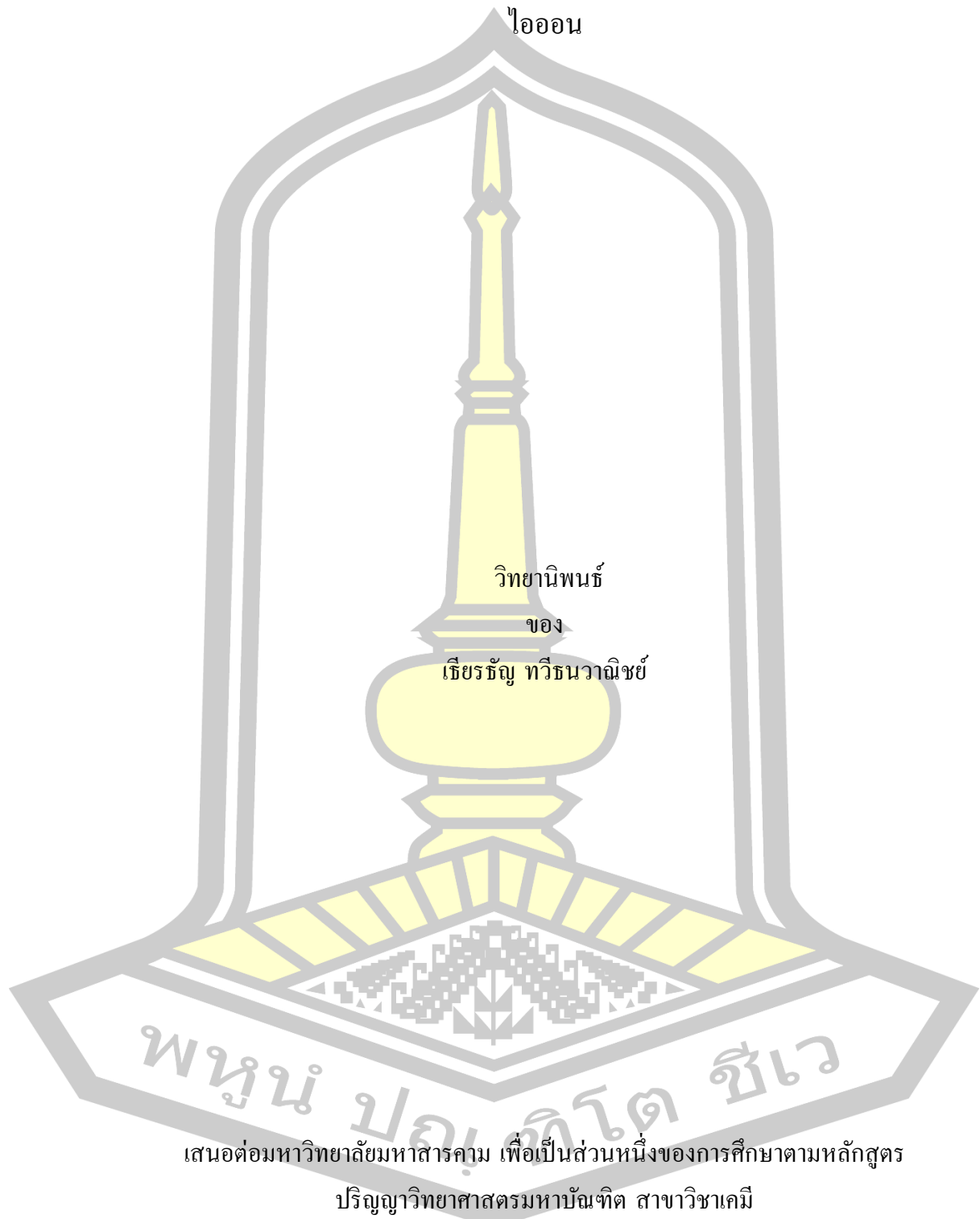
Thianthan Taweetanavanich

A Thesis Submitted in Partial Fulfillment of Requirements for  
degree of Master of Science in Chemistry

October 2018

Copyright of Mahasarakham University

การดัดแปรของฟลูออเรสเซนซ์โพรบที่มีโรดามีน สำหรับการตรวจวัดที่จำเพาะต่อแคทไอออน



เสนอต่อมหาวิทยาลัยมหาสารคาม เพื่อเป็นส่วนหนึ่งของการศึกษาตามหลักสูตร

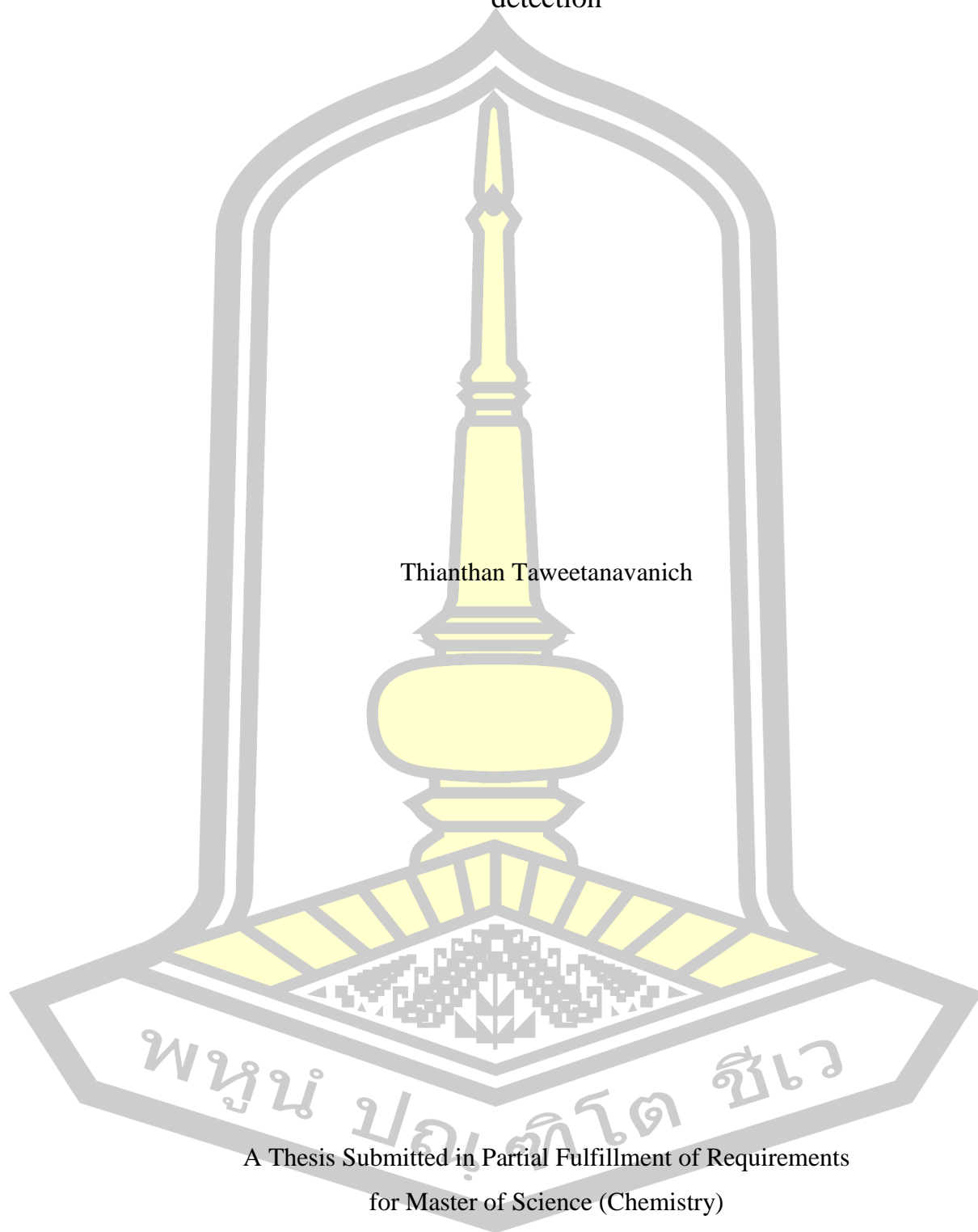
ปริญญาวิทยาศาสตรมหาบัณฑิต สาขาวิชาเคมี

ตุลาคม 2561

สงวนลิขสิทธิ์เป็นของมหาวิทยาลัยมหาสารคาม

Modification of rhodamine-based fluorescence probe for specific cation  
detection

Thianthan Taweetanavanich



A Thesis Submitted in Partial Fulfillment of Requirements  
for Master of Science (Chemistry)

October 2018

Copyright of Mahasarakham University



The examining committee has unanimously approved this Thesis, submitted by Mr. Thianthan Taweetanavanich , as a partial fulfillment of the requirements for the Master of Science Chemistry at Mahasarakham University

Examining Committee

Chairman

(Asst. Prof. Burapol Singhana  
Ph.D.)

Advisor

(Assoc. Prof. Chatthai Kaewtong ,  
Ph.D.)

Co-advisor

(Asst. Prof. Banchob Wanno ,  
Ph.D.)

Committee

(Asst. Prof. Prapairat Seephonkai ,  
Ph.D.)

Committee

(Asst. Prof. Widchaya  
Radchatawedchakoon , Ph.D.)

Mahasarakham University has granted approval to accept this Thesis as a partial fulfillment of the requirements for the Master of Science Chemistry

(Prof. Pairoit Pramual , Ph.D.)  
Dean of The Faculty of Science

(Asst. Prof. Krit Chaimoon , Ph.D.)  
Dean of Graduate School

Day.....Month.....Year.....

<b>TITLE</b>	Modification of rhodamine-based fluorescence probe for specific cation detection		
<b>AUTHOR</b>	Thianthan Taweetanavanich		
<b>ADVISORS</b>	Associate Professor Chatthai Kaewtong , Ph.D. Assistant Professor Banchob Wanno , Ph.D.		
<b>DEGREE</b>	Master of Science	<b>MAJOR</b>	Chemistry
<b>UNIVERSITY</b>	Maharakham University	<b>YEAR</b>	2018

### ABSTRACT

The rhodamine-cyclohexane (L1-L3) were synthesized via a coupling reaction between Rhen and cyclohexane dicarboxylic acid under estimated condition to obtain moderate isolated yield.

The various of PEG ( $M_n$  400, 4000, and 6000) were coupling with rhodamine ethylenediamine to obtained the rhodamine-PEG (L5-L7) in high yield. Moreover, the rhodamine-PEG (L5) showed a rapid response to pH from 1 to 3 through color and fluorescent changes.

A rhodamine-based colorimetric and fluorescent pH chemosensor (L8) was designed and synthesized by a coupling reaction between rhodamine ethylenediamine and succinic anhydride. The L8 showed excellent pH response in aqueous solution. In addition, common cations did not interfere ( $Na^+$ ,  $K^+$ ,  $Ag^+$ ,  $Mg^{2+}$ ,  $Ca^{2+}$ ,  $Pb^{2+}$ ,  $Co^{2+}$ ,  $Ni^{2+}$ ,  $Cu^{2+}$ ,  $Zn^{2+}$ ,  $Cd^{2+}$ ,  $Hg^{2+}$ ,  $Al^{3+}$ ,  $Cr^{3+}$ ,  $Fe^{3+}$ ,  $Au^{3+}$ ,  $Pt^{2+}$ ,  $Ru^{2+}$ ) with the pH response process. To further study it's potential as a portable pH sensor, L8 was immobilized on activated cellulose paper using *N,N'*-dicyclohexylcarbodiimide (DCC) and *N,N'*-dimethylpyridin-4-amine (DMAP) as coupling reagent to obtain the composite pH sensor (CP- L8). The CP- L8 was characterized by ATR-FTIR, UV-vis, Fluorescence and SEM techniques. The CP-L8 showed a rapid response to pH range from 1 to 8 through color and fluorescent changes. Moreover, a paper pH sensor can be reused by dipping in NaOH. Therefore, our work demonstrates the potential of rhodamine-dye composites for visualizing pH changes in real systems.

Keyword : Rhodamine, cyclohexane, PEG, pH sensor paper

## ACKNOWLEDGEMENTS

The thesis was granted by the Center of Excellence for innovation in Chemistry (PERCH-CIC) and the Thailand Research Fund (RSA5980072) for financially support.

The thesis would not have been accomplished if without the help from several people. First of all, I would like to thank Assoc. Prof. Chatthai Kaewtong (advisor), Asst. Prof. Banchob Wanno (co-advisor), Prof. Thawatchai Tuntulani, Assoc. Prof. Buncha Pulpoka, Asst. Prof. Prapairat Seephonkai, Asst. Prof. Widchaya Radchatawedchakoon and Asst. Prof. Burapol Singhana for their suggestions and comments as committee members and thesis examiners.

However, I would like to thank all members of the Nanotechnology and Supramolecular Chemistry Research Unit at the Department of Chemistry Mahasarakham University for all the helps and Supramolecular Chemistry Research Unit at the Department of Chemistry Chulalongkorn University for NMR and Mass experiments.

Finally, I would like to thank my parents and my family for their love, kindness, encouragement, and financial support all over my life.

Thianthan Taweetanavanich

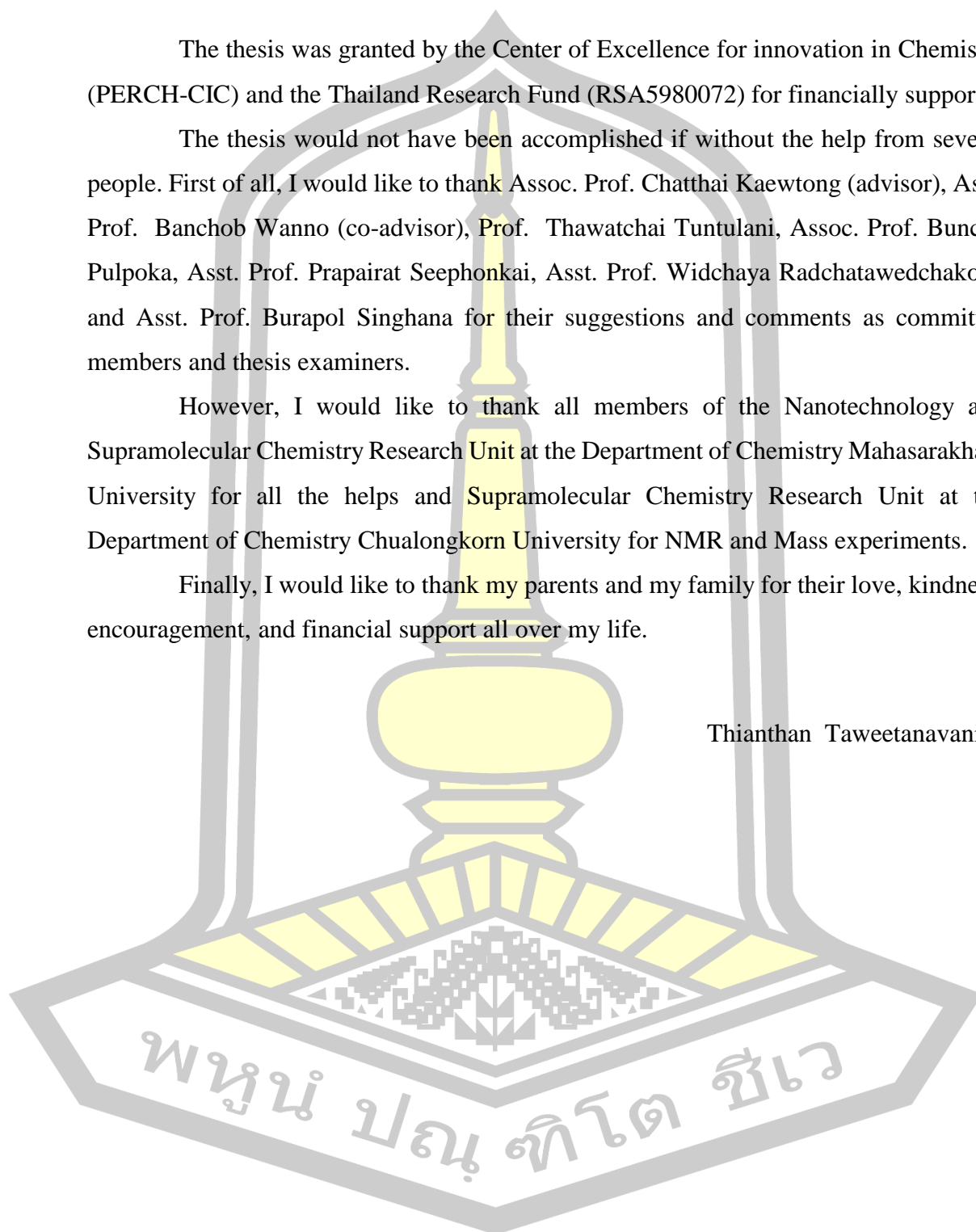


## TABLE OF CONTENTS

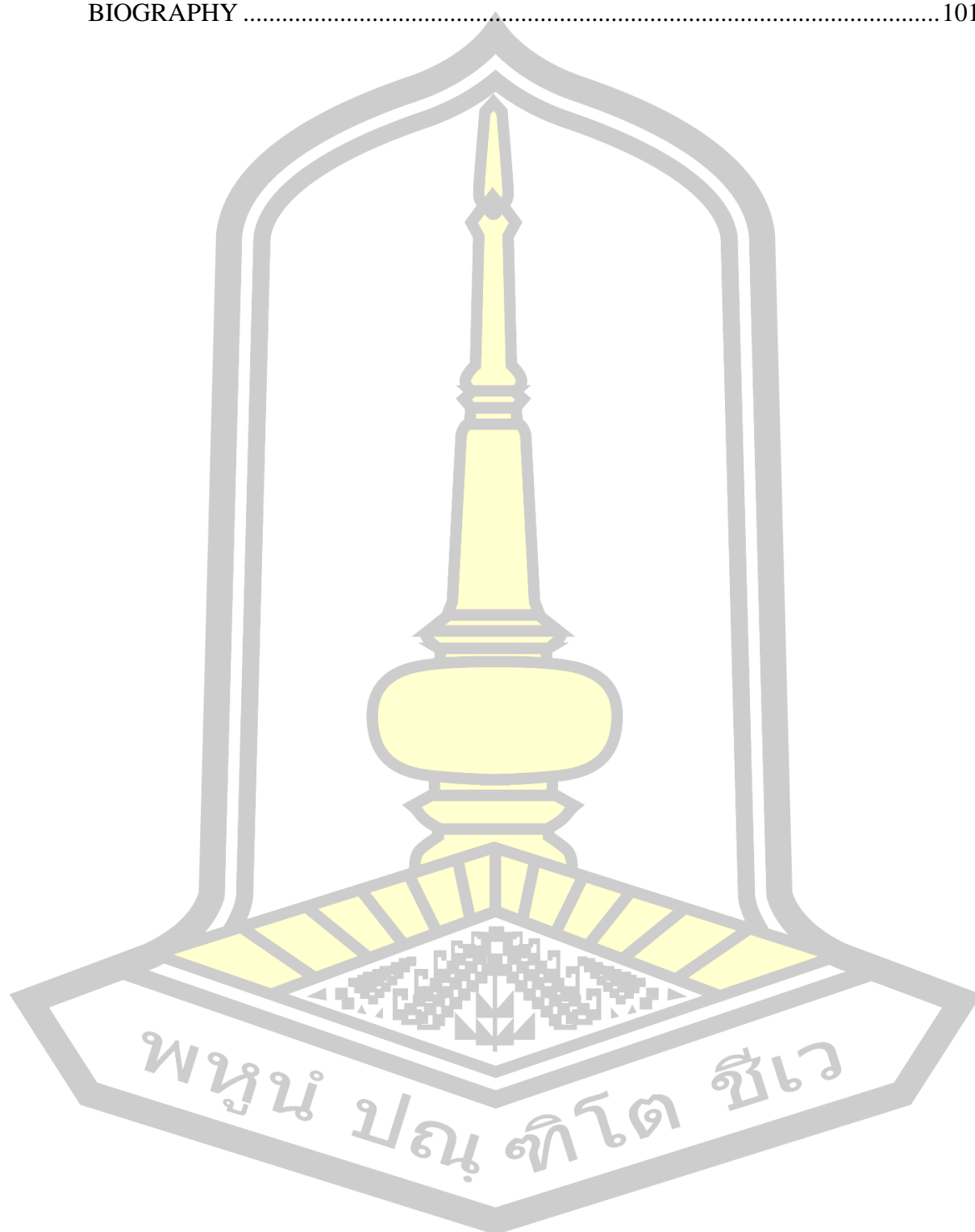
	<b>Page</b>
ABSTRACT.....	D
ACKNOWLEDGEMENTS.....	E
TABLE OF CONTENTS.....	F
LIST OF TABLE.....	J
LIST OF FIGURE.....	K
LIST OF SCHEME.....	O
CHAPTER 1 .....	1
INTRODUCTION .....	1
1.1 Supramolecular chemistry .....	1
1.2 Molecular recognition and chemical sensor .....	3
1.3 Fluorescence sensor .....	5
1.4 The most efficient dyes for labeling .....	7
1.5 Introduction to Rhodamine B .....	8
1.6 Introduction to Rhodamine B derivative .....	9
1.7 Rhodamine Based chemosensor .....	9
1.8 Introduction to the research problem and its significant.....	10
1.9 Objectives of research.....	12
CHAPTER 2 .....	13
LITERATURE REVIEW .....	13
2.1 Rhodamine-cyclohexane chemosensor.....	13
2.2 Rhodamine-polyethylene glycol (PEG) chemosensor.....	20
2.3 Rhodamine base chemosensor.....	27
2.4 Metal ions sensor based Rhodamine derivative.....	32
CHAPTER 3 .....	42
MATERIALS AND METHODS.....	42

3.1 Materials .....	42
3.1.1 Instrumentals .....	42
3.1.2 Chemicals .....	42
3.2 Methods .....	43
3.2.1 Synthesis of Rhodamine ethylenediamine (Rhen) .....	43
3.2.2 Rhodamine-cyclohexane.....	44
3.2.2.1 Synthesis of 1,3-cyclohexane N-(Rhodamine B)-lactam-ethylene diamines (L1, L2). .....	44
3.2.2.1.1 Condition I.....	47
3.2.2.1.2 Condition II.....	48
3.2.2.1.3 Condition III.....	49
3.2.2.1.4 Condition IV.....	50
3.2.2.1.5 Condition V.....	51
3.2.2.1.6 Condition VI.....	52
3.2.2.1.7 Condition VII.....	53
3.2.2.1.8 Condition VIII.....	54
3.2.2.1.9 Condition IX.....	55
3.2.2.1.10 Condition X.....	56
3.2.2.2 Synthesis of 1,4-cyclohexane N-(Rhodamine B)-lactam-ethylene diamines (L3, L4) .....	57
3.2.2.2.1 Condition I.....	58
3.2.2.2.2 Condition II.....	59
3.2.2.2.3 Condition III.....	60
3.2.3 Rhodamine-PEG (L5, L6 and L7).....	61
3.2.3.1 Synthesis of PEG-COOH.....	61
3.2.3.2 Synthesis of Rhodamine-PEG (L5).....	62
3.2.3.3 Synthesis of Rhodamine-PEG (L6).....	63
3.2.3.4 Synthesis of Rhodamine-PEG (L7).....	64
3.2.4 Rhodamine anhydride (L8) .....	64
3.2.4.1 Synthesis of Rhodamine anhydride (L8).....	64



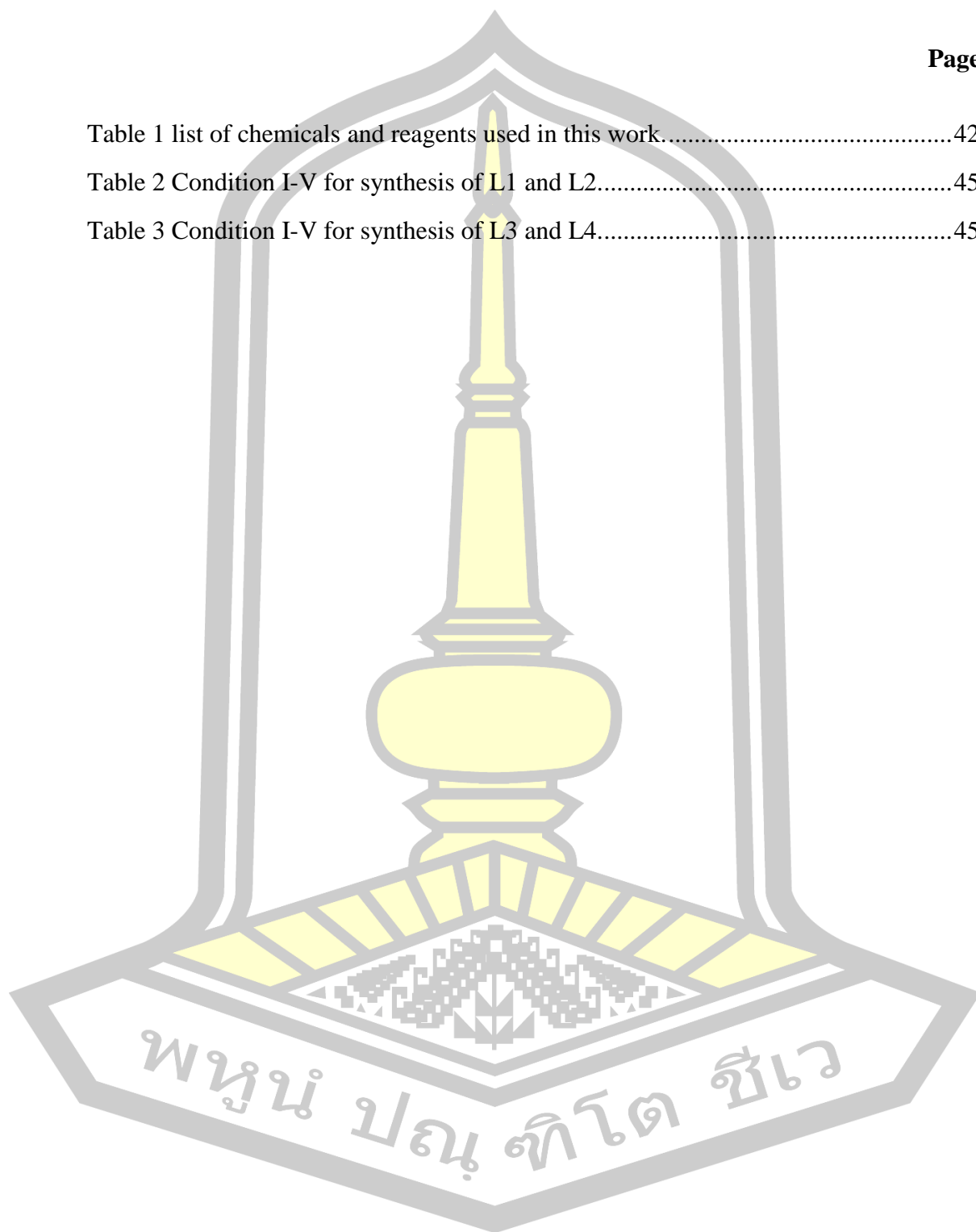
3.2.4.2 Preparation of paper based sensor (CP-L8).....	65
3.3 Characterization.....	65
3.4 Complexation studies of ligand and metal ions.....	66
3.5 The estimated pH of ligand.....	66
3.6 The estimated pH of ligand.....	67
CHAPTER 4 .....	68
RESULTS AND DISCUSSION .....	68
4.1 Synthesis of Rhodamine ethylenediamine (Rhen).....	68
4.2 Rhodamine-cyclohexane (L1-L4).....	69
4.2.1 Synthesis and characterization of L1-L4.....	69
4.2.1.1 Synthesis and characterization of L1.....	70
4.2.1.2 Synthesis and characterization of L2.....	71
4.3 Rhodamine-PEG (L5, L6 and L7) .....	72
4.3.1 Synthesis and characterization of PEG-COOH, L5-L7.....	72
4.3.1.1 Synthesis and characterization of PEG-COOH.....	72
4.3.1.2 Synthesis and characterization of L5-L7.....	73
4.3.2 Complexation study with metal ions .....	77
4.3.3 Micellar sensor study.....	79
4.3.4 pH study of L5.....	80
4.4 Rhodamine Anhydride (L8).....	81
4.4.1 Synthesis and characterization of L8.....	81
4.4.2 Selectivity of L8 .....	82
4.4.3 Characterization of L8 and application. ....	83
4.4.4 Computational calculations of L8 .....	86
CHAPTER 5 .....	88
CONCLUSION.....	88
5.1 Rhodamine-cyclohexane (L1-L4).....	88
5.2 Rhodamine-PEG (L5).....	88
5.3 Rhodamine anhydride (L8).....	89

REFERENCES .....	91
BIOGRAPHY .....	101



## LIST OF TABLE

	Page
Table 1 list of chemicals and reagents used in this work.....	42
Table 2 Condition I-V for synthesis of L1 and L2.....	45
Table 3 Condition I-V for synthesis of L3 and L4.....	45



## LIST OF FIGURE

	Page
Figure 1 Graphic representations of (a) [2]rotaxane and (b) [2]catenane [3].	1
Figure 2 Molecule of (a) [2]rotaxane and (b) [2]catenane [3].	2
Figure 3 Molecular Recognition (a) Static and dynamic (b) molecular recognition	3
Figure 4 Pyrene-based sensor that functions as a fluorescent probe for $Pb^{2+}$ [7].	4
Figure 5 Typical absorption and fluorescence emission spectra. fluorescence spectrum is located at longer wavelengths with respect to the absorption spectrum. The area between absorption and emission spectrum is shadowed. The distance between their band maxima is called the Stokes shift.	5
Figure 6 The range of application of fluorescence sensing technologies.	6
Figure 7 Structure of mesomeric dyes; fluorescein (1) and cyanines dye (2).	7
Figure 8 Structure of xanthene and Rhodamine.	8
Figure 9 Position structure of Rhodamine B.	9
Figure 10 (a) synthesis route of 12, (b) change in excimer/monomer ratio for P1 in MeCN upon titration with ( $\Delta$ ) $CsNO_3$ , (x) $RbNO_3$ , ( $\bullet$ ) $KNO_3$ , (O) $NaNO_3$ , ( $\blacksquare$ ) $NH_4NO_3$ and (+) $HNO_3$ . (c) change in excimer/monomer ratio for P1 upon titration with $CaCl_2$ . Excitation at 346 nm, monomer emission at 397 nm, excimer emission at 470 nm.	14
Figure 11 (a) structure of P2, P3, Fluorescence enhancement of (b) (S)-P2 and (c) (R)-P2 ( $1.0 \times 10^{-5}$ M in benzene/0.05% DME) versus concentration of (R)- and	15
Figure 12 (a) structure of P4•succinate, P5•malonate. A fluorescence spectra (in DMSO $10^{-5}$ M, $\lambda_{ex}$ 290 nm) of (b) P4 + increasing amounts of succinate,	16
Figure 13 (a) structure of P6 and P7, (b) UV spectra in DMSO of P6 ( $10^{-5}$ M) +	17
Figure 14 (a) structure of P8, (b) Absorption spectra of metal-free P8 (10 mM) and in the presence of 10 equiv. of various metal ions in MeCN:H <sub>2</sub> O (4:1, v/v, 10 mM HEPES buffer, pH = 7) medium. (c) emission spectra of P8 (10 mM) and that of in the presence of 10 equiv. of various metal ions in a MeCN: H <sub>2</sub> O (4:1, v/v, 10 mM...	19
Figure 15 (a) Structure of P9, illustration for the fabrication of thermoresponsive P9, of $Zn^{2+}$ Ions and Temperature. (c) Fluorescence emission spectra of P9 (0.2 g/L, [ZQMA] = $5.0 \times 10^{-6}$ M) upon addition of 4.0 equiv (relative to ZQMA moieties) of	

various metal ions ( $\text{Zn}^{2+}$ ,  $\text{Al}^{3+}$ ,  $\text{Ba}^{2+}$ ,  $\text{Ca}^{2+}$ ,  $\text{Co}^{2+}$ ,  $\text{Cu}^{2+}$ ,  $\text{Fe}^{2+}$ ,  $\text{Fe}^{3+}$ ,  $\text{Ag}^+$ ,  $\text{Hg}^{2+}$ ,  $\text{Li}^+$ ,  $\text{Mg}^{2+}$ ,  $\text{Mn}^{2+}$ ,  $\text{Ni}^{2+}$ ,  $\text{Pb}^{2+}$ , and  $\text{Cd}^{2+}$ ), respectively. (d) changes in relative fluorescence of P9 ( $5.0 \times 10^{-6}$  M) upon sequential addition of 4.0 equiv of  $\text{Zn}^{2+}$  ions and EDTA ....21

Figure 16 (a) structures of the functionalized PEG-PS resin with the peptide sensor (P10) and (b) the fluorescent measuring of PG1-PEG-PS suspension. (c) Fluorescence response of PG1-PEG-PS (50  $\mu\text{M}$ ) in the presence of  $\text{Zn}(\text{II})$  (1 equiv.) and additional metal ions (1 equiv.). (d) Fluorescence emission spectra of PG1-PEG-PS (50  $\mu\text{M}$ ) in the presence of (left)  $\text{Cu}^{2+}$  (50  $\mu\text{M}$ ) and EDTA (2 mM) (right)  $\text{Zn}^{2+}$  (50  $\mu\text{M}$ ) and EDTA (2 mM).....23

Figure 17 (a) palladium detection based on the Tsuji–Trost reaction. (b) of P11 fluorescent spectra of P11 (1  $\mu\text{M}$ ) in the presence of various metal ions (1  $\mu\text{M}$ ) in PEG400 solutions incubated for 2 h at  $55^\circ\text{C}$ . (c) the emission intensity at 526 nm. ....24

Figure 18 (a) structure of P12. (b) UV-Vis absorption spectra of P12 in aqueous solutions (10 mM) upon addition of various metal ions. (c) reversible changes in absorbance intensity of P12 (10 mM) at 561 nm upon alternate addition of  $\text{Cu}^{2+}$  and EDTA ions. (d) colorimetric changes of P12 in aqueous solutions (10 mM) upon addition of various metal ions.....25

Figure 19 (a) structure of P13. (b) Fluorescence spectra of P13 (10  $\mu\text{mol/L}$ ) in aqueous solution the presence of 10 equiv. of various metal ions. (c) fluorescence intensity of P13 (10  $\mu\text{mol/L}$ ) in aqueous solution the presence of 10 equiv. of various metal ions.....26

Figure 20 (a) structure of P14 , (b) structure of P15 , Absorbance spectra (c) P14 and (d) P15 at various values of pH. Measured using 0.37  $\mu\text{M}$  solutions.....27

Figure 21 (a) structure of P16. (b) changes of color of RBDAB in MeCN/water (10/90, v/v) buffer solution (0.1 M citrate buffer solutions) with different pH. The pH from left to right is 4.0, 5.0, 6.0 and 7.0. (c) and UV-Vis absorption spectra of 10 mM P16 at different pH.....28

Figure 22 (a) pH sensing mechanism of P18. (b) Fluorescence images of RCE in buffers of various pH values under ultraviolet light (365 nm). From left to right: 7.51, 5.25, 4.76, 4.01. (c) fluorescence spectra of P18 (10  $\mu\text{M}$ ) in buffer at various pH values. ....29

Figure 23 (a) pH sensing mechanism of P19. (b) Absorption spectra of P19 (25  $\mu\text{M}$ ) in solution (buffer-EtOH, v/v = 1:1) with different pH. (c) The fluorescence spectrum of P19 (25  $\mu\text{M}$ ) in solution (buffer-EtOH, v/v = 1:1) with different pH,  $\lambda_{\text{ex}}$  = 562 nm. (d) The color change of P19 (25  $\mu\text{M}$ , buffer-EtOH, v:v = 1:1) at different pH.....30

Figure 24 (a) structure of P20 (b) pH reversibility study of 1 between pH 4.0 and pH 7.0 ( $\lambda_{\text{ex}} = 550 \text{ nm}$ , $\lambda_{\text{em}} = 588 \text{ nm}$ ). (c) UV/Vis Absorption and (d) fluorescence spectra of 1 (10 $\mu\text{M}$ ) in BR buffer solution containing 1% MeCN with different pH.....	31
Figure 25 (a) structure of P21, (b) fluorescence titration spectra of 1 ( $c = 4.41 \times 10^{-5} \text{ M}$ ) in $\text{CH}_3\text{CN}$ –water (4:1, v/v; 10 $\mu\text{M}$ tris HCl buffer, pH 7.0) upon addition of $\text{Hg}^{2+}$ ; Inset: Color change of the receptor solution under illumination of UV light.....	32
Figure 26 (a) structure of P22, (b) Absorption spectra (c) fluorescence spectra of P22 (10 $\mu\text{M}$ ) in water with the presence of 10 equiv. of various species. ....	33
Figure 27 (a) structure of P23, (b) color of P23 in the presence of the specified metal ions ( $c = 8.25 \times 10^{-4} \text{ M}$ ) in water. (c) Absorption spectra and (d) fluorescence spectrum of P23 after keeping the beads in contact with aqueous solutions of .....	34
Figure 28 (a) structure of P24, (b) UV-Vis absorption spectra of probe 1 (10.0 $\mu\text{M}$ ) in the presence of $\text{Hg}^{2+}$ (0-2 equiv.) in $\text{C}_2\text{H}_5\text{OH}$ -water (4:6, v/v) buffered with HEPES pH = 7.0 solution at room temperature. Inset: (c) showing the change in the color of P24 (10 $\mu\text{M}$ ) upon addition of $\text{Hg}^{2+}$ ions (2 equiv.); (d) Job's plot for determining the stoichiometry of P24 and $\text{Hg}^{2+}$ ion by absorbance at 561 nm, the total concentration of $[\text{Hg}^{2+}] + [\text{P24}]$ was 10 $\mu\text{M}$ . ....	35
Figure 29 (a) structure of P25, Absorption titration spectra of 1 ( $c = 2.25 \times 10^{-4} \text{ M}$ ) in $\text{CH}_3\text{CN}/\text{H}_2\text{O}$ (4:1, v/v; 10 mM tris HCl buffer; pH 6.8) upon addition of .....	36
Figure 30 (a) structure of P25 (left) and $\text{P25-Fe}^{3+}$ complex (right). Inset: (b) P25- only colorless solution, and (c) P25 plus $\text{Fe}^{3+}$ , violet color solution, both in EtOH.....	37
Figure 31 (a) structure of P26. (b) Fluorescence spectra of L2 (10 mM) in $\text{CH}_3\text{CH}_2\text{O-H}_2\text{O}$ (1/1, v/v) with the presence of 10 equiv. of various species Inset: fluorogenic color response of P26 (10 mM) in $\text{CH}_3\text{CH}_2\text{O-H}_2\text{O}$ (1/1, v/v) .....	38
Figure 32 (a) structure of P27. (b) fluorescence spectra of 2 (10 $\mu\text{M}$ ) in $\Theta$ ( $\text{CH}_3\text{OH}$ , $\text{H}_2\text{O}$ ) = 3/7 (1 mM Tris-HCl buffer, pH = 7.40) solution with the presence of 10.....	39
Figure 33 (a) structure of P28 and P29. Fluorescence spectra of P28 (b) and P29 (c) (10 $\mu\text{M}$ ) in EtOH/ $\text{H}_2\text{O}$ (8:2, v/v) upon addition of 10 equiv $\text{Ag}^+$ , $\text{Li}^+$ , $\text{K}^+$ , $\text{Fe}^{2+}$ , $\text{Pb}^{2+}$ , $\text{Ba}^{2+}$ , $\text{Cd}^{2+}$ , $\text{Ce}^{3+}$ , $\text{Ni}^{2+}$ , $\text{Co}^{2+}$ , $\text{Mn}^{2+}$ , $\text{Fe}^{3+}$ , $\text{Zn}^{2+}$ , $\text{Mg}^{2+}$ , $\text{Hg}^{2+}$ , $\text{NH}_4^+$ , $\text{Ca}^{2+}$ , $\text{Cu}^{2+}$ , $\text{Na}^+$ ; (d) The color changes of P28 and P29 (100 $\mu\text{M}$ ) in the presence of different metal cations (2 eq) under UV light (365 nm). ....	40
Figure 34 (a) structure of P30. (b) Selectivity of P30 toward $\text{Au}^{3+}$ among various metal ions. Solutions of P30 (60 $\mu\text{M}$ , orange bars) with metal ions (1 equiv.) in EtOH- $\text{H}_2\text{O}$ (1:1, v/v). Solutions of P30 (60 $\mu\text{M}$ , green bars) with various metal ions .....	41
Figure 35 $^1\text{H-NMR}$ spectrum of Rhen. ....	68

Figure 36 Structure of L1, L2, L3 and L4.....	69
Figure 37 $^1\text{H}$ -NMR spectrum of L1.....	70
Figure 38 $^1\text{H}$ -NMR spectrum of L2.....	71
Figure 39 Structure of PEG-COOH and L5-L7.....	72
Figure 40 $^1\text{H}$ -NMR spectrum of PEG-COOH.....	73
Figure 41 $^1\text{H}$ -NMR spectrum of L5.....	74
Figure 42 $^1\text{H}$ -NMR spectrum of L6.....	75
Figure 43 (a) UV-Vis spectrum of L5 and (b) fluorescence spectrum of L5 .....	76
Figure 44 (a) UV-Vis spectra (b) fluorescence spectra of L5 ( $10^{-5}$ M) added various metal ion ( $10^{-5}$ M) in EtOH.....	77
Figure 45 (a) UV-Vis (b) fluorescence spectra of L5 ( $10^{-5}$ M).....	78
Figure 46 Fluorescence spectra of (a) L5 ( $5 \times 10^{-5}$ M)+SDS and (b) L5 ( $5 \times 10^{-5}$ M) +TX-100 added 5 metal ion ( $10^{-3}$ M) in EtOH. ....	79
Figure 47 (a) UV-Vis spectra (b) fluorescence spectra of L5 ( $10^{-5}$ M) .....	80
Figure 48 $^1\text{H}$ -NMR spectrum of L8.....	81
Figure 49 Fluorescence spectra of L8 in the present various metal ions (10 $\mu\text{M}$ ) and proton in MeOH:H <sub>2</sub> O (Ratio 1:1). ....	82
Figure 50 FT-IR spectra of CP-L8 and CP-L8•H <sup>+</sup> .....	83
Figure 51 SEM images of (a) original cellulose paper, (b) paper-grafted L6 and (c) paper-grafted L8 treated with H <sup>+</sup> . ....	84
Figure 52 Colorimetric (a) and fluorescence (b) photographs of CP-L8.....	85
Figure 53 The solid-state fluorescence spectra of CP-L8 (a) upon soak in vary pH (1-12) from 540-700 nm, (b) The plot of maximum fluorescence intensities .....	86
Figure 54 Molecular orbital energy level of L8 in natural and protonated form. ....	87
Figure 55 Structure of L1 and L3. ....	88
Figure 56 Structure of L5.....	89



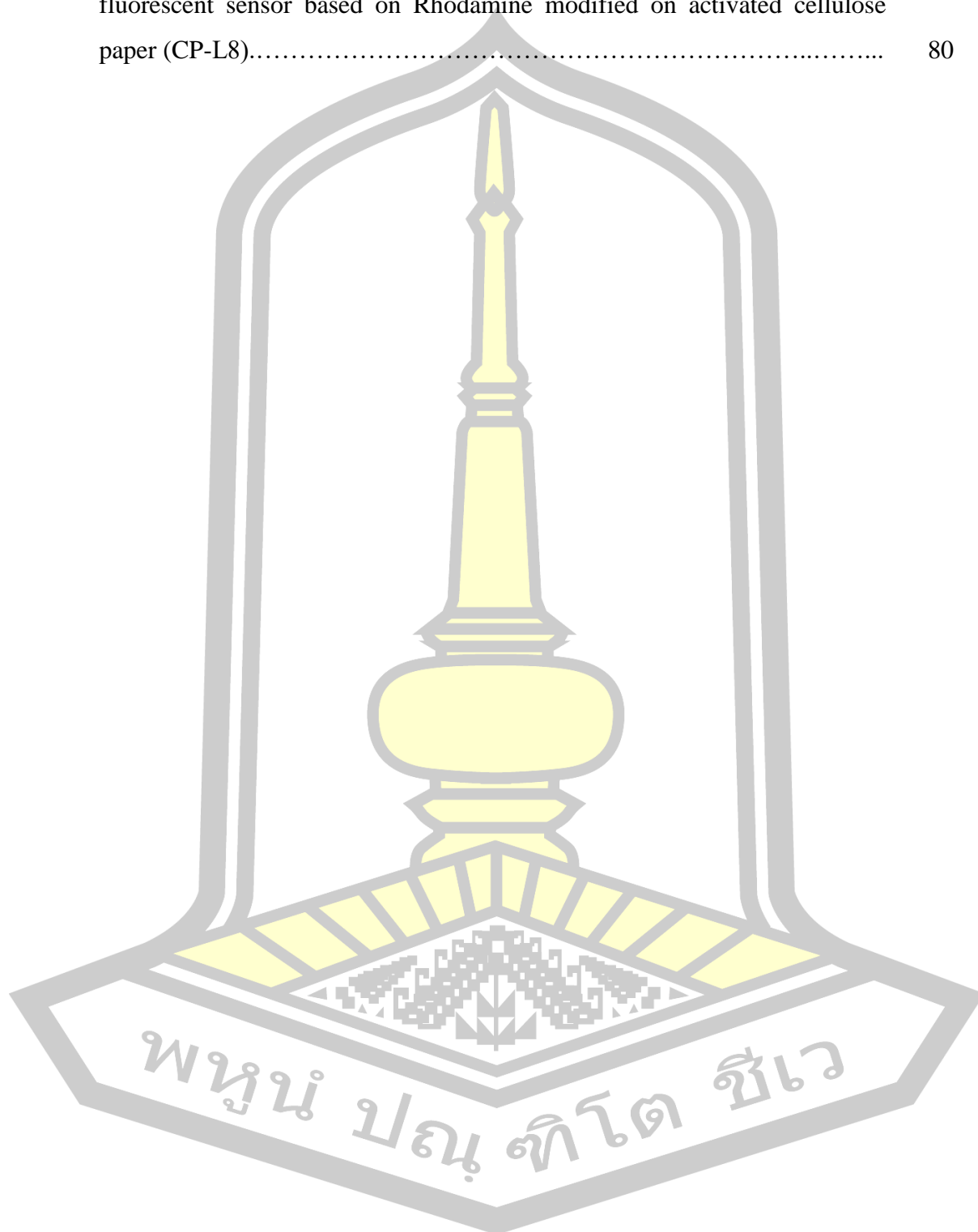
## LIST OF SCHEME

	Page
Scheme 1 Component of supramolecular chemistry.....	2
Scheme 2 Diagram of a sensor that produces an electrical output in..... response to the presence of an input quantity.....	4
Scheme 3 Spirolactam ring-opening process of Rhodamine derivatives.....	10
Scheme 4 Cu <sup>2+</sup> induced spirolactam ring opening mechanism.....	10
Scheme 5 Synthesis route of Rhen.....	43
Scheme 6 Synthesis route of L1 and L2.....	46
Scheme 7 The synthesis route of L1 and L2 under condition I .....	47
Scheme 8 The synthesis route of L1 and L2 under condition II .....	48
Scheme 9 The synthesis route of L1 and L2 under condition III .....	49
Scheme 10 The synthesis route of L1 and L2 under condition IV.....	50
Scheme 11 The synthesis route of L1 and L2 under condition V.....	51
Scheme 12 The synthesis route of L1 and L2 under condition VI.....	52
Scheme 13 The synthesis route of L1 and L2 under condition VII.....	53
Scheme 14 The synthesis route of L1 and L2 under condition VIII.....	54
Scheme 15 The synthesis route of L1 and L2 under condition IX.....	55
Scheme 16 The synthesis route of L1 and L2 under condition X.....	56
Scheme 17 Synthesis route of L3 and L4.....	57
Scheme 18 The synthesis route of L3 and L4 under condition I.....	58
Scheme 19 The synthesis route of L3 and L4 under condition II.....	59
Scheme 20 The synthesis route of L3 and L4 under condition III.....	60
Scheme 21 Synthesis route of PEG-COOH.....	61
Scheme 22 Synthesis route of L5.....	62
Scheme 23 Synthesis route of L6.....	63
Scheme 24 Synthesis route of L7.....	64
Scheme 25 Synthesis route of L8.....	64
Scheme 26 Synthesis route of CP-L8.....	66



Scheme 27 Proposed selective detection mechanism of pH optical and fluorescent sensor based on Rhodamine modified on activated cellulose paper (CP-L8).....

80



# CHAPTER 1

## INTRODUCTION

### 1.1 Supramolecular chemistry

Supramolecular chemistry, also known as “chemistry beyond the molecule”, focuses on the study of molecular recognition and high-order assemblies formed by noncovalent interactions. In 1987, the Nobel Prize in Chemistry was awarded jointly to Donald J. Cram, Jean-Marie Lehn, and Charles J. Pedersen “for their development and use of molecules with structure-specific interactions of high selectivity”. This established supramolecular chemistry as a well-accepted chemical discipline. Because supramolecular systems are made from building blocks that are linked together by noncovalent interactions, they can show stimuli-responsive behavior. What’s more, fascinating chemical architectures, such as rotaxanes, catenanes, and knots (Figure 1 and 2), which are difficult to prepare from covalent chemistry, can be easily prepared through templated synthesis [1].

A supramolecule is a well-defined discrete system generated through interactions between a molecule (receptor or host) having convergent binding sites such as donor atoms, sites for formation of hydrogen bonds and sizable cavity, and another molecule (analyte or guest) having divergent binding sites such as hydrogen bonding, dipole-dipole, charge transfer, van der Waals, and  $\pi$ - $\pi$  stacking interactions (scheme 1) [2].

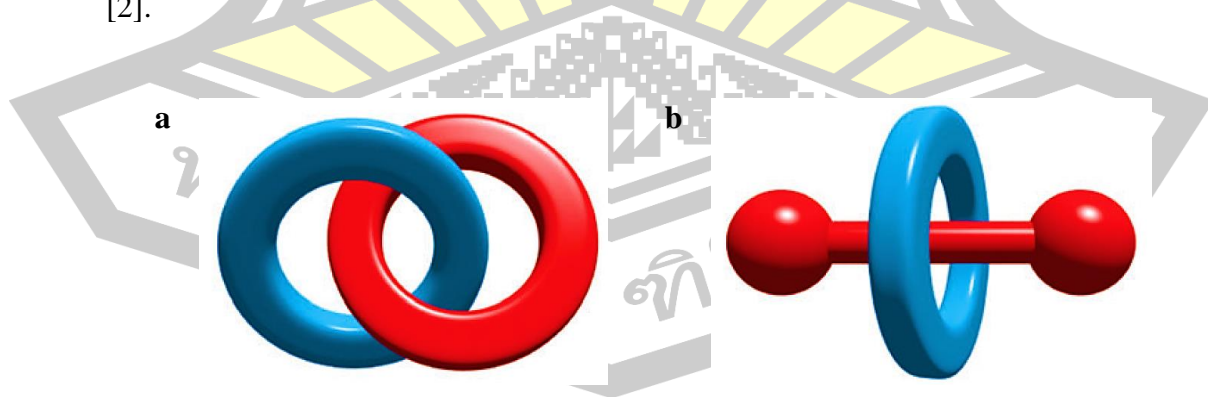


**Figure 1** Graphic representations of (a) [2]rotaxane and (b) [2]catenane [3].

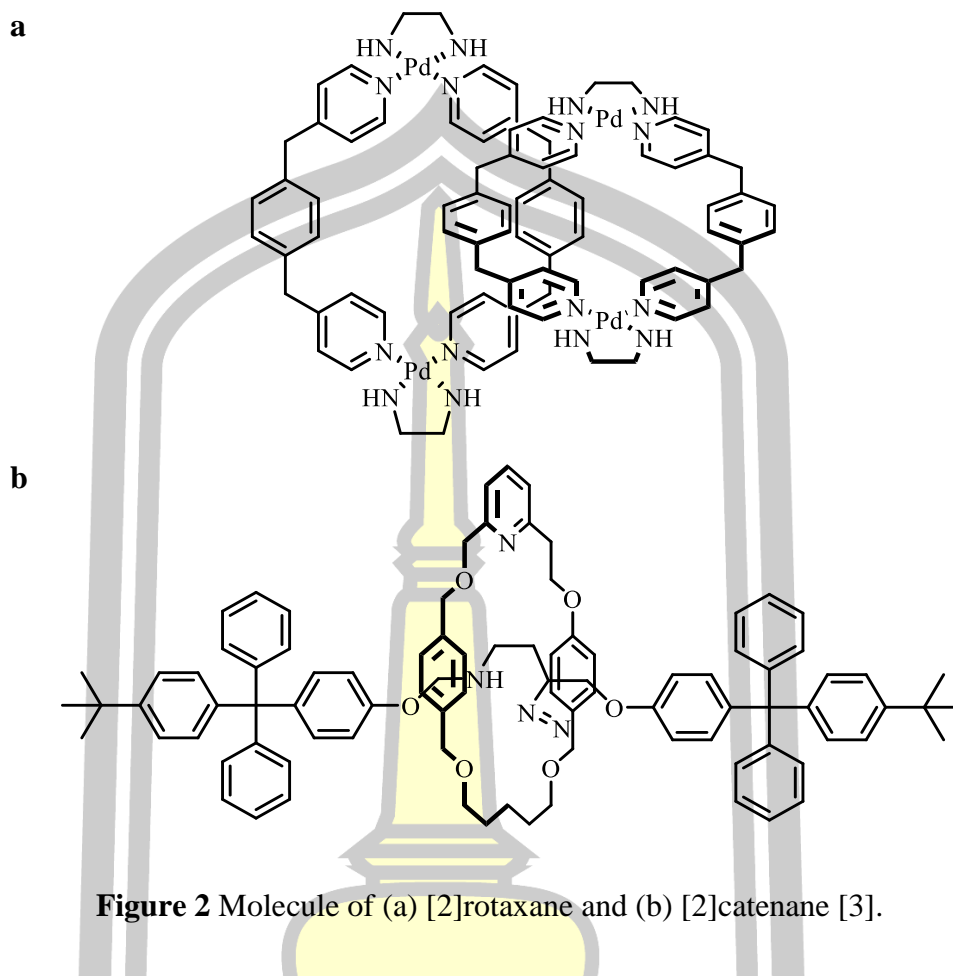
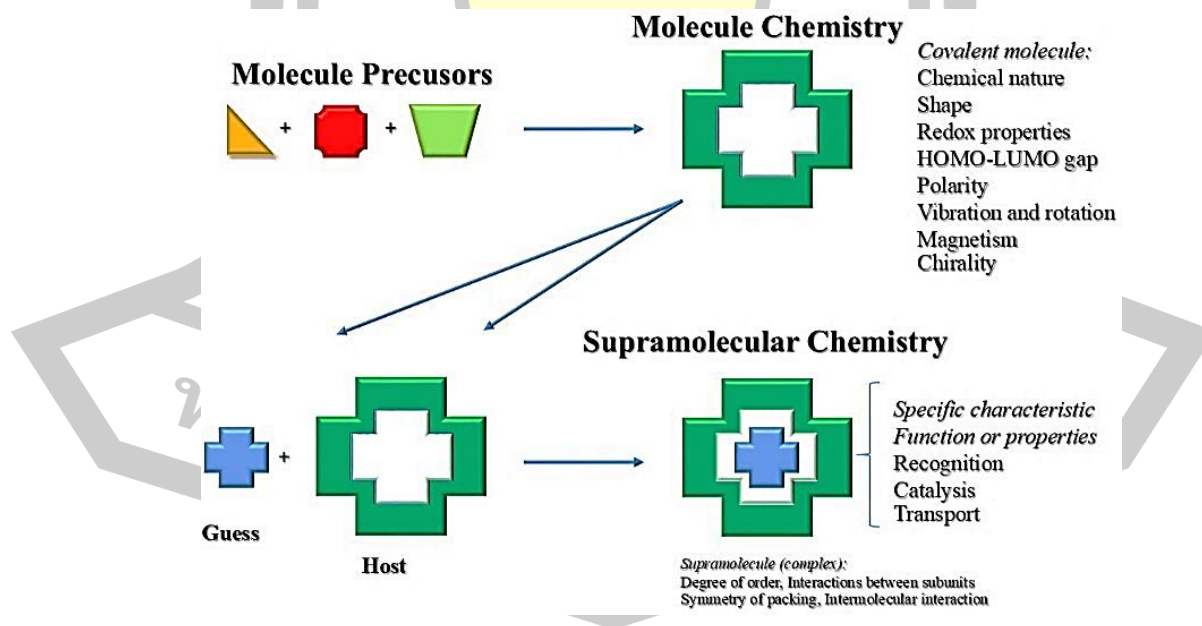


**Figure 2** Molecule of (a) [2]rotaxane and (b) [2]catenane [3].



**Scheme 1** Component of supramolecular chemistry [4].

## 1.2 Molecular recognition and chemical sensor

Molecular recognition is defined by the energy and the information involved in the binding and selection of substrate by a given receptor molecule; it may also involve a specific function. Mere binding is not recognition, although it is often taken as such. One may say that recognition is binding with a purpose, like receptors are ligands with a purpose. It implies a pattern recognition process through a structurally well-defined set of intermolecular interactions. Binding of a top forms a complex or supermolecule characterized by its (thermodynamic and kinetic (Figure 3)) stability and selectivity, i.e., by the amount of energy and of information brought into operation [5].

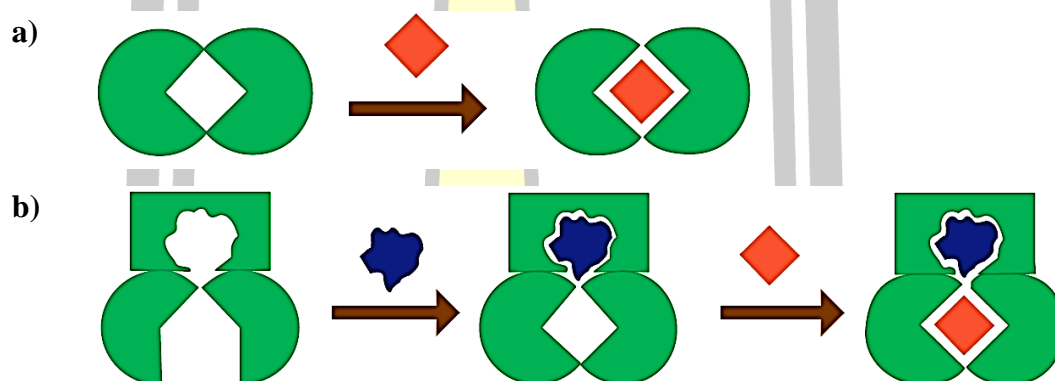
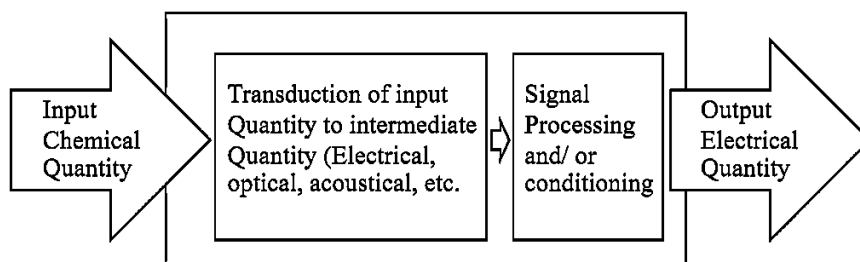


**Figure 3** Molecular Recognition (a) Static and dynamic (b) molecular recognition

The chemical sensor is an analyzer that responds to a particular analyte in a selective and reversible way and transforms input chemical quantity, ranging from the concentration of a specific sample component to a total composition analysis, into an analytically electrical signal, as depicted in scheme 2. The chemical information may originate from a chemical reaction by a biomaterial, chemical compound, or a combination of both attached onto the surface of a physical transducer toward the analyte. The chemical sensor subject is an emerging discipline formed by the multidisciplinary study among chemistry, biology, electricity, optics, mechanics, acoustics, thermology, semiconductor technology, microelectronics technology, and membrane technology [6]. The example of chemical sensor was presented in Figure 4.



**Scheme 2** Diagram of a sensor that produces an electrical output in response to the presence of an input quantity [6].

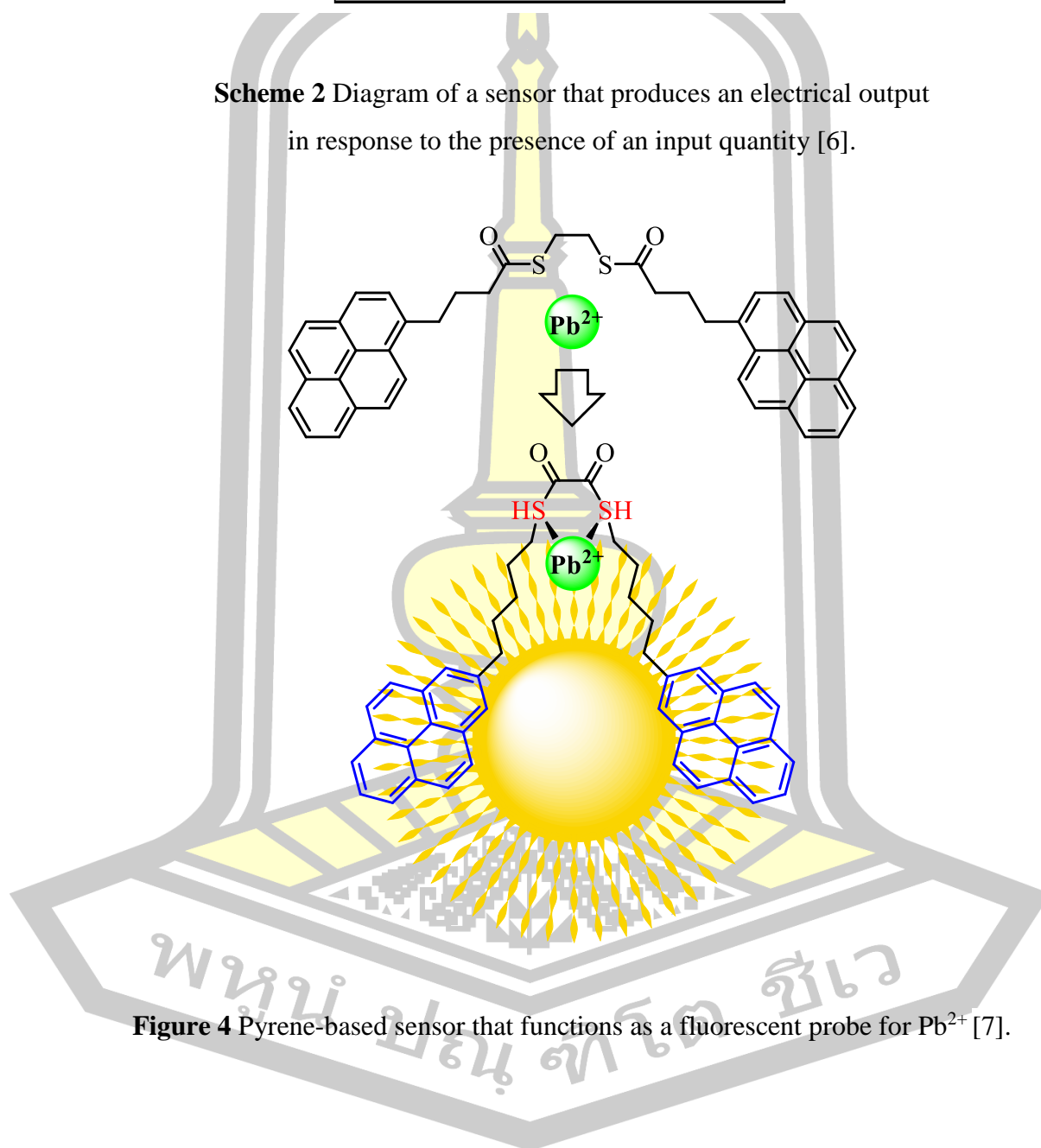


**Figure 4** Pyrene-based sensor that functions as a fluorescent probe for  $\text{Pb}^{2+}$  [7].

### 1.3 Fluorescence sensor

Fluorescence is the phenomenon of emission of light quanta by a molecule or supramolecular structure (fluorophore) after initial electronic excitation in a light-absorption process. After excitation by absorbing the light quanta, a molecule resides for some time in the so-called excited state and its fluorescence emission can be observed usually with a lower energy (longer wavelength) than the excitation. Such change in fluorescence emission color with respect to the color of incident light was first observed by Irish scientist George Stokes and is called the Stokes shift. The time scale of fluorescence emission depends on both the fluorophore and its interactions with local environment. Thus, for organic dyes the fluorescence lifetime is in picosecond (ps) to nanosecond (ns) time range, typically  $10^{-8}$  to  $10^{-11}$  s.

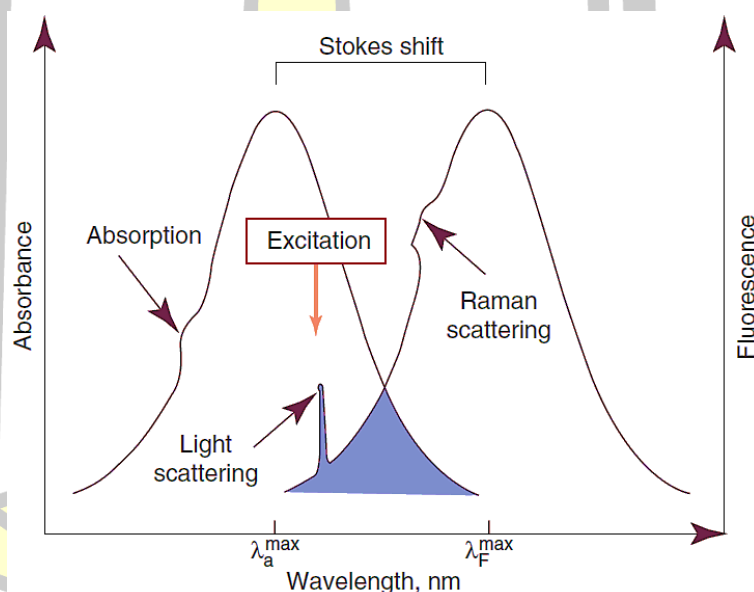


**Figure 5** Typical absorption and fluorescence emission spectra. fluorescence spectrum is located at longer wavelengths with respect to the absorption spectrum. The area between absorption and emission spectrum is shadowed. The distance between their band maxima is called the Stokes shift.

Molecular constructs can be made in such a way that they integrate both the recognition and reporter elements of a sensor, allowing target detection in a direct way. Such sensors are essentially the ‘direct sensors’, since the transduction of signal generated on the step of recognition does not need any additional steps or additional interacting partners. Such molecular sensors are ‘affinity-based’ because the signal is produced by the target-sensor interaction itself, in contrast to ‘catalytic sensors’, in which the signal is caused by a catalytic substrate transformation. The label in most cases is a fluorescent dye or nanoparticle (a fluorophore), leading to a signal of fluorescence emission that is relatively easy to record. Fluorescence is often very sensitive to the changes of molecular environment and not only to target binding. If its change is coupled with molecular recognition event, this property can be also applied in sensing. In a broader sense, fluorescence allows visualization of sensor-target interactions with high spatial resolution (Figure. 6).

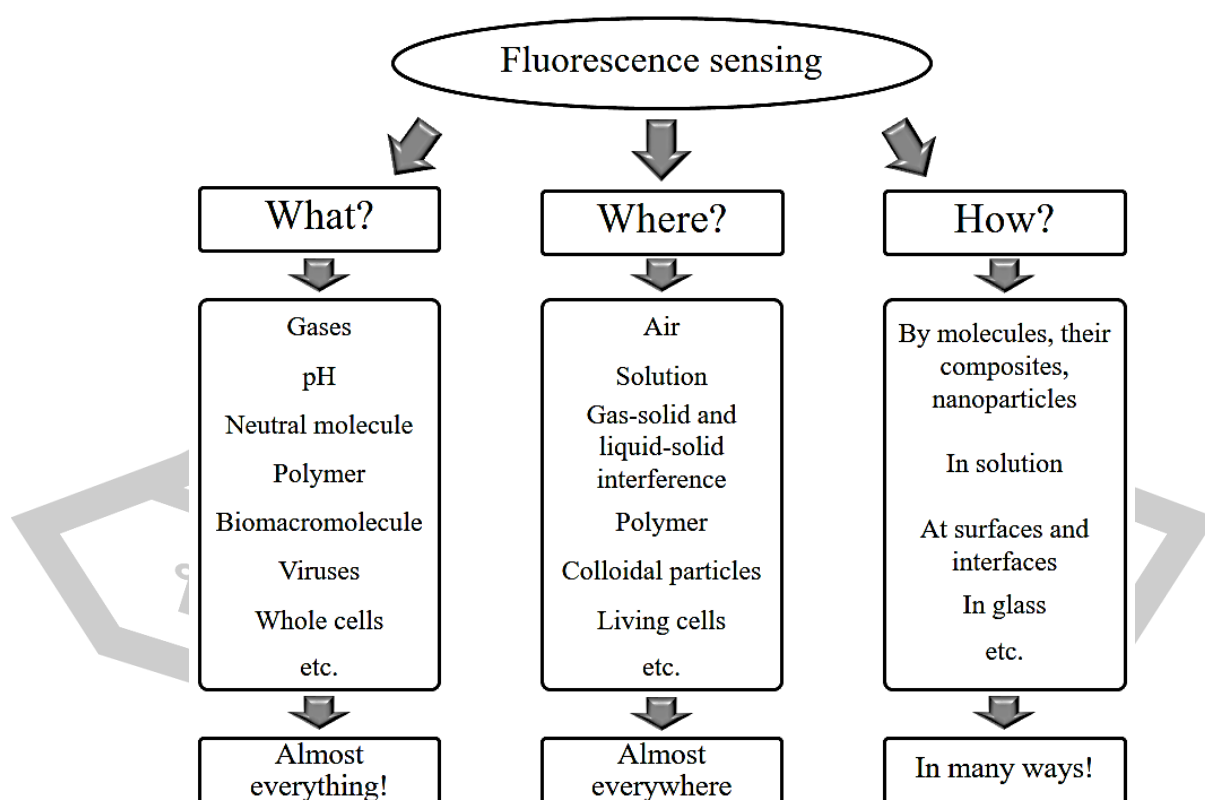


**Figure 6** The range of application of fluorescence sensing technologies.

Thus, fluorescence sensing is essentially a label-based approach (intrinsic fluorophores, such as tryptophan in proteins, can be considered as naturally imposed labels). When comparing this approach with the label-free methods based on detection of changes of refractive index, charge or mass at the sensor surface or heat effects, one has to note the following important point. Testing often involves side effects produced by contaminants. These contaminants also have mass and charge; they change refractive index and produce heat effects. This results in background signal that may induce a serious complication when these techniques are used for testing realistically complex samples, such as blood serum. In contrast, specific labeling in sensing technologies always makes the response more specific leading to reduction of false positive complications in results [8].

#### 1.4 The most efficient dyes for labeling

High quantum yield of fluorescence emission in solutions can be achieved in the case of resonant or mesomeric dyes, such as fluoresceins (**1**), Rhodamines (**4**), and cyanines (**2**). Their skeleton is rigid, which allows minimizing the vibrations-related energy losses and their electronic density is delocalized over the whole fluorophore. Because of the absence of strong charge asymmetry their interaction with polar environment is small and it is the reason why we observe their small Stokes shift and low spectral sensitivity to the environment.

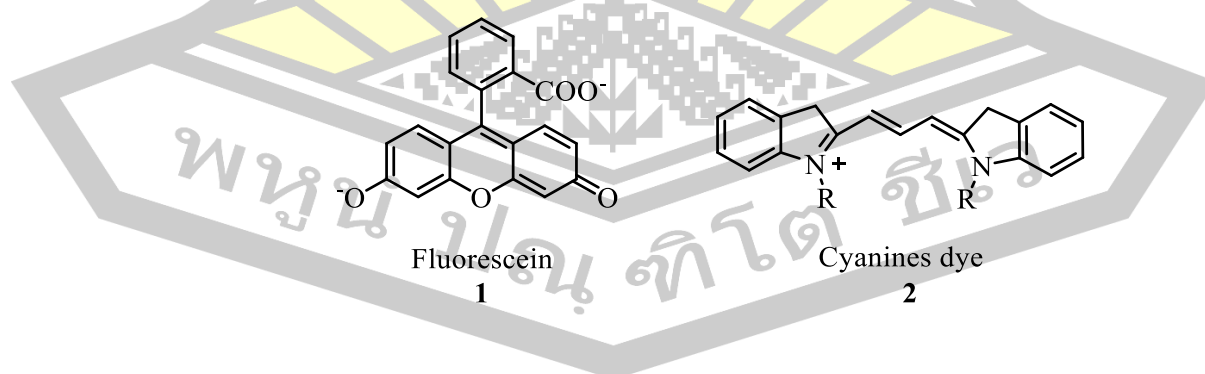


**Figure 7** Structure of mesomeric dyes; fluorescein (**1**) and cyanines dye (**2**).



There are several classes of dyes that conform in the best way to the criteria for optimal labels and tags. They can be efficiently used if a 'responsive' function is not needed. Those are the modified fluorescein and Rhodamine derivatives, BODIPY and also cyanine dyes. Synthetic chemistry suggests many improvements in their properties.

### 1.5 Introduction to Rhodamine B

Rhodamine is classes of highly fluorescent dyes, Rhodamines are derivatives of xanthene (3). Rhodamine (4) was divided into 2 type: Rhodamine 6G (5) and Rhodamine B (6). Which the first fluorescent dyes to be used as laser dyes. Their absorption and emission spectra are quite narrow and the Stokes shift is small. They emit fluorescence in the range 500-700 nm [9]. Rhodamine are, owing there structural rigid affect to fluorescent. In addition, their fluorescence efficiency show a peculiar depend on the substitution pattern of amino group. If these are only partially substituted by alkyl group, the fluorescence efficiency is close to unity and nearly independent of solvent polarity and temperature [10].

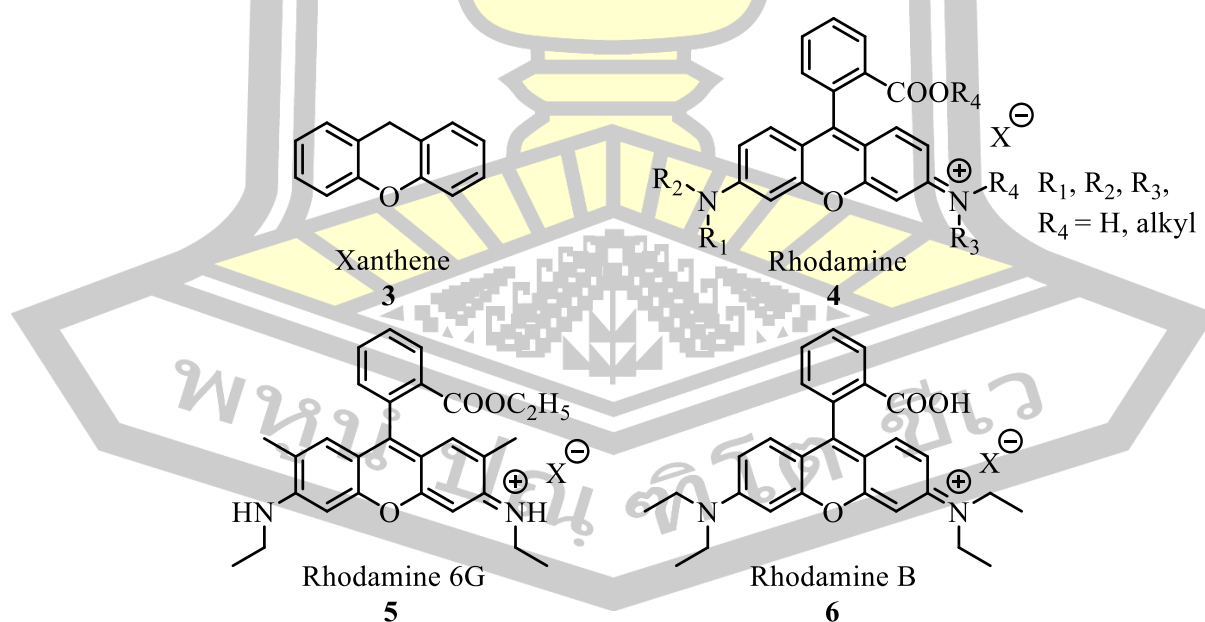


**Figure 8** Structure of xanthene and Rhodamine.

## 1.6 Introduction to Rhodamine B derivative

Three types of modification of Rhodamine derivatives can be envisioned: modification of the amino groups of xanthene moiety (positions 3 and 6); modification of the carboxyphenyl ring at positions 4' and/ or 5' or modification of the position 2 carboxylic group (Figure 1.9). Although 2'-position could be seen as the easiest to functionalize since it bears already a functional group (a carboxylic acid or ester, depending on the Rhodamine) and 2' -position modified called Rhodamine spirolactam derivative [11].

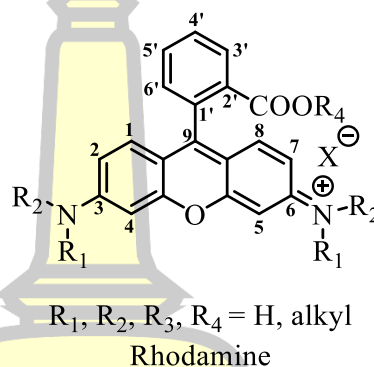
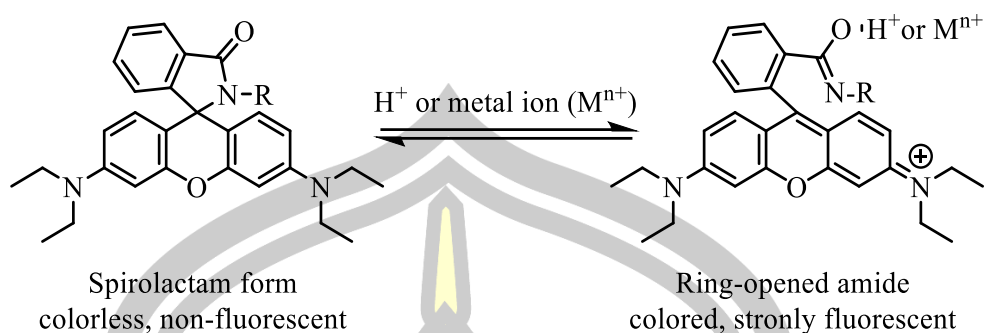


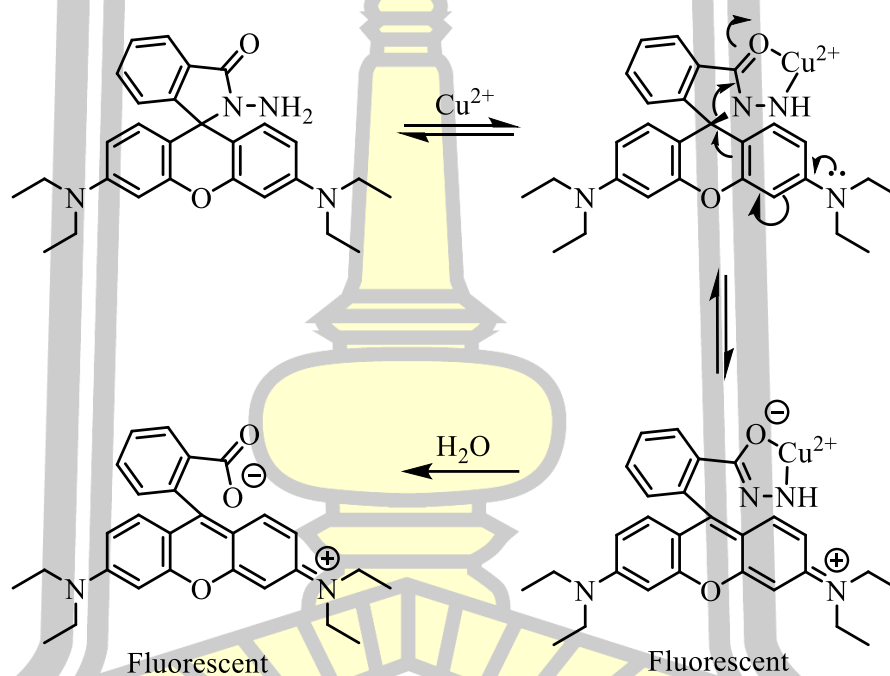
**Figure 9** Position structure of Rhodamine B.

## 1.7 Rhodamine Based chemosensor

Rhodamine spirolactam derivatives is colorless and non-fluorescent in common (protic or aprotic) solvents, which structurally equilibrates to a colored and highly fluorescent ring-opened amide form upon analyte induced binding or reaction. For example, acidic pH and metal can induce a non-fluorescent Rhodamine spirolactam to be a highly fluorescent Rhodamine derivatives (Scheme 3) [12]. The mechanism for spirolactam open ring by cation of Rhodamine derivatives shown as Scheme 4 [13].



**Scheme 3** Spirolactam ring-opening process of Rhodamine derivatives [12].



**Scheme 4**  $\text{Cu}^{2+}$  induced spirolactam ring opening mechanism [13].

### 1.8 Introduction to the research problem and its significant

In topic 1.4-1.7 mentioned about Rhodamine B based chemosensor. It show Rhodamine B as fluorophore which specific with metal ion and  $\text{H}^+$ . This is a reason for interesting to apply Rhodamine B as a sensor for metal ions and pH detection.

Heavy metals are defined as metallic elements that have a relatively high density compared to water. With the assumption that heaviness and toxicity are inter-related, and that are able to induce toxicity at low level of exposure [14]. They can affect many different areas of the brain and their associated functions, resulting in a variety of symptoms. These include personality changes (irritability, shyness, nervousness), tremors, changes in vision (constriction (or narrowing) of the visual field), deafness, muscle incoordination, loss of sensation, and difficulties with memory [15]. The traditional methods used for quantification of heavy metal ions are atomic absorption spectrometry (AAS) [16], inductively coupled plasma atomic emission spectrometry (ICP-AES) [17], X-ray fluorescence [18]. However, these methods are mostly labor-intensive and time consuming. Therefore, sensor was developed for easy to detect by simple instrument and save cost to detection such as UV-Vis, fluorescence spectrometer.

The detection of pH is also importance because it commonly plays a key role in a variety of systems including chemical and biological properties such as the hardness of water and oxygen consumption depend on pH value that effect to survival of marine [19,20]. Moreover pH value is important experimentally in the laboratory. Several detection methods such as acid–base titration [21,22] and potentiometric titration [23,24] have been employed to detect pH value, however these technique can be inaccurate and many other factors have to be taken into consideration to get the correct value. Nowadays, There are many techniques using organic materials for pH detection, for example, logic gates [25], optical sensors [26], and fluorescence sensors [27,28]. Fluorescence sensors have been especially used for pH detection due to their high sensitivity, high selectivity and save cost [29].

This thesis is focusing an 3 topic:

I) Rhodamine-cyclohexane: In this topic will present about the synthesis of Rhodamine derivative coupling with cyclohexane dicarboxylic acid. The synthesis was proceeded by various of coupling reagent, solvent , precursor amount and temperature.

II) Rhodamine-Polyethylene glycol (PEG): The second topic represent a various of molecular weight (400, 4000 and 6000) of polyethylene glycol (PEG). Which it was linked with Rhodamine derivative by coupling reaction. Moreover, The

probe was study of selectivity with metal ions, pH estimated and applied to micelle sensor.

III) Rhodamine anhydride: The last topic will present about the synthesis of Rhodamine derivative coupling with succinic anhydride. Moreover, the probe was study selectivity with metal ions, pH estimated and applied to portable sensor.

### **1.9 Objectives of research**

1.9.1 To synthesize of Rhodamine derivative with cyclohexane dicarboxylic acid via coupling reaction

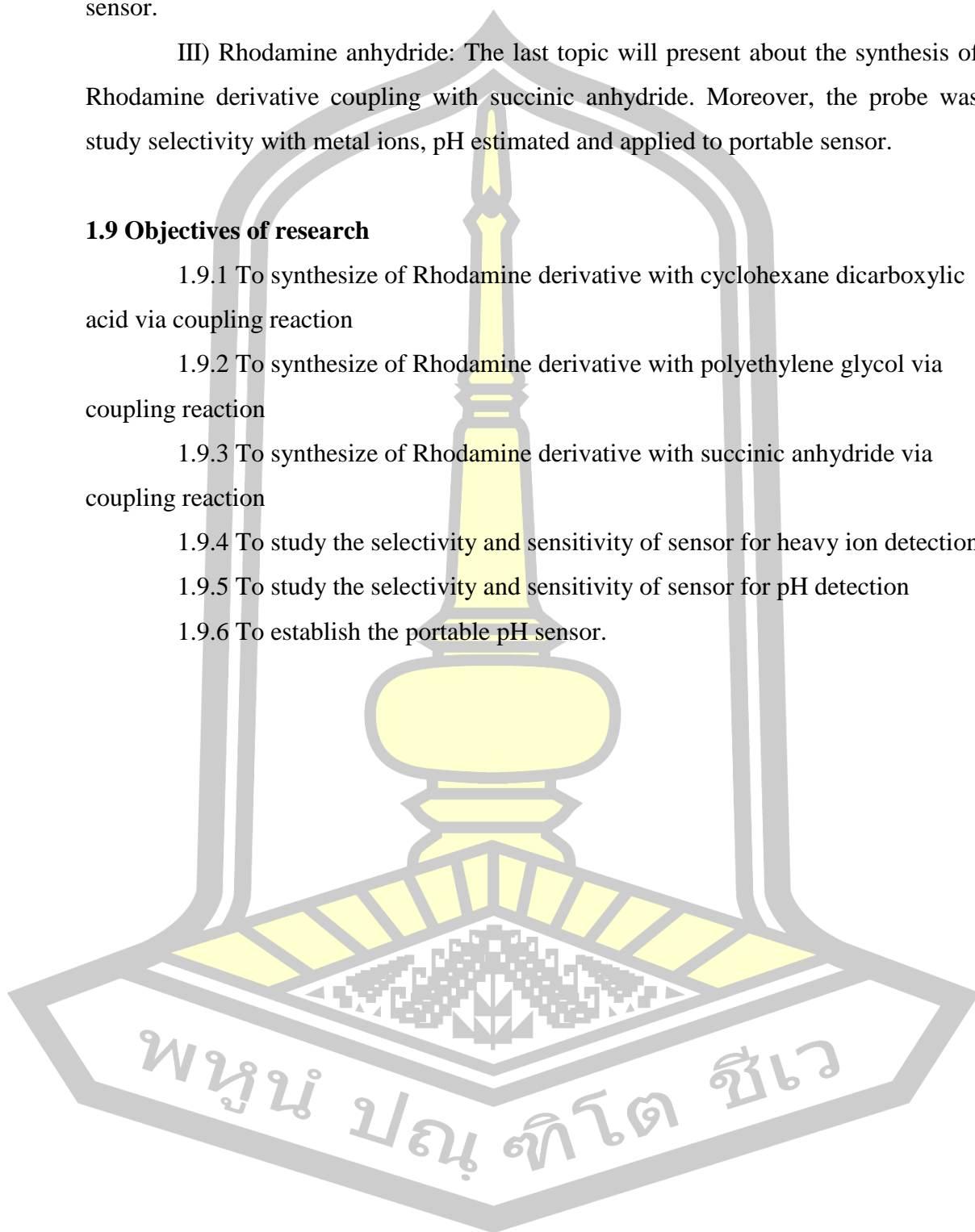
1.9.2 To synthesize of Rhodamine derivative with polyethylene glycol via coupling reaction

1.9.3 To synthesize of Rhodamine derivative with succinic anhydride via coupling reaction

1.9.4 To study the selectivity and sensitivity of sensor for heavy ion detection

1.9.5 To study the selectivity and sensitivity of sensor for pH detection

1.9.6 To establish the portable pH sensor.



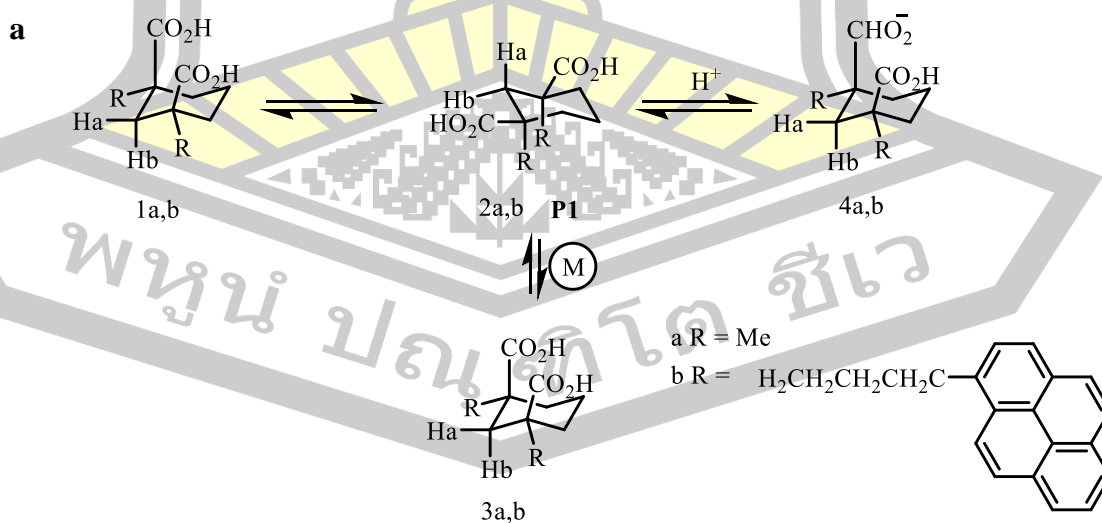
## CHAPTER 2

### LITERATURE REVIEW

#### 2.1 Rhodamine-cyclohexane chemosensor

During the past of decayed, the cyclohexane system for designing fluorescence sensor have play importance rule due to structure flexible and good properties to establish a chemical sensor.

In 1998, C. Monahan and coworkers [30] synthesized the excimer/ monomer fluorescence probe for a pyrene functionalized cis-cyclohexane-1,3-dicarboxylate (**P1**). The conformational switching can be induced by divalent and monovalent metal cations (Figure 10a), as well as strong and weak acids. Analogue **P1** exhibits large changes in fluorescence and is thus sensor for Lewis and Brønsted acids. Moreover, The two pyrenyl groups in structure **P1** are in close proximity to each other and are able to exhibit intramolecular excimer fluorescence. With structures 1b, 3b and 4b, the pyrenyl groups are separated and the favorability of excimer formation is decreased. This was found to be the case in MeCN solution where titration of the bis(tetrabutylammonium) salt of 2b with strong acid resulted in a stoichiometric decrease in the excimer/monomer fluorescence ratio. The titration curve (Figure 10b) indicates that only 1 equiv. of nitric acid is needed to completely switch the excimer/ monomer ratio.



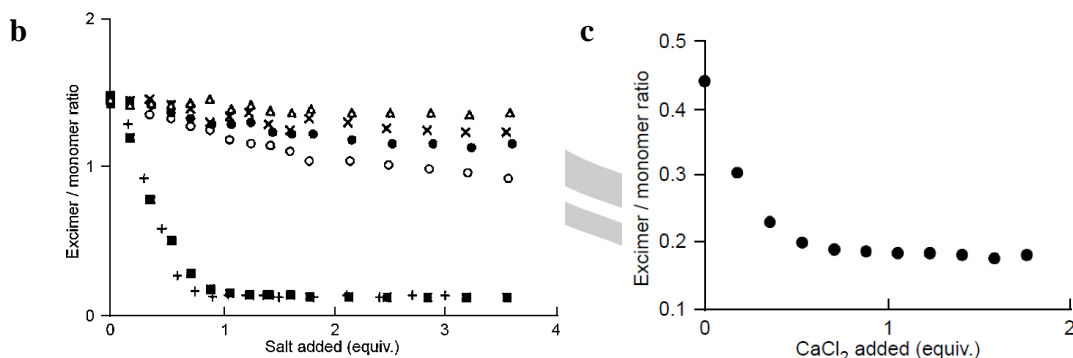


**Figure 10** (a) synthesis route of **12**, (b) change in excimer/monomer ratio for **P1** in MeCN upon titration with ( $\Delta$ ) CsNO<sub>3</sub>, ( $\times$ ) RbNO<sub>3</sub>, ( $\bullet$ ) KNO<sub>3</sub>, ( $\circ$ ) NaNO<sub>3</sub>, ( $\blacksquare$ ) NH<sub>4</sub>NO<sub>3</sub> and ( $+$ ) HNO<sub>3</sub>. (c) change in excimer/monomer ratio for **P1** upon titration with CaCl<sub>2</sub>. Excitation at 346 nm, monomer emission at 397 nm, excimer emission at 470 nm.

Cyclohexane-1,2-diamine-based bisbinaphthyl macrocycles ((*S*)-/(*R*)-**P2**) and their cyclic and acyclic analogues were synthesized by Z. B. Li and coworkers in 1998 [31]. The interactions of these compounds with various chiral acids are studied. Compounds (*S*)-/(*R*)-**P2** exhibit highly enantioselective fluorescent responses and high fluorescent sensitivity toward *R*-hydroxycarboxylic acids and N-protected amino acids. Among these interactions, (*S*)-mandelic acid ( $10^{-3}$  M) led to over 20-fold fluorescence enhancement of (*S*)-**P2** ( $1.0 \times 10^{-5}$  M in benzene/0.05% DME) at the monomer emission, and (*S*) hexahydromandelic acid ( $10^{-3}$  M) led to over 80-fold fluorescence enhancement. These results demonstrate that (*S*)-**P2** is useful as an enantioselective fluorescent sensor for the recognition of the chiral acids. On the basis of the study of the structures of (*S*)- **P2** and the previously reported 1,2-diphenylethylenediamine-based bisbinaphthyl macrocycle (*S*)- **P2**, the large fluorescence enhancement of (*S*)- **P3** with a chirality-matched *R*-hydroxycarboxylic acid is attributed to the formation of a structurally rigidified host-guest complex and the further interaction of this complex with the acid to suppress the photoinduced electron-transfer fluorescent quenching caused by the nitrogens in (*S*)-**P2**.

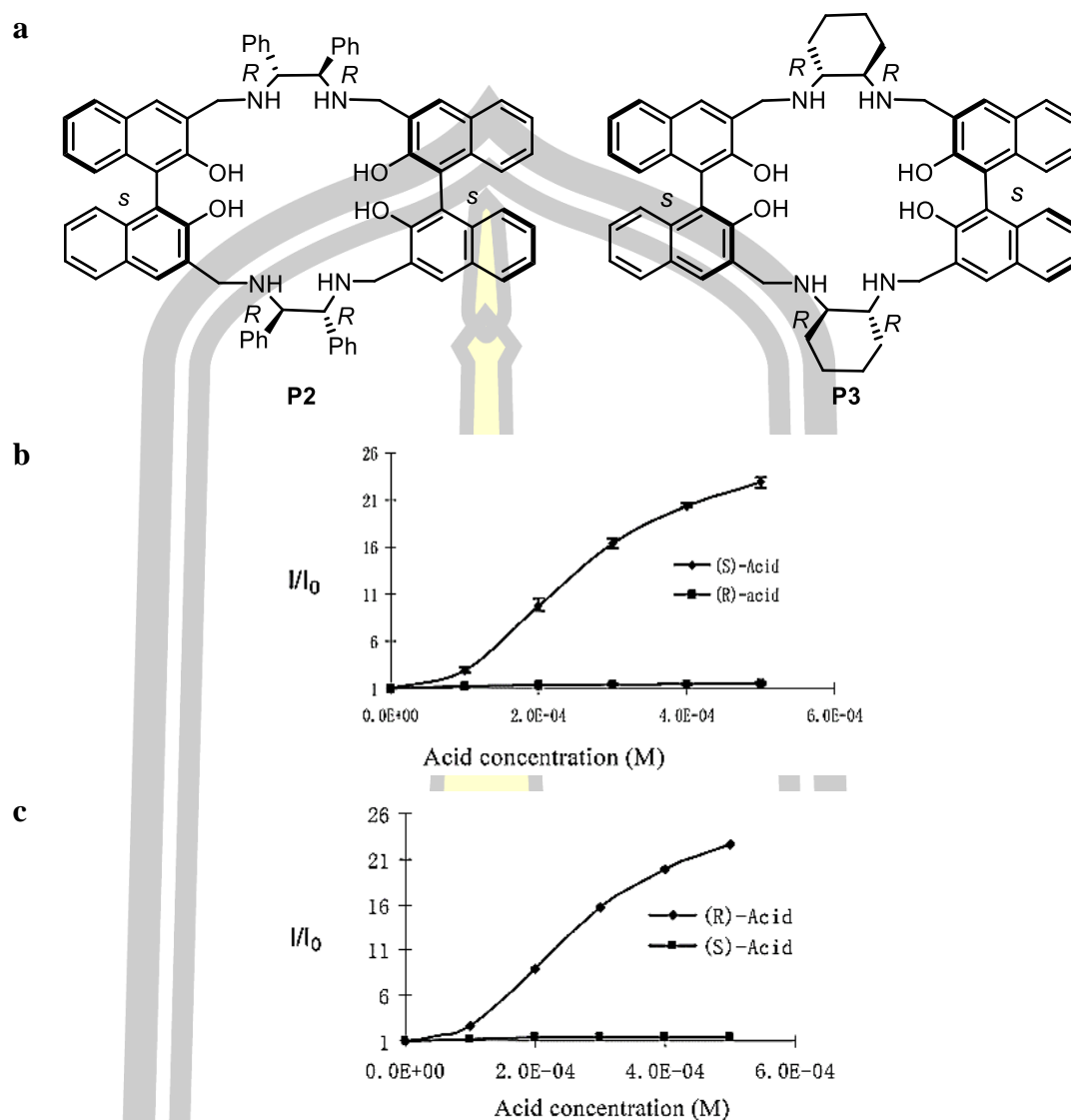


**Figure 11** (a) structure of **P2**, **P3**, Fluorescence enhancement of (b) (S)-**P2** and (c) (R)-**P2** ( $1.0 \times 10^{-5}$  M in benzene/0.05% DME) versus concentration of (R)- and (S)-mandelic acid ( $\lambda_{\text{ex}}=332$  nm).

พหุ ประทีป ชีวะ



Aliphatic  $\alpha,\omega$ -dicarboxylates of five cyclohexane (**P4**, **P5**) were synthesized by Costero and coworkers in 1998 [32]. The studied **P4** and **P5** have been designed following the binding site-signalling unit approach and they all possess thiourea groups as recognition moieties. Ligands **P4** and **P5** containing naphthalene units can be used as fluorescent sensors as they form intramolecular or intermolecular excimers in the presence of appropriate dicarboxylates. Studies carried out with **P4** and **P5** demonstrated that in the presence of succinate and malonate a new band appears around 490 nm and 495 nm respectively show as Figure 12a and 12b.

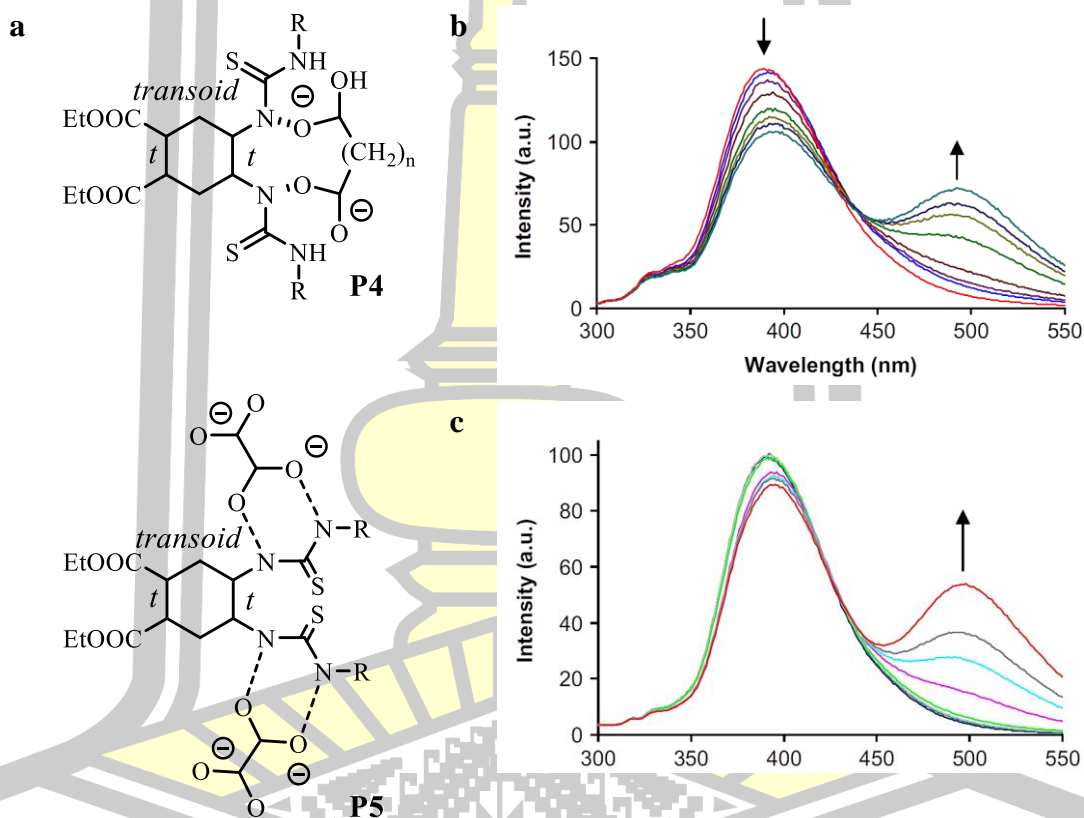
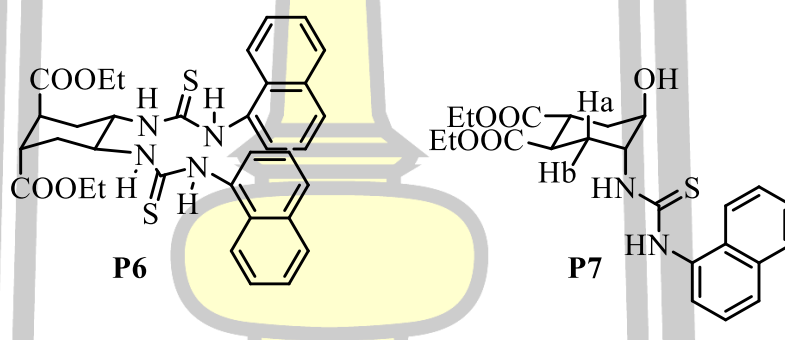


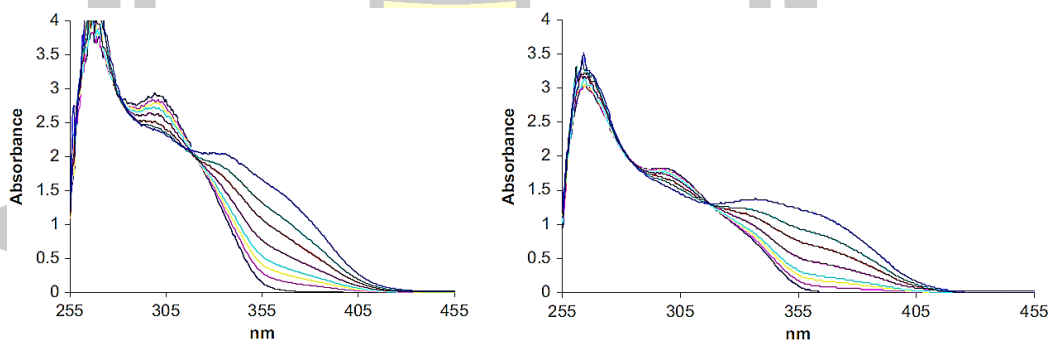
**Figure 12** (a) structure of **P4**•succinate, **P5**•malonate. A fluorescence spectra (in DMSO  $10^{-5}$  M,  $\lambda_{\text{ex}}$  290 nm) of (b) **P4** + increasing amounts of succinate, (c) **P5** + increasing amounts of succinate.

In 2008, M. A. Costero and coworkers [33] synthesized a new chiral cyclohexyl based fluorescent anion receptors and their absolute configuration has been determined by using circular dichroism (CD). The stoichiometries and equilibrium constants were determined by fitting the UV spectra of equilibrium mixtures (Figure 13b) for **P6** and **P7** with L-aspartate and for other ligands and dicarboxylates. The stoichiometry of the complexes formed by ligands **P6** and **P7** was 1:1 with all the studied dicarboxylates. The complexation constant values were also very similar. By contrast, ligands **P6** and **P7** showed a 2:1 stoichiometry in their complexes with L-, D-aspartate and L-, D-glutamate, and a 1:1 stoichiometry with L-, D-tartrate. The chiral discrimination ability of these ligands for chiral dicarboxylates has been studied and the best results have been obtained with TMA aspartate.

**a**



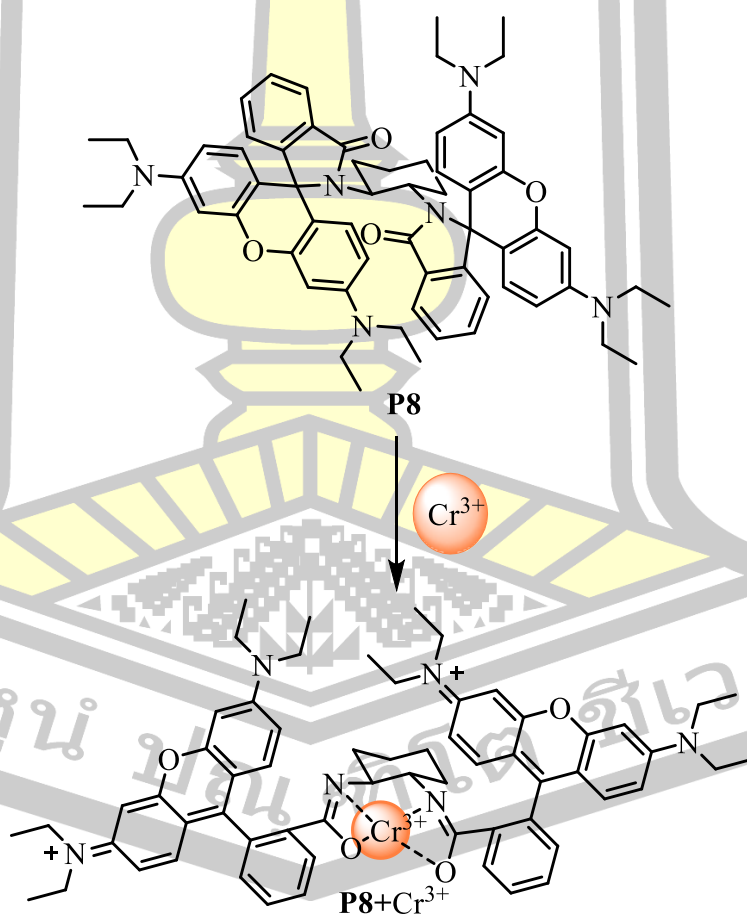
**b**



**Figure 13** (a) structure of **P6** and **P7**, (b) UV spectra in DMSO of **P6** ( $10^{-5}$  M) + TMA L-aspartate (left) and **P7** ( $10^{-5}$  M)+TMA L-aspartate (right).

A new Rhodamine Based fluorescent turn on sensor **P8** were synthesized by S. Sahana and coworkers in 2018 [34]. The result is highly selective and sensitive chemosensor for the  $\text{Cr}^{3+}$  ion in a  $\text{CH}_3\text{CN-H}_2\text{O}$  solution. In presence of  $\text{Cr}^{3+}$  ion, the strong fluorescence enhancement is attributed due to the interaction of  $\text{Cr}^{3+}$  with **P8** (Figure 14b), leading to opening of the spirolactam ring of Rhodamine B to the amide form. The  $\text{Cr}^{3+}$  sensing mechanism is also supported by the Job's plot, ESI-MS,  $^1\text{H}$ -NMR titration experiments. Importantly, **P8** shows high selectivity over other biologically relevant metal ions. Also, anions do not show any effect (Figure 14c). In addition, the detection limit is found to be up to 7.5 nM which is acceptable within the EPA (US) limit. The probe is also able to function within a broad biological pH range of 4–8.

**a**



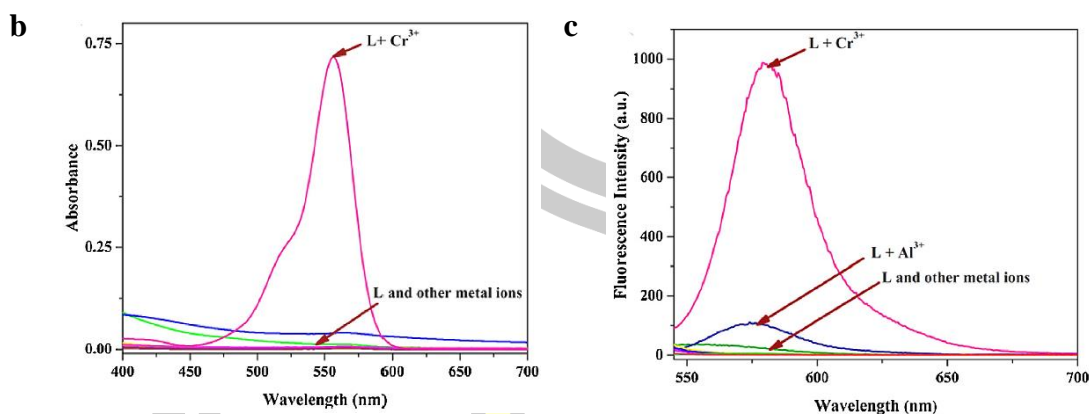
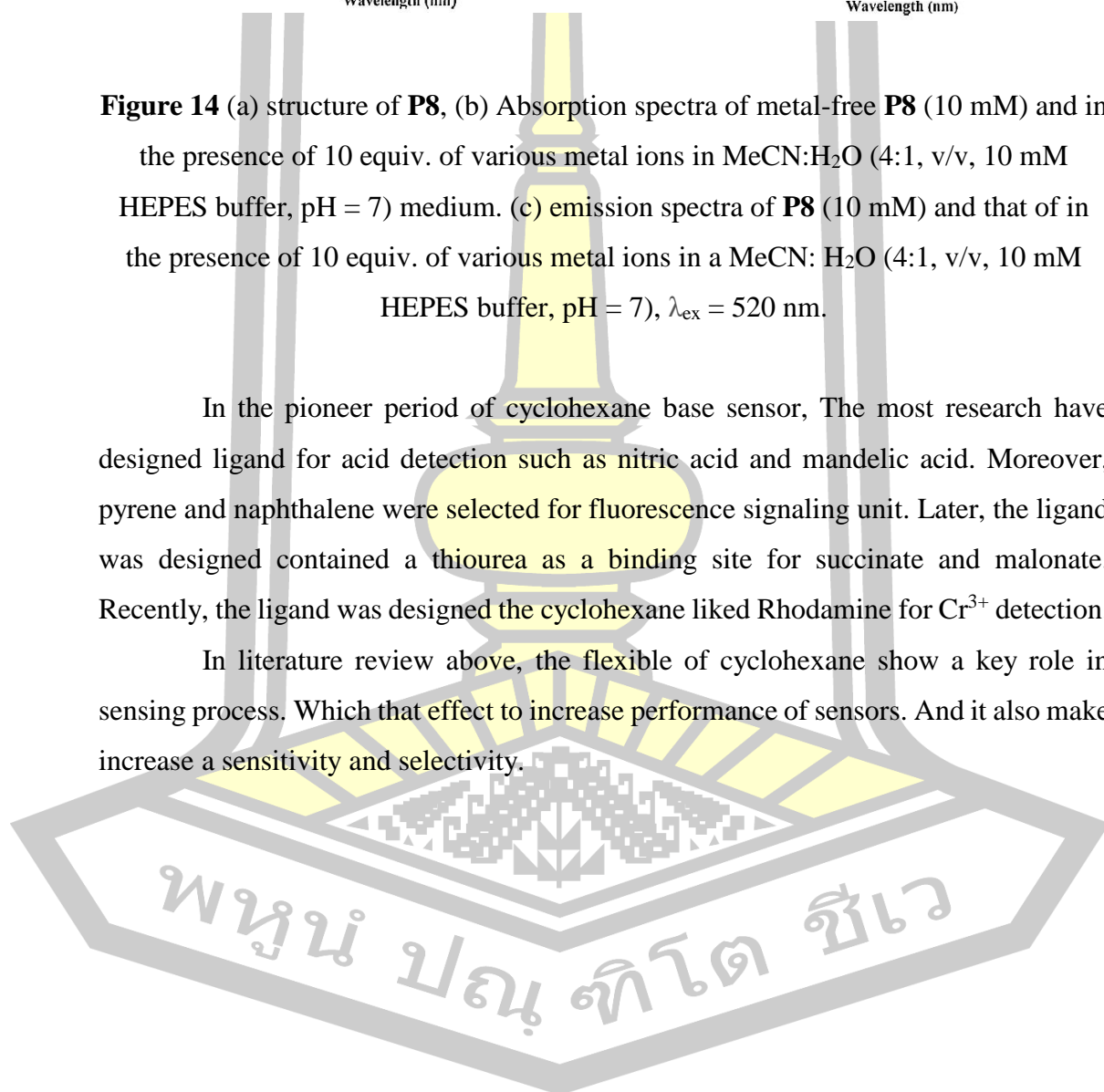


**Figure 14** (a) structure of **P8**, (b) Absorption spectra of metal-free **P8** (10 mM) and in the presence of 10 equiv. of various metal ions in MeCN:H<sub>2</sub>O (4:1, v/v, 10 mM HEPES buffer, pH = 7) medium. (c) emission spectra of **P8** (10 mM) and that of in the presence of 10 equiv. of various metal ions in a MeCN: H<sub>2</sub>O (4:1, v/v, 10 mM HEPES buffer, pH = 7),  $\lambda_{ex} = 520$  nm.

In the pioneer period of cyclohexane base sensor, The most research have designed ligand for acid detection such as nitric acid and mandelic acid. Moreover, pyrene and naphthalene were selected for fluorescence signaling unit. Later, the ligand was designed contained a thiourea as a binding site for succinate and malonate. Recently, the ligand was designed the cyclohexane liked Rhodamine for  $Cr^{3+}$  detection.

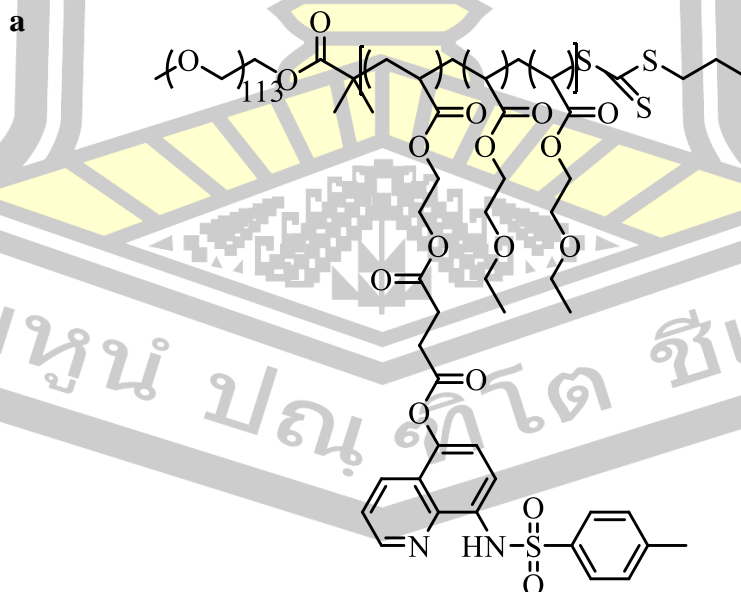
In literature review above, the flexible of cyclohexane show a key role in sensing process. Which that effect to increase performance of sensors. And it also make increase a sensitivity and selectivity.

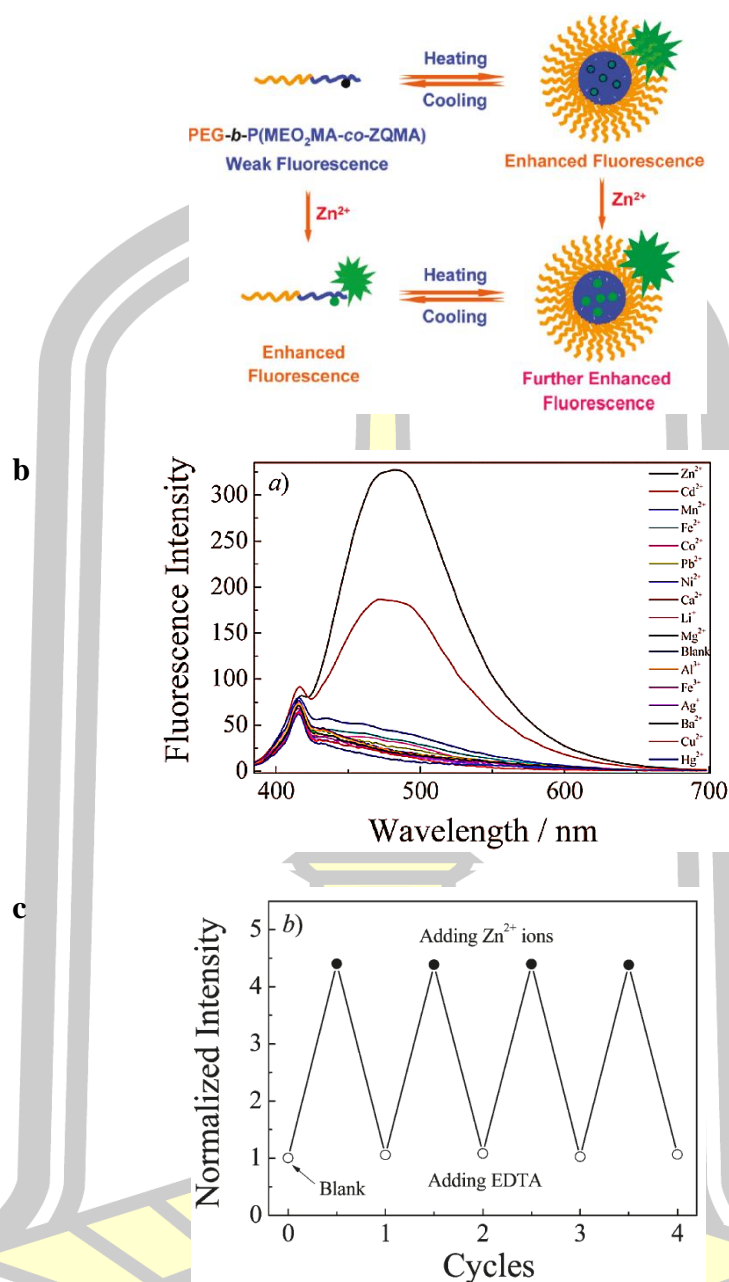


## 2.2 Rhodamine-polyethylene glycol (PEG) chemosensor

The advantage of PEG is highly soluble in water. Therefore, we selected the PEG in this work for increasing polarity of sensor and detect metal ions in aqueous solution.

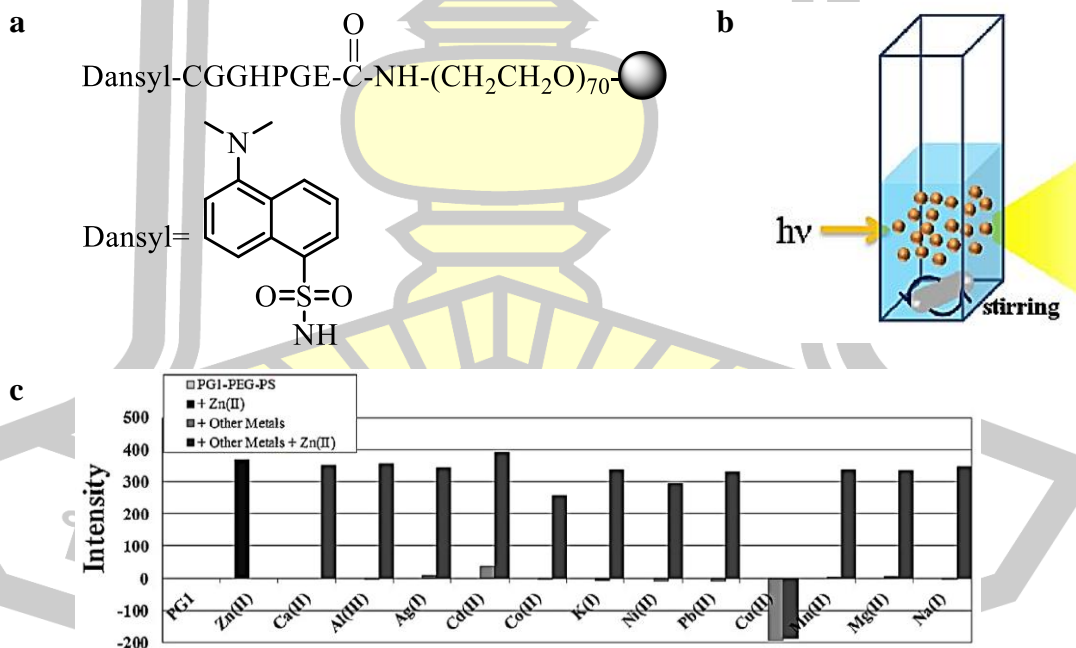
In 2011, T. Liu and coworker [35] synthesized PEG-b-P(MEO<sub>2</sub>MA-co-OEGMA-co-ZQMA) (**P9**), which can serve as dual fluorescent chemosensors for temperature and Zn<sup>2+</sup> ions (Figure 15b). At 20°C, **P9** can selectively bind Zn<sup>2+</sup> ions over other common metal ions (Figure 15c), leading to the prominent fluorescence enhancement with a detection limit down to ~3.0 nM. Upon heating above the critical micellization temperature (CMT), the fluorescence intensity of **P9** in the absence of Zn<sup>2+</sup> ions exhibits a 6.0-fold increase in a narrow temperature range of 26-32°C. Furthermore, the effective detection range of temperatures can be facily tuned by simply varying OEGMA molar contents in the thermoresponsive block. A part from this, reversible sensing of Zn<sup>2+</sup> ions can be achieved at 37 °C (Figure 15d), although the detection limits slightly increased to ~14 nM for **P9** and ~10 nM for **P9** In vitro fluorescence imaging studies demonstrated that the micelles can effectively enter into living cells and sensitively respond to Zn<sup>2+</sup> ions.



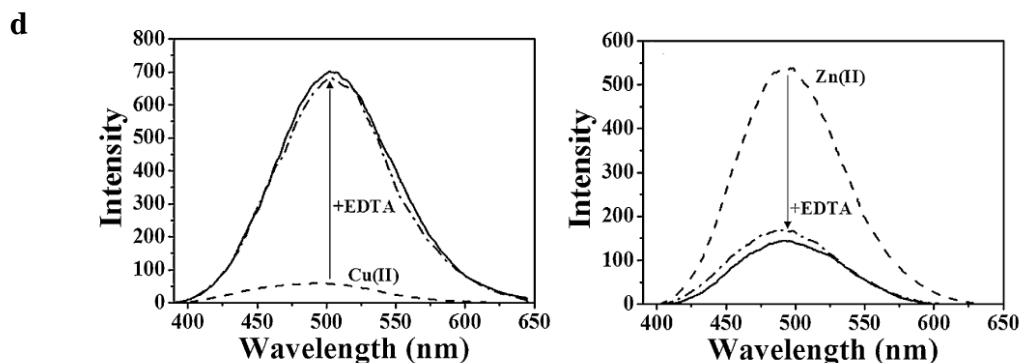


**Figure 15** (a) Structure of **P9**, illustration for the fabrication of thermoresponsive **P9**, of Zn<sup>2+</sup> Ions and Temperature. (c) Fluorescence emission spectra of **P9** (0.2 g/L, [ZQMA] = 5.0 × 10<sup>-6</sup> M) upon addition of 4.0 equiv (relative to ZQMA moieties) of various metal ions (Zn<sup>2+</sup>, Al<sup>3+</sup>, Ba<sup>2+</sup>, Ca<sup>2+</sup>, Co<sup>2+</sup>, Cu<sup>2+</sup>, Fe<sup>2+</sup>, Fe<sup>3+</sup>, Ag<sup>+</sup>, Hg<sup>2+</sup>, Li<sup>+</sup>, Mg<sup>2+</sup>, Mn<sup>2+</sup>, Ni<sup>2+</sup>, Pb<sup>2+</sup>, and Cd<sup>2+</sup>), respectively. (d) changes in relative fluorescence of **P9** (5.0 × 10<sup>-6</sup> M) upon sequential addition of 4.0 equiv of Zn<sup>2+</sup> ions and EDTA at 37 °C, four cycles were tested in each case.

In 2014, P. J. Bishnu and coworkers [36] prepared a functionalized resin by immobilization of the fluorescent peptide sensor into PEG-PS resin beads (**P10**) and investigated the sensing ability for the metal ions in aqueous solutions. The functionalized resin was easily used for detecting heavy metal ions in aqueous solutions using spectrofluorometer with stirrer (Figure 16b). The functionalized resin with the peptide sensor showed a selective response to Cu(II) and Zn(II) ions among 13 metal ions in aqueous solutions (Figure 16c). The functionalized resin with the peptide sensor, showed a turn off response to Cu(II) and a turn on response to Zn(II) ions in aqueous solutions. The resin showed a very sensitive response to Cu(II) and Zn(II) ions; about 1 equiv. of the metal ions was enough to saturate the fluorescent change of the resin. Furthermore, the recycle of the resin bead for detecting metal ions was demonstrated by simply washing of the resin with EDTA solution and fluorescent response for Cu(II) ions (Figure 16d).

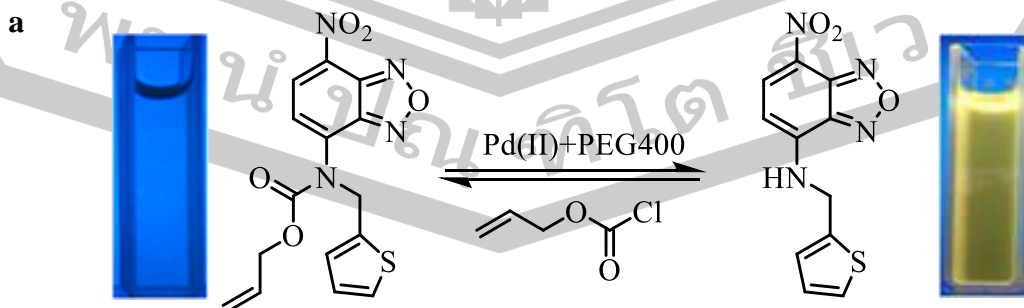






**Figure 16** (a) structures of the functionalized PEG-PS resin with the peptide sensor (P10) and (b) the fluorescent measuring of PG1-PEG-PS suspension. (c) Fluorescence response of PG1-PEG-PS (50  $\mu\text{M}$ ) in the presence of Zn(II) (1 equiv.) and additional metal ions (1 equiv.). (d) Fluorescence emission spectra of PG1-PEG-PS (50  $\mu\text{M}$ ) in the presence of (left)  $\text{Cu}^{2+}$  (50  $\mu\text{M}$ ) and EDTA (2 mM) (right)  $\text{Zn}^{2+}$  (50  $\mu\text{M}$ ) and EDTA (2 mM).

7-nitro-2,1,3-benzoxadiazole-4-allyl-*N*-(thiophen-2-ylmethyl)carbamate (**P11**) was synthesized by Z. Y. Xu and coworkers [37] (Figure 17a). **P11** displayed specific and ratiometric fluorescent responses toward palladium species (Figure 17b, c). The chemosensor showed more than 50-fold enhancement in fluorescence intensity with the presence of PEG400 and palladium because **P11** can be transformed to **P11'** under palladium-catalyzing Tsuji-Trost reaction. **P11** displayed high selectivity and sensitivity for palladium species with the detection limit of  $1.13 \times 10^{-9}$  M.





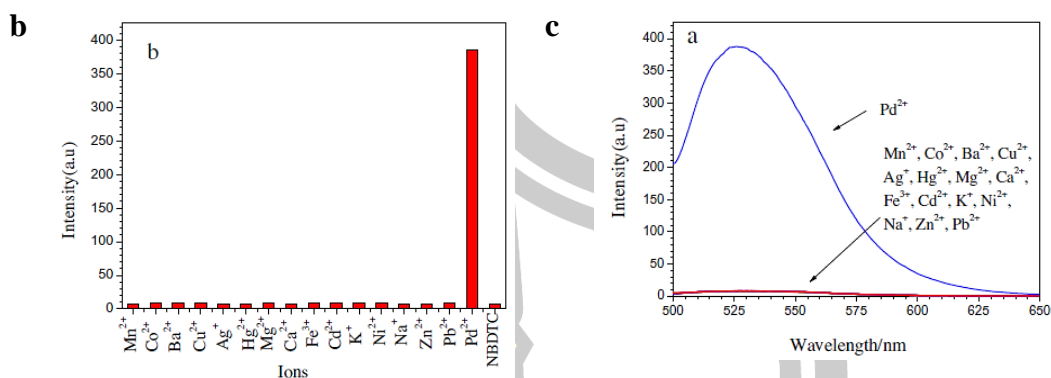


**Figure 17** (a) palladium detection based on the Tsuji–Trost reaction. (b) of **P11** fluorescent spectra of **P11** (1 μM) in the presence of various metal ions (1 μM) in PEG400 solutions incubated for 2 h at 55°C. (c) the emission intensity at 526 nm.

In 2017, G. Li and coworkers [38] developed a water-soluble polymer based colorimetric chemosensor, **P12**, which showed real-time and turn-on colorimetric responses to Cu<sup>2+</sup> ions with high selectivity and sensitivity over other competitive ions in pure aqueous solution (Figure 18b, c). The detection limit ( $2.5 \times 10^{-8}$  M) of **P12** for Cu<sup>2+</sup> fell sufficiently below the safe limit of Cu<sup>2+</sup> in drinking water (20 mM). Furthermore, the absorption intensity of the **P12**-Cu<sup>2+</sup> complex remained unaffected over a wide pH range of 4–10 (Figure 18d), and **P12** could be applied to analyse Cu<sup>2+</sup> in real environmental samples within the wide pH range. In addition, the response to Cu<sup>2+</sup> ions has been found to be reversible by the EDTA-titration experiments (Figure 18e). Moreover, a test paper based on **P12** has been fabricated, which could serve as a practical colorimetric sensor for the convenient detection of Cu<sup>2+</sup> ions in real samples. Based on these results, we believe that **P12** will be an excellent prototype to develop chemosensors based on water-soluble polymers for the detection of metal ions in pure aqueous solutions.

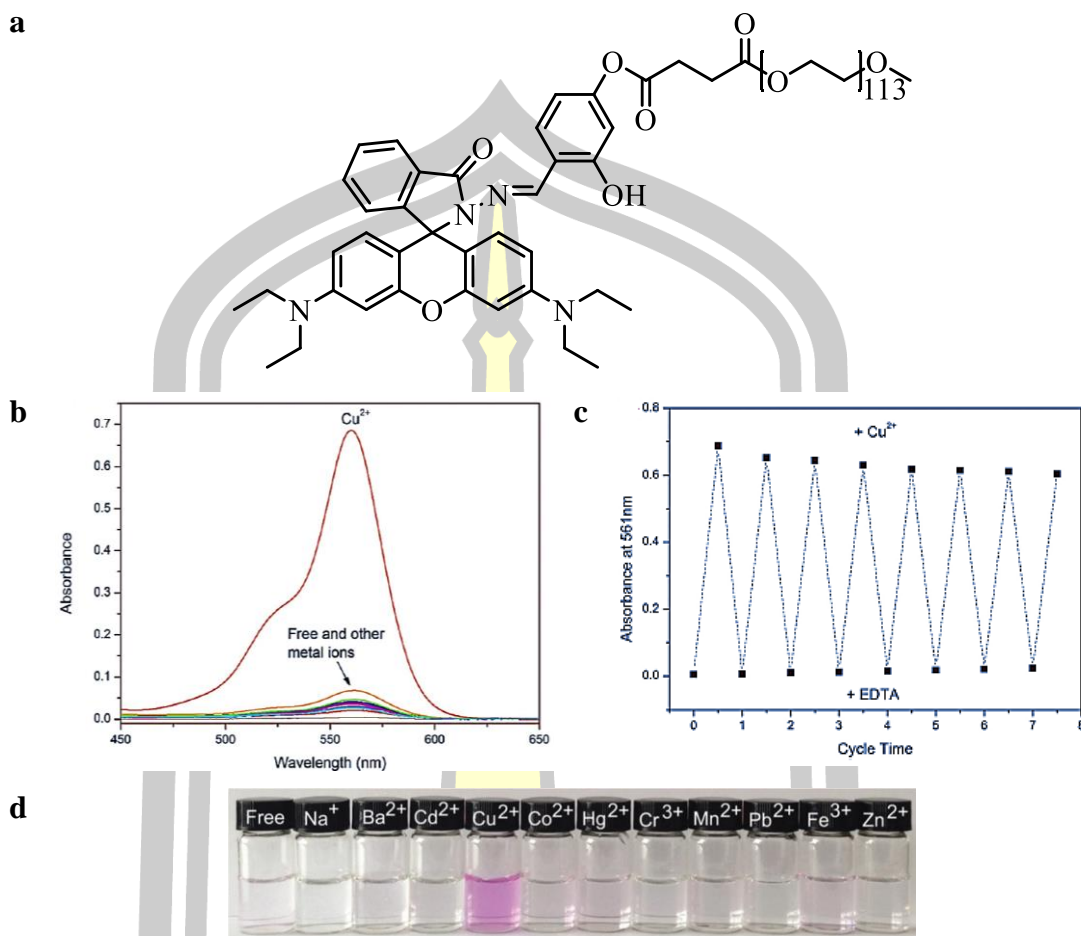


**Figure 18** (a) structure of **P12**. (b) UV-Vis absorption spectra of **P12** in aqueous solutions (10 mM) upon addition of various metal ions. (c) reversible changes in absorbance intensity of **P12** (10 mM) at 561 nm upon alternate addition of  $\text{Cu}^{2+}$  and EDTA ions. (d) colorimetric changes of **P12** in aqueous solutions (10 mM) upon addition of various metal ions.

The water-soluble fluorescent sensor **P13** for mercury ion has been designed and synthesized by W. Du and coworkers in 2017 [39]. This **P13** display 1:1 complex formation with mercury ion (Figure 19a), which could be monitored by the spectral changes as well as color changes. It showed high sensitivity and selectivity for  $\text{Hg}^{2+}$  recognition in comparison to other metal ions in pure aqueous solution (Figure 19b). Especially, it should be noted that these fluorescence experiments were performed in a pure aqueous solution (Figure 19c), which is different from other probes determined in organic solvent or mixed solutions. Based on these conditions, this sensor show a great

potential in the detection and analysis of diverse mercury-related cases in biological, medical and environmental areas.

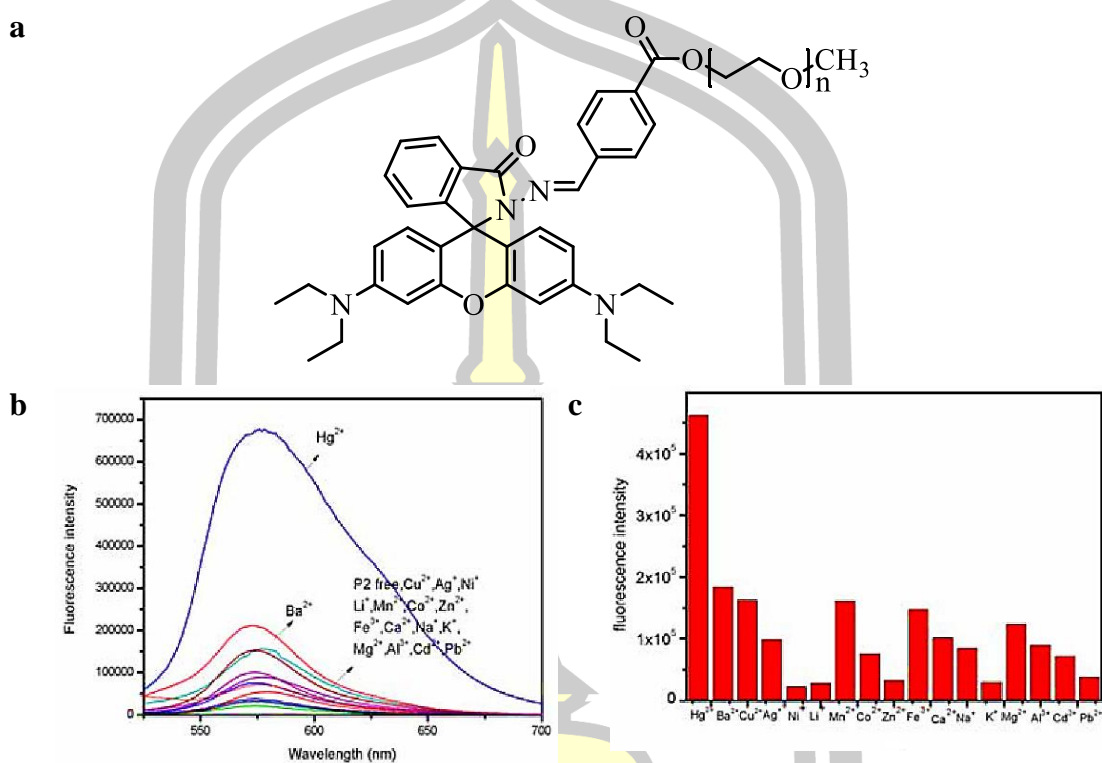


**Figure 19** (a) structure of **P13**. (b) Fluorescence spectra of **P13** (10  $\mu\text{mol/L}$ ) in aqueous solution the presence of 10 equiv. of various metal ions. (c) fluorescence intensity of **P13** (10  $\mu\text{mol/L}$ ) in aqueous solution the presence of 10 equiv. of various metal ions.

literature review in topic 2.4 represents performance of PEG for establish a sensor. They increase a polarity of sensor which effect to sensitivity and sensitivity. Most systems consist of water which is a simulation in real examples.

### 2.3 Rhodamine base chemosensor

Rhodamine, a classical fluorescent dye, has been widely used as a probe for metal ions detection. Because they have a high selectivity and high sensitivity with metal ions. However, it also can detect  $\text{H}^+$ . Therefore, Rhodamine was used for pH detection.

In 2010, Best Q. A. and coworkers [40] synthesized Rhodamine derivative (**P14**, **P15**) for the fluorescence based detection of pH. **P14**, **P15** exhibited “off-on” quenching as solutions went from basic to acidic, which was characterized as a spirocyclic structure by UV-Vis and NMR. **P14** has been proposed to be the most biologically relevant probe, because of its dynamic response in the “acidic window” (Figure 20c). **P15** has interesting photophysical behavior and is related to a PET-type mechanism (Figure 20d); further spectroscopic interrogation is underway.

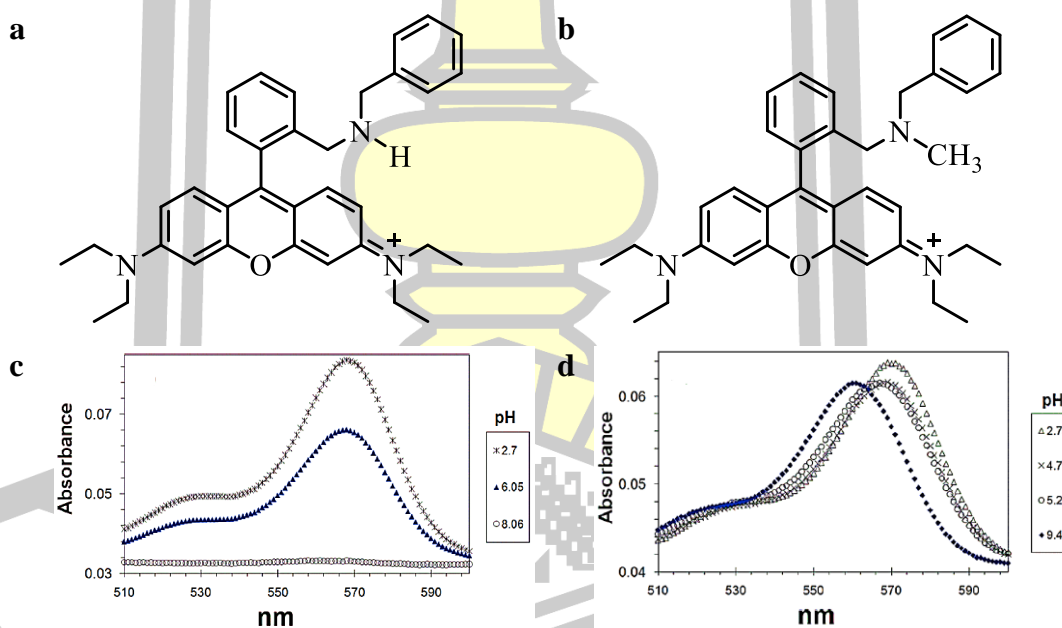


**Figure 20** (a) structure of **P14**, (b) structure of **P15**, Absorbance spectra (c) **P14** and (d) **P15** at various values of pH. Measured using  $0.37 \mu\text{M}$  solutions in 15% EtOH/ $\text{H}_2\text{O}$  (v/v).

In 2013, Hu Z. Q. and coworker [41] were fabricated a highly sensitive fluorescent acidic pH probe based on Rhodamine B-2-aminobutenedioate conjugate. When the  $H^+$  concentration falls within the pH range of 4.0-6.5 (Figure 21c), the spirolactam unit of **P16** was opened, which resulted in the dramatic enhancement of both fluorescence and absorbance intensity as well as the color change of the solution (Figure 21b). Background metal ions showed small or no interference with the detection of  $H^+$ . Confocal laser scanning microscopy experiments showed that **P16** can be applied to detect acidic pH variations in living cells with a turn-on signal.

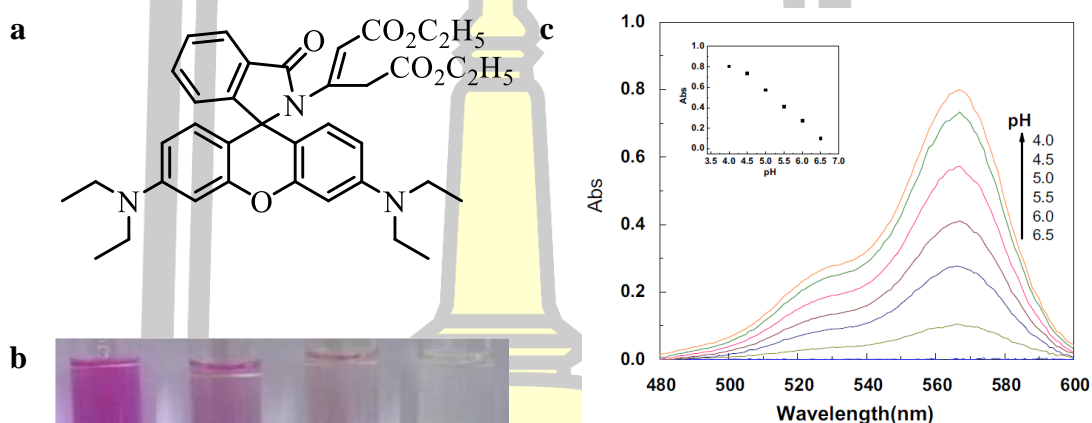


**Figure 21** (a) structure of **P16**. (b) changes of color of RBDAB in MeCN/water (10/90, v/v) buffer solution (0.1 M citrate buffer solutions) with different pH. The pH from left to right is 4.0, 5.0, 6.0 and 7.0. (c) and UV-Vis absorption spectra of 10 mM **P16** at different pH.

In 2013, Lv H. S. coworkers [42] were synthesized a new pH fluorescent probe (**P17**), based on structural changes of Rhodamine dye at different pH values. The **P17** exhibits high selectivity, high sensitivity and quick response to acidic pH (Figure 22 (b)), as well as low cytotoxicity, excellent photostability, reversibility and cell membrane permeability. Fluorescence intensity at 584 nm was increased more than 150-fold within pH range 7.51-3.53 (Figure 22c). This probe has pKa value 4.71, which is valuable for studying acidic organelles. Because of its long absorption and emission

wavelengths, **P17** can avoid associated cell damage. The probe can selectively stain lysosomes and monitor lysosomal pH changes in living cells.

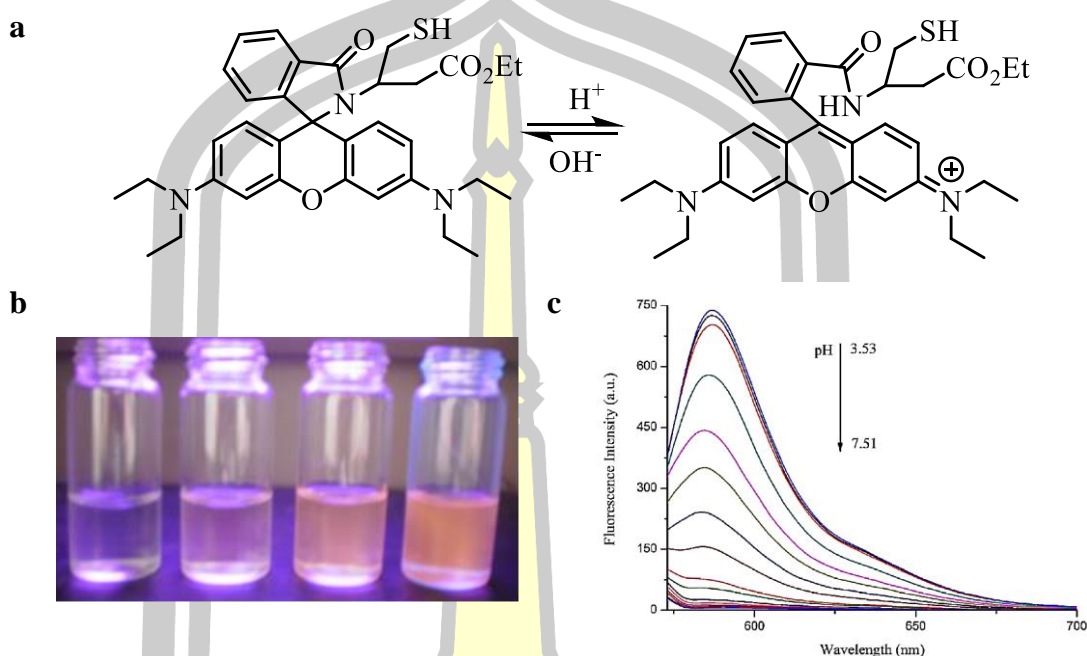


**Figure 22** (a) pH sensing mechanism of **P18**. (b) Fluorescence images of RCE in buffers of various pH values under ultraviolet light (365 nm). From left to right: 7.51, 5.25, 4.76, 4.01. (c) fluorescence spectra of **P18** (10  $\mu$ M) in buffer at various pH values.

In 2015, Tan J. L coworkers [43] synthesized and characterized a “off–on” colorimetric and fluorescent Rhodamine analogue, and used to monitor extreme acidity (below pH 3.5) via the photophysical response to pH (Figure 23d). The colorless spirocyclic structure at high pH ( $pH > 7.0$ ) opened to the colored and highly fluorescent form at very low pH ( $pH < 3.0$ ) (Figure 23b, c). This sensitive pH probe was characterized with short response time, good reversibility and no interaction with interfering metal ions, and the quantitative relationship between the fluorescence intensity and pH value was consistent with the equilibrium equation

$$pH = pK_a - \log[(I_{\max} - I)/(I - I_{\min})].$$



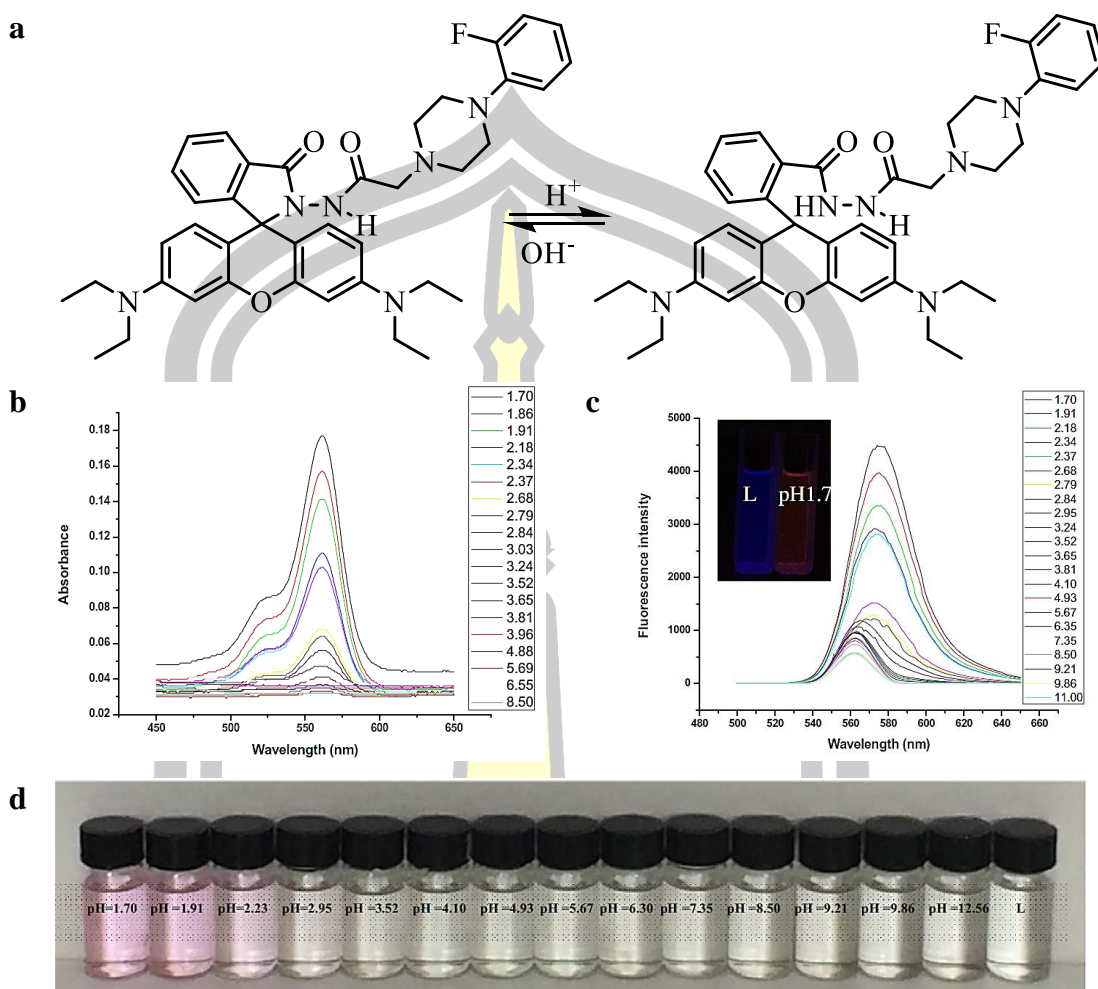


**Figure 23** (a) pH sensing mechanism of **P19**. (b) Absorption spectra of **P19** (25  $\mu$ M) in solution (buffer-EtOH, v/v = 1:1) with different pH. (c) The fluorescence spectrum of **P19** (25  $\mu$ M) in solution (buffer-EtOH, v/v = 1:1) with different pH,  $\lambda_{ex}$  = 562 nm. (d) The color change of **P19** (25  $\mu$ M, buffer-EtOH, v:v = 1:1) at different pH.

Recently, D. Lee coworkers [44] developed a highly sensitive and selective pH sensor, Rhodamine-based fluorescence dye **P20**. The fluorescent emission of **P20** at 588 nm increased with the pH decreasing from pH 7.0-4.0 (Figure 24c, d) due to the ring-opening of spirolactam by  $H^+$ . **P20** exhibited good water solubility, high quantum yield, and fast response to pH changes. Moreover, **P20** can stain lysosomes in living cells with high photostability and low cytotoxicity. Importantly, **P20** was used for monitoring pH changes in lysosomes induced by chloroquine, artesunate and dexamethasone.

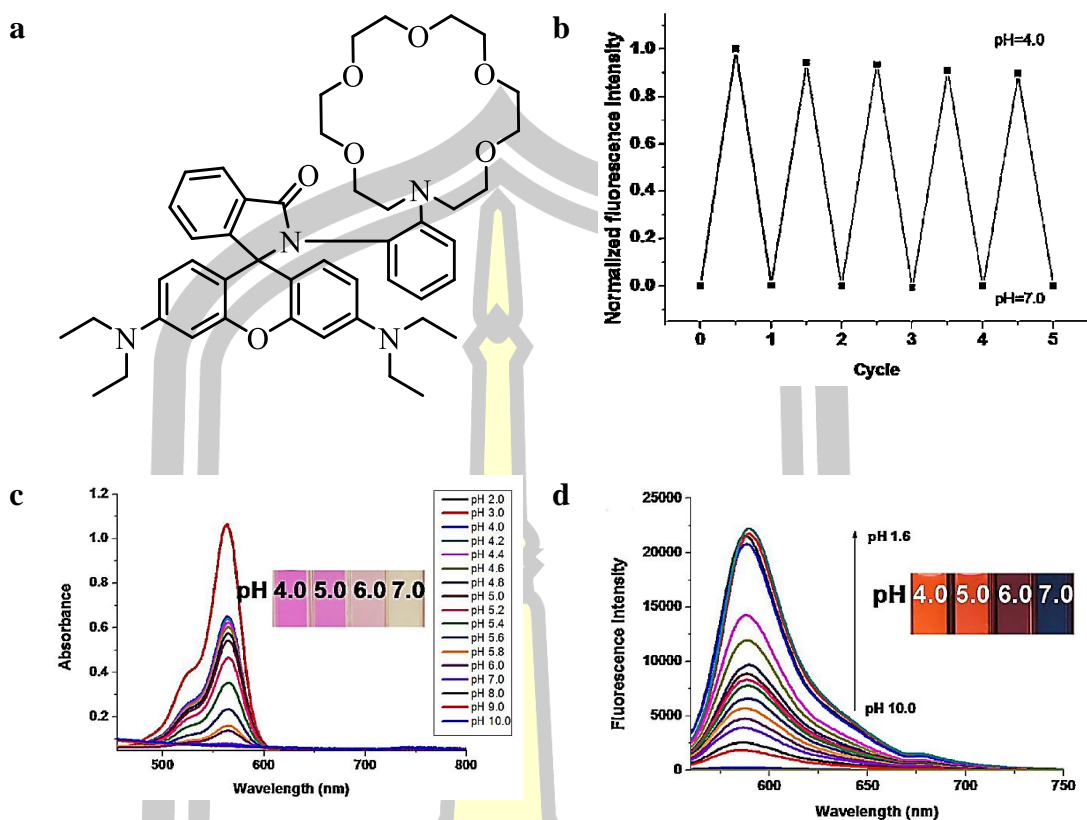


**Figure 24** (a) structure of **P20** (b) pH reversibility study of **1** between pH 4.0 and pH 7.0 ( $\lambda_{\text{ex}} = 550 \text{ nm}$ ,  $\lambda_{\text{em}} = 588 \text{ nm}$ ). (c) UV/Vis Absorption and (d) fluorescence spectra of **1** ( $10 \mu\text{M}$ ) in BR buffer solution containing 1% MeCN with different pH.

In topic 2.3 show a high performance of sensor based Rhodamine as the result of highlight of color when spirolactam ring was opened. Moreover, Rhodamine probes have a good work on specific length of pH.

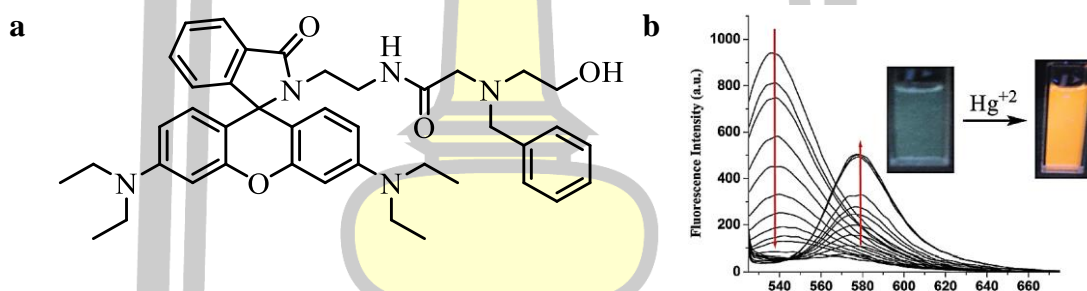
พหุ ประสิทธิภาพ



## 2.4 Metal ions sensor based Rhodamine derivative

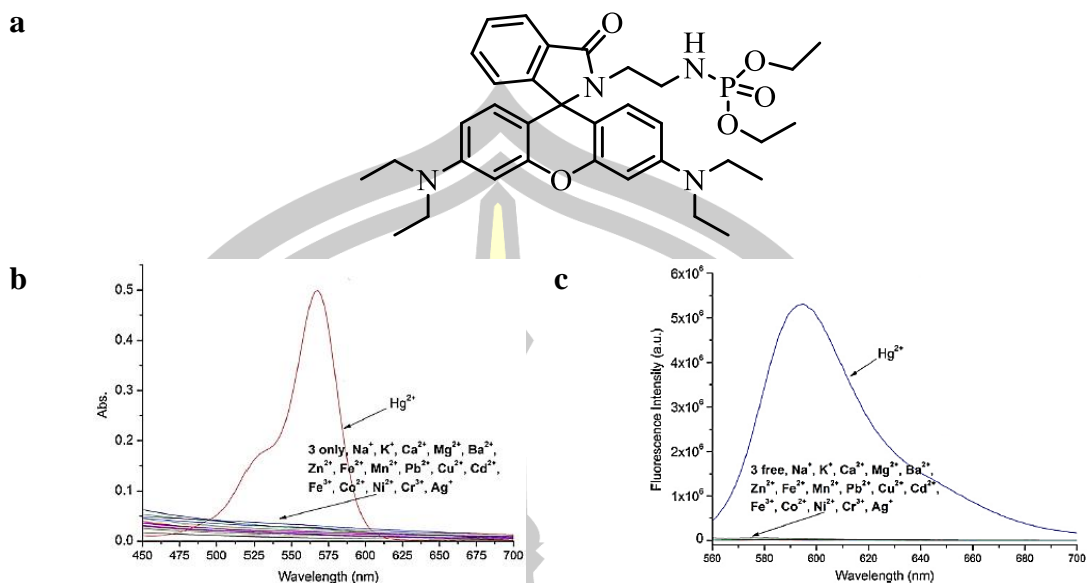
In chapter 1, we mentioned about mechanism of spirolactam ring opening of Rhodamine with metal ion. Therefore, Many research attempted to design and synthesis Rhodamine probe that can detect a metal ion or more. In topic 2.4 will show research about Rhodamine probe with metal ions detection.

Rhodamine appended tripodal (**P21**) were designed and synthesized Kumaresh G. coworkers [45] in 2012. The receptor selectively recognizes  $\text{Hg}^{2+}$  ions in  $\text{CH}_3\text{CN}$ –water (4:1, v/v; 10  $\mu\text{M}$  tris HCl buffer, pH 7.0) by displaying a ratiometric change in emission (Figure 25b). Additionally, the visual detection is possible by a sharp change in color. The receptor shows in vitro detection of  $\text{Hg}^{2+}$  ions in human cervical cancer (HeLa) cells.



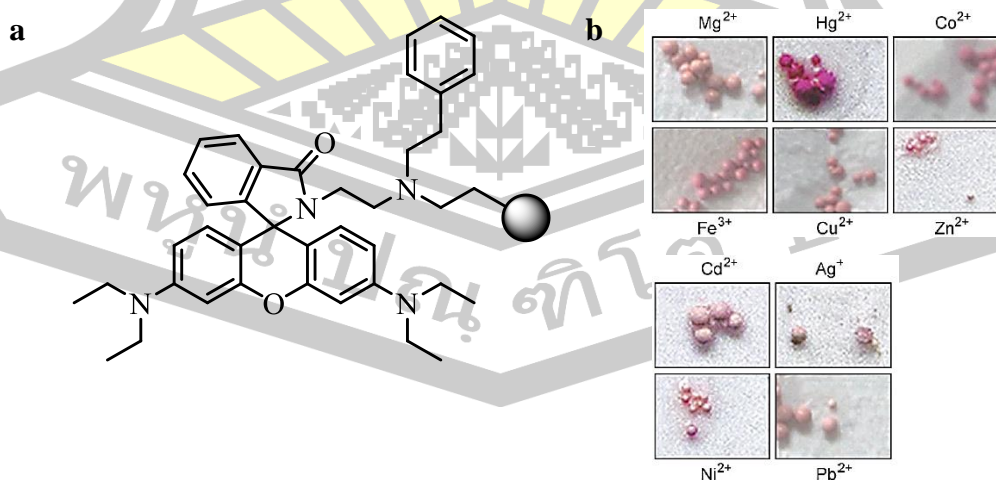
**Figure 25** (a) structure of **P21**, (b) fluorescence titration spectra of **1** ( $c = 4.41 \times 10^{-5}$  M) in  $\text{CH}_3\text{CN}$ –water (4:1, v/v; 10  $\mu\text{M}$  tris HCl buffer, pH 7.0) upon addition of  $\text{Hg}^{2+}$ ; Inset: Color change of the receptor solution under illumination of UV light.

In 2013, Z. Di coworkers [46] designed and synthesized Rhodamine-based fluorescent (**P22**), which contained a hydrophilic group, were designed as fluoroionophores and chromophores (Figure 26a) for the optical detection of  $\text{Hg}^{2+}$  ions in water with a broad pH span (3–10). As expected, it exhibited high selectivity and sensitivity for  $\text{Hg}^{2+}$  over other commonly coexistent metal ions in water (Figure 26b, c). Its selectivity was excellent, and the detection limit was measured to be 0.2 ppm. The significant changes in the fluorescence color could be used for naked-eye detection.



**Figure 26** (a) structure of P22, (b) Absorption spectra (c) fluorescence spectra of P22 (10  $\mu$ M) in water with the presence of 10 equiv. of various species.

In 2013, G. Kumaresh coworkers [47] synthesized Rhodamine-based recognizes  $\text{Hg}^{2+}$  and  $\text{Cu}^{2+}$  ions in aqueous  $\text{CH}_3\text{CN}$ , but when immobilized onto Merrifield resin to give **P23**, this sensor system selectively detects  $\text{Hg}^{2+}$  ions over a series of other metal cations in water (Figure 27c, d). The detection can be performed colorimetrically and fluorimetrically. The ensemble **P23**- $\text{Hg}^{2+}$  can also distinguish dl-homocysteine from l-cysteine in water by both analytical methods.



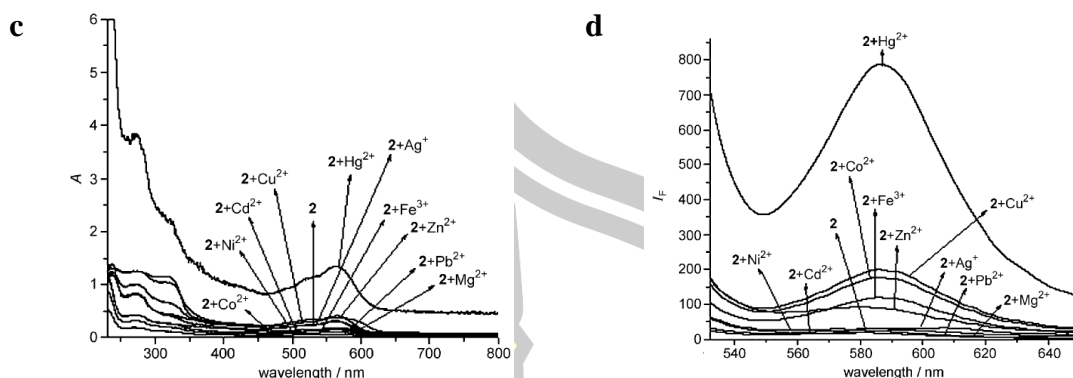


**Figure 27** (a) structure of **P23**, (b) color of **P23** in the presence of the specified metal ions ( $c=8.25 \times 10^{-4}$  M) in water. (c) Absorption spectra and (d) fluorescence spectrum of **P23** after keeping the beads in contact with aqueous solutions of different metal salt.

In 2013, Y. Fanyong and coworkers [48] designed and prepared **P24** from Rhodamine B and Phthalimido Gly. The sensing behavior of **P24** was studied by UV-Vis and fluorescence spectroscopy. **P24** showed excellent high selectivity and sensitivity towards  $\text{Hg}^{2+}$  over commonly coexistent metal ions in neutral solution (Figure 28b, c), which could be attributed to the  $\text{Hg}^{2+}$ -triggered ring opening of the spirolactam of the Rhodamine moiety and the formation of a 1:1 **P24**- $\text{Hg}^{2+}$  complex (Figure 28d). The limit of detection (LOD) based on  $3\delta_{\text{blank}}/k$  was calculated to be  $2.8 \times 10^{-8}$  M, as well as an excellent linear relationship with the concentration of  $\text{Hg}^{2+}$  in the range from  $0.1 \times 10^{-6}$  to  $1.0 \times 10^{-6}$  mol/L ( $R^2 = 0.98927$ ). In addition, the effects of pH, coexisting metal ions, and the reversibility were investigated in detail.

พหุ ประสิทธิภาพ

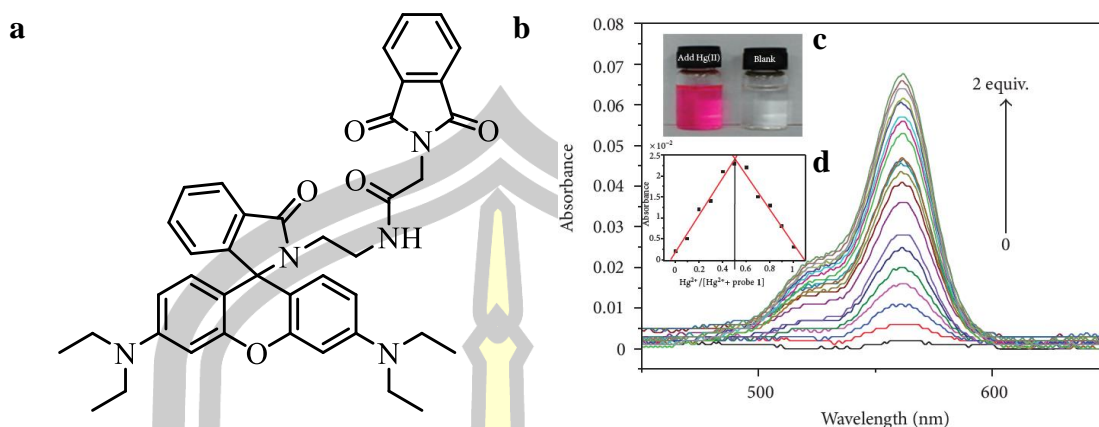


**Figure 28** (a) structure of **P24**, (b) UV-Vis absorption spectra of probe 1 (10.0  $\mu\text{M}$ ) in the presence of  $\text{Hg}^{2+}$  (0-2 equiv.) in  $\text{C}_2\text{H}_5\text{OH}$ -water (4:6, v/v) buffered with HEPES pH = 7.0 solution at room temperature. Inset: (c) showing the change in the color of **P24** (10  $\mu\text{M}$ ) upon addition of  $\text{Hg}^{2+}$  ions (2 equiv.); (d) Job's plot for determining the stoichiometry of **P24** and  $\text{Hg}^{2+}$  ion by absorbance at 561 nm, the total concentration of  $[\text{Hg}^{2+}] + [\text{P24}]$  was 10  $\mu\text{M}$ .

In 2013, G. Kumaresh and coworkers [49] were designed and synthesized a Rhodamine-based chemosensor (**P25**) The receptor selectively recognizes  $\text{Co}^{2+}$  (Figure 29b) and  $\text{Hg}^{2+}$  ions (Figure 29c) in  $\text{CH}_3\text{CN}$ /water (4:1, v/v;  $10^{-1}$  M tris HCl buffer, pH 6.8) by showing different extents of change in emission. The disappearance of colour of mercury-ensemble of **P25** followed by appearance of distinct bluish color under UV illumination upon addition of L-cysteine distinguishes  $\text{Hg}^{2+}$  from  $\text{Co}^{2+}$  ions (inset Figure 29b). The receptor shows in vitro detection of both the ions in human cervical cancer (HeLa) cells.

พหุ ประถมศึกษา

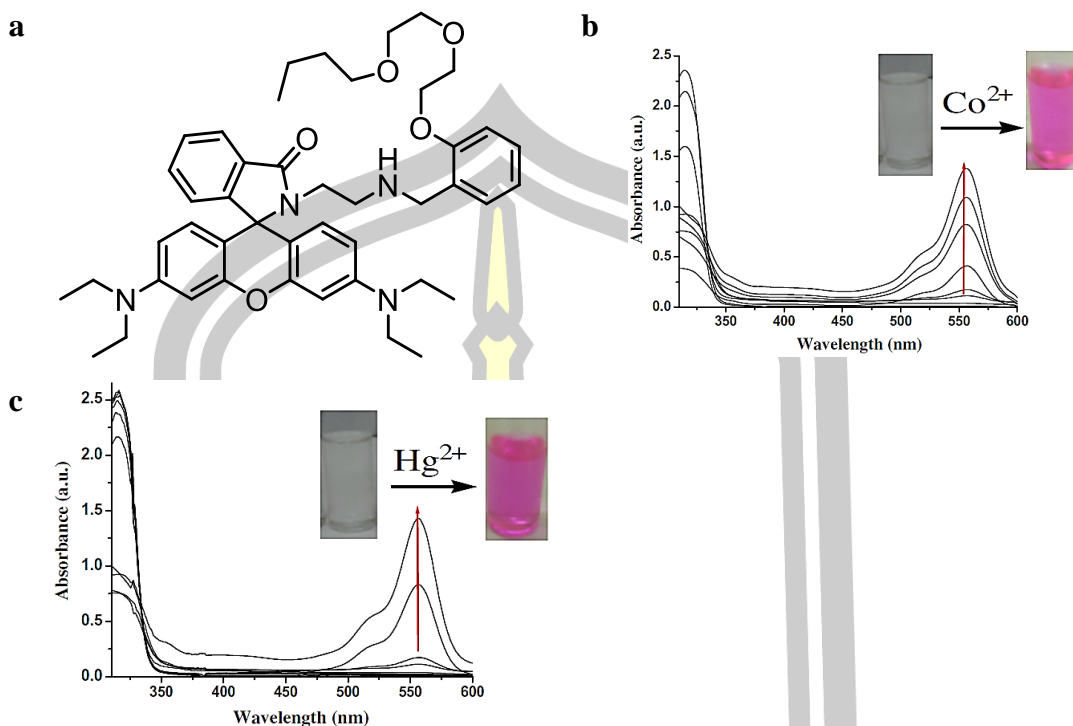


**Figure 29** (a) structure of **P25**, Absorption titration spectra of **1** ( $c = 2.25 \times 10^{-4}$  M) in  $\text{CH}_3\text{CN}/\text{H}_2\text{O}$  (4:1, v/v; 10 IM tris HCl buffer; pH 6.8) upon addition of (b)  $\text{Co}^{2+}$ , and (c)  $\text{Hg}^{2+}$ .

In 2013, B. Jeane and coworkers [50] synthesized fluorescent sensor (**P25**) for iron. Its electronic absorption spectrum in ethanol has bands at 410 ( $\epsilon = 500 \text{ cm}^{-1} \text{ mol}^{-1} \text{ L}$ ), 316 ( $\epsilon = 14 \times 10^3 \text{ cm}^{-1} \text{ mol}^{-1} \text{ L}$ ), and 272 nm ( $\epsilon = 32 \times 10^3 \text{ cm}^{-1} \text{ mol}^{-1} \text{ L}$ ), and it is pH sensitive (Figure 30e) with two pKa values (1.2 and 2.8). It reacts promptly with  $\text{Fe}^{3+}$ , with a pseudo-first order rate constant of  $1 \times 10^3 \text{ s}^{-1}$ , with an equilibrium constant of  $1.3 \times 10^6 \text{ mol}^{-1} \text{ L}$ , forming a violet complex ( $\lambda_{\text{max}} = 540 \text{ nm}$ ) with a fluorescent emission at 582 nm, with a higher sensitivity and selectivity compared to those of  $\text{Fe}^{2+}$ ,  $\text{Ba}^{2+}$ ,  $\text{Al}^{3+}$ ,  $\text{K}^+$ ,  $\text{Ca}^{2+}$ ,  $\text{Ni}^{2+}$ ,  $\text{Co}^{2+}$ ,  $\text{Cd}^{2+}$ ,  $\text{Cr}^{3+}$ ,  $\text{Hg}^{2+}$ ,  $\text{Mg}^{2+}$ ,  $\text{Mn}^{2+}$ ,  $\text{Na}^+$ , or  $\text{Cu}^{2+}$  (Figure 30d).

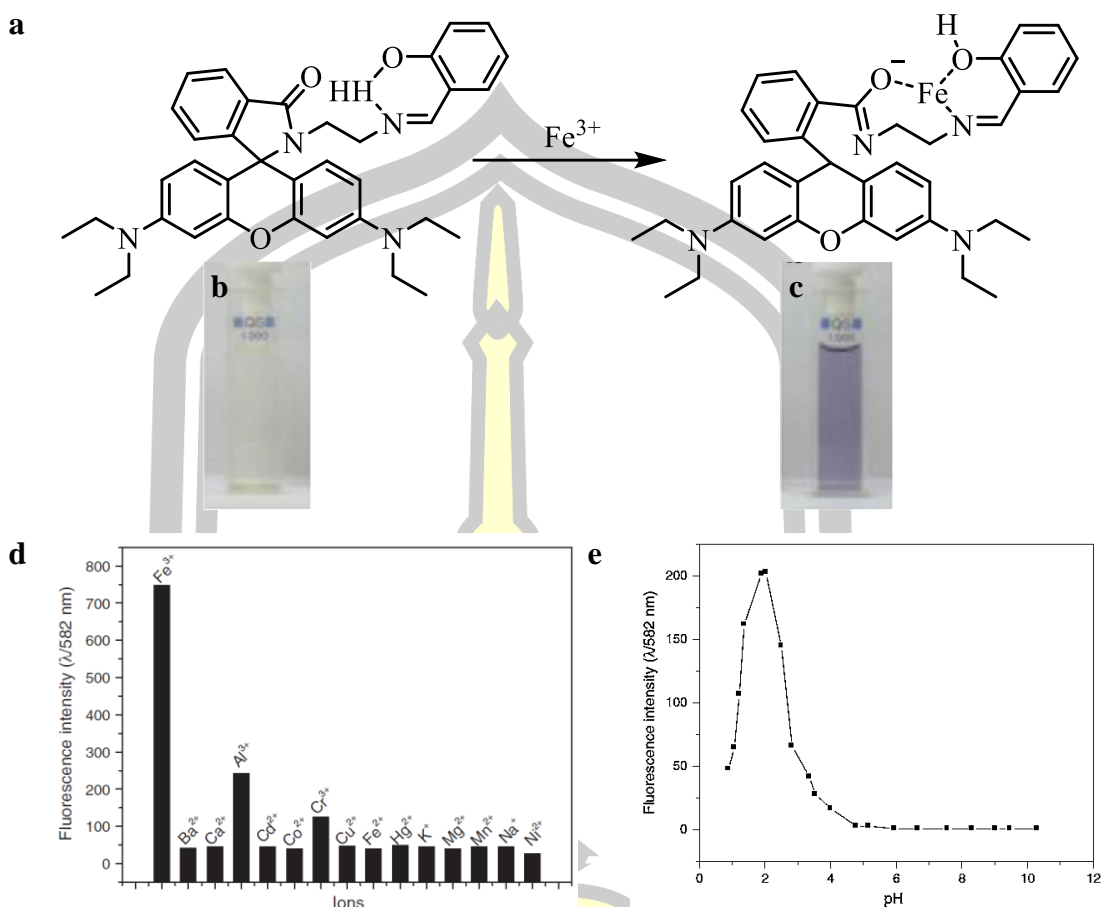


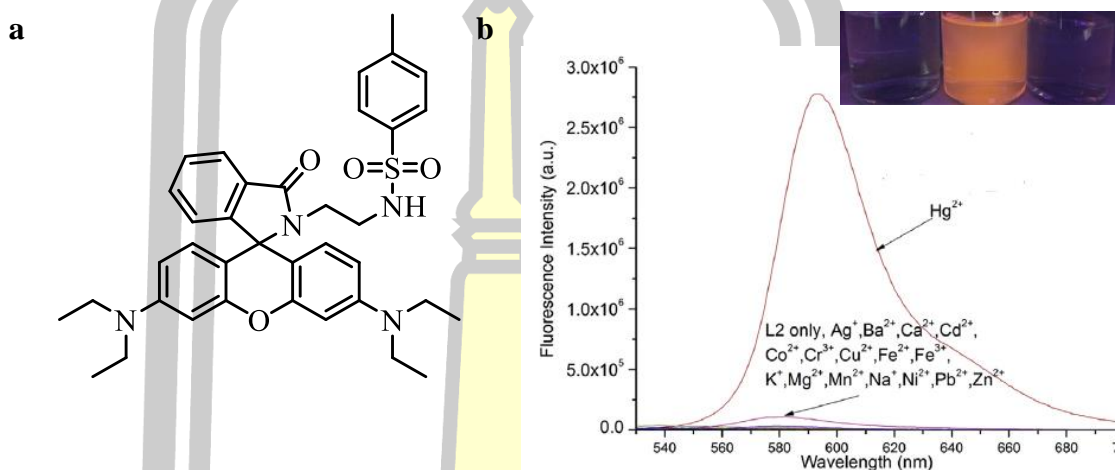
**Figure 30** (a) structure of **P25** (left) and **P25-Fe<sup>3+</sup>** complex (right). Inset: (b) **P25**- only colorless solution, and (c) **P25** plus  $\text{Fe}^{3+}$ , violet color solution, both in EtOH.

(d) Fluorescence spectra of the mixture of rhodanal ethanolic solution (1 mL of  $1.4 \times 10^{-4} \text{ mol L}^{-1}$ ) with 2.6 equivalents of various metal ion (1.4 mL of  $9.0 \times 10^{-4} \text{ mol L}^{-1}$ ) pH 7.0, 20 mM Tris-HCl buffer. (e) Effect of pH on the fluorescence intensity of rhodanal (20  $\mu\text{L}$ ,  $7.0 \times 10^{-3} \text{ mol L}^{-1}$ ) in EtOH:universal buffer (1:1, v:v) solution. Resting time of each sample before the measurement was 18 h. pH dependent fluorescence at 582 nm.

A Rhodamine-based chemodosimeter (**P26**) were synthesized by Z. Di and coworkers [51] in 2013. **P26** contained an osyl group acted as a strong electron acceptor. As expected, **P26** exhibited high selectivity and excellent sensitivity in both absorbance and fluorescence detection of  $\text{Hg}^{2+}$  in aqueous solution. The coordination of **P26** with  $\text{Hg}^{2+}$  was chemically nonreversible and it was based on the fact that  $\text{Hg}^{2+}$  exhibited a

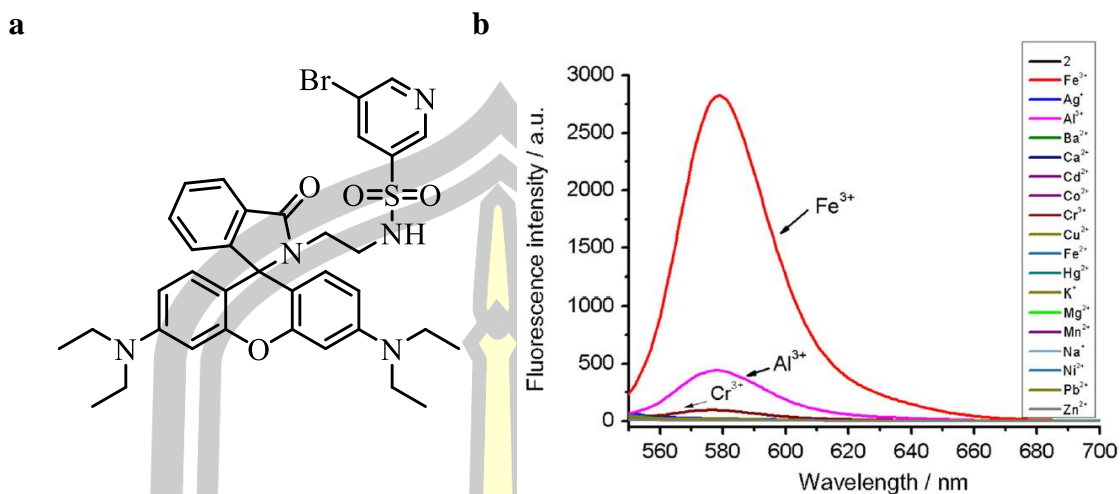


strong thiophilic affinity (Figure 31b). Addition of  $\text{Hg}^{2+}$  to an ethanol aqueous solution of **P26** resulted in a color change from colorless to obvious pink color, these significant changes in color could be used for naked-eye detection. Furthermore, fluorescence imaging experiments of  $\text{Hg}^{2+}$  ions in living MGC803 cells demonstrated its value of practical applications in biological systems.



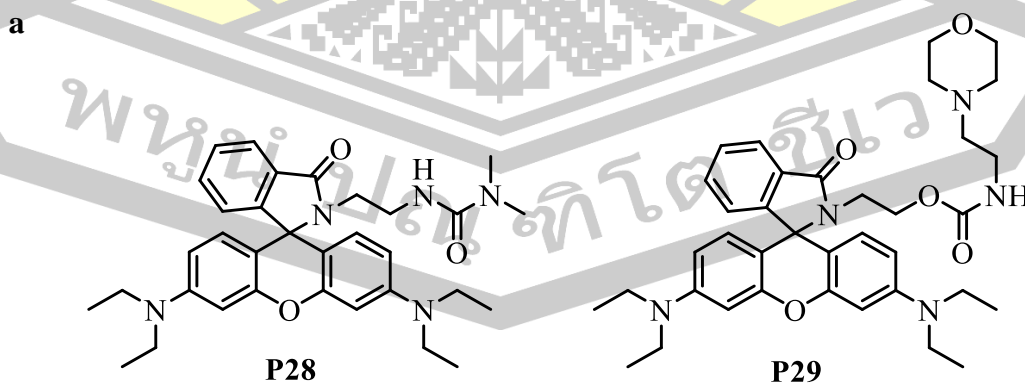
**Figure 31** (a) structure of **P26**. (b) Fluorescence spectra of L2 (10 mM) in  $\text{CH}_3\text{CH}_2\text{O}-\text{H}_2\text{O}$  (1/1, v/v) with the presence of 10 equiv. of various species Inset: fluorogenic color response of **P26** (10 mM) in  $\text{CH}_3\text{CH}_2\text{O}-\text{H}_2\text{O}$  (1/1, v/v) to  $\text{Hg}^{2+}$  (10 eq.) under UV illumination (365 nm).

In 2015, L. Yao and coworker [52] synthesized chemosensor (**P27**) which contained a strong electron-withdrawing group. As expected, the **P27** exhibited high selectivity and excellent sensitivity in both absorbance and fluorescence detection of  $\text{Fe}^{3+}$  ( $\theta$  ( $\text{CH}_3\text{OH}$ ,  $\text{H}_2\text{O}$ ) = 3/7, 1 mM Tris-HCl buffer, pH = 7.40) (Figure 32b). Upon addition of  $\text{Fe}^{3+}$ , the solution of the **P27** resulted in a color change from colorless to obvious pink. These significant changes in color could be used for naked-eye detection. Furthermore, fluorescence imaging experiments of  $\text{Fe}^{3+}$  ions in living MGC-803 cells demonstrated its value of practical applications in biological systems.



**Figure 32** (a) structure of **P27**. (b) fluorescence spectra of **2** (10  $\mu$ M) in  $\Theta$  ( $\text{CH}_3\text{OH}$ ,  $\text{H}_2\text{O}$ ) = 3/7 (1 mM Tris-HCl buffer, pH = 7.40) solution with the presence of 10 equiv. of various species.

Two low cytotoxic fluorescence probes (**P28** and **P29** were synthesized by J. Cuicui and coworkers in 2015 [53]). **P28** and **P29** exhibited an excellent selectivity to  $\text{Fe}^{3+}$  (Figure 33b, c, d), which was not disturbed by  $\text{Ag}^+$ ,  $\text{Li}^+$ ,  $\text{K}^+$ ,  $\text{Na}^+$ ,  $\text{NH}_4^+$ ,  $\text{Fe}^{2+}$ ,  $\text{Pb}^{2+}$ ,  $\text{Ba}^{2+}$ ,  $\text{Cd}^{2+}$ ,  $\text{Ni}^{2+}$ ,  $\text{Co}^{2+}$ ,  $\text{Mn}^{2+}$ ,  $\text{Zn}^{2+}$ ,  $\text{Mg}^{2+}$ ,  $\text{Hg}^{2+}$ ,  $\text{Ca}^{2+}$ ,  $\text{Cu}^{2+}$ ,  $\text{Ce}^{3+}$ ,  $\text{AcO}^-$ ,  $\text{Br}^-$ ,  $\text{Cl}^-$ ,  $\text{HPO}_4^{2-}$ ,  $\text{HSO}_3^-$ ,  $\text{I}^-$ ,  $\text{NO}_3^-$ ,  $\text{S}_2\text{O}_3^{2-}$ ,  $\text{SO}_3^{2-}$  and  $\text{SO}_4^{2-}$  ions. The detection limits were  $1.8 \times 10^{-7}$  M for **P28** and  $5.60 \times 10^{-7}$  M for **P29**, respectively. 1:1 stoichiometry and 1:2 stoichiometry were the most likely recognition mode of **P28** or **P29** towards  $\text{Fe}^{3+}$ , and the corresponding OFF–ON fluorescence mechanisms of **P28** and **P29** were proposed.





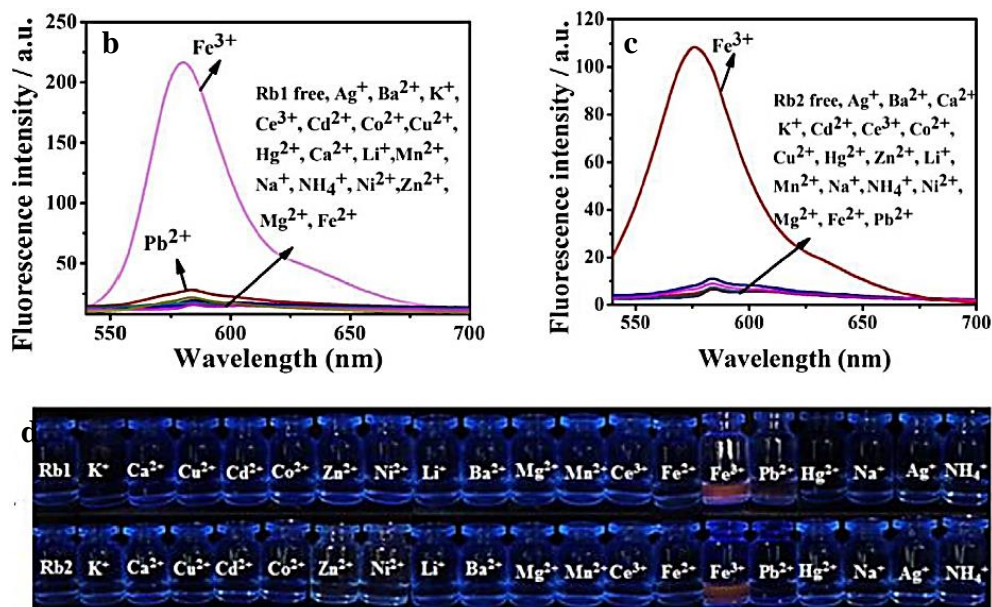


**Figure 33** (a) structure of **P28** and **P29**. Fluorescence spectra of **P28** (b) and **P29** (c) (10 μM) in EtOH/H<sub>2</sub>O (8:2, v/v) upon addition of 10 equiv Ag<sup>+</sup>, Li<sup>+</sup>, K<sup>+</sup>, Fe<sup>2+</sup>, Pb<sup>2+</sup>, Ba<sup>2+</sup>, Cd<sup>2+</sup>, Ce<sup>3+</sup>, Ni<sup>2+</sup>, Co<sup>2+</sup>, Mn<sup>2+</sup>, Fe<sup>3+</sup>, Zn<sup>2+</sup>, Mg<sup>2+</sup>, Hg<sup>2+</sup>, NH<sub>4</sub><sup>+</sup>, Ca<sup>2+</sup>, Cu<sup>2+</sup>, Na<sup>+</sup>; (d) The color changes of **P28** and **P29** (100 μM) in the presence of different metal cations (2 eq) under UV light (365 nm).

In 2015, S. Pailin and coworker [54] synthesized Rhodamine-alkyne conjugate (**P30**) for selective detection of Au<sup>3+</sup> in a reversible manner. Rhodamine was coupled with *o*-phenylenediamine bearing a propargyl moiety. **P30** displayed high selectivity and sensitivity toward Au<sup>3+</sup> with a 148-fold “turn-on” fluorescence response in EtOH-H<sub>2</sub>O (1:1 v/v) (Figure 24b). The stoichiometry of the chemosensor and Au<sup>3+</sup> was 1:1 based on the Job plot analysis with the detection limit of 10.5 nM. The chemosensor is membrane permeable and capable of monitoring Au<sup>3+</sup> in cultured HeLa cells.

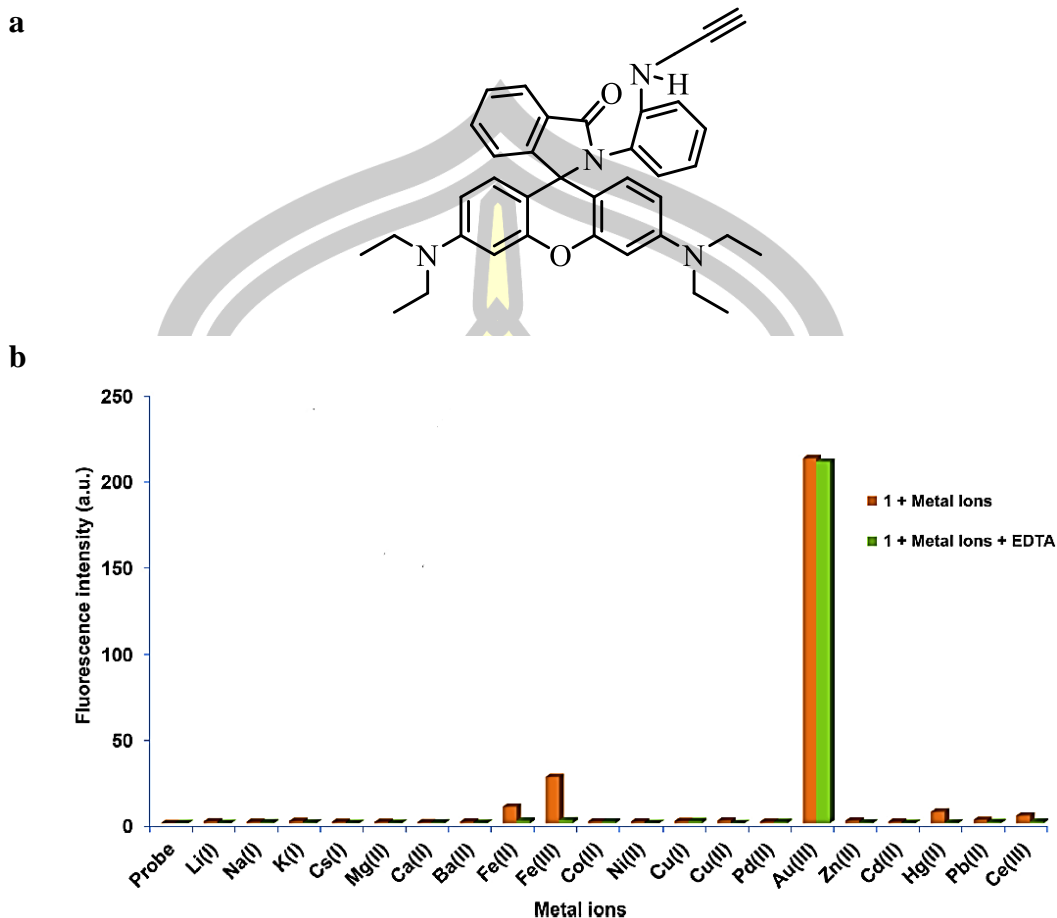


**Figure 34** (a) structure of **P30**. (b) Selectivity of **P30** toward  $\text{Au}^{3+}$  among various metal ions. Solutions of **P30** (60  $\mu\text{M}$ , orange bars) with metal ions (1 equiv.) in EtOH- $\text{H}_2\text{O}$  (1:1, v/v). Solutions of **P30** (60  $\mu\text{M}$ , green bars) with various metal ions (1 equiv.) in EtOH- $\text{H}_2\text{O}$  (1:1, v/v) and EDTA (1 equiv.). Upon the addition of  $\text{Au}^{3+}$ , the colorless solution of **P30** changes to pink and a strong fluorescence emission is observed.

In topic 2.4 show a high performance of metal ions detection by Rhodamine probe. It can detect one or more metal ions that high selectivity and sensitivity. Moreover, some sensors can reuse by added chelating agent. This literature review is being guide for a research in further.

## CHAPTER 3

### MATERIALS AND METHODS

#### 3.1 Materials

##### 3.1.1 Instrumentals

<sup>1</sup>H-NMR was measured with a Varian 400 MHz spectrometer in CDCl<sub>3</sub> and DMSO-*d*<sub>6</sub> with TMS as internal reference. High resolution mass spectra (HRMS) was measure on a Biflex Bruker Mass spectrometer at Department of Chemistry, Chulalongkorn University. Fluorescence spectra in solution was measured with a Perkin Elmer LS 50B and absorbance spectra were recorded with a Perkin Elmer Lambda 25 UV/Vis spectrometer at Department of Chemistry, Maha Sarakham University. Solid state fluorescence was measured on Fluoromax-4 at Rajabhat Maha Sarakham University. FT-IR spectra were recorded with a Bruker Tensor 27 FT-IR. Scanning Electron Microscopy (SEM) was performed with a Zeiss (LEO) 1450VP at Faculty of Science, Khon Kaen University. The pH value was adjusted with a Metrohm 713 pH Meter.

##### 3.1.2 Chemicals

**Table 1** list of chemicals and reagents used in this work.

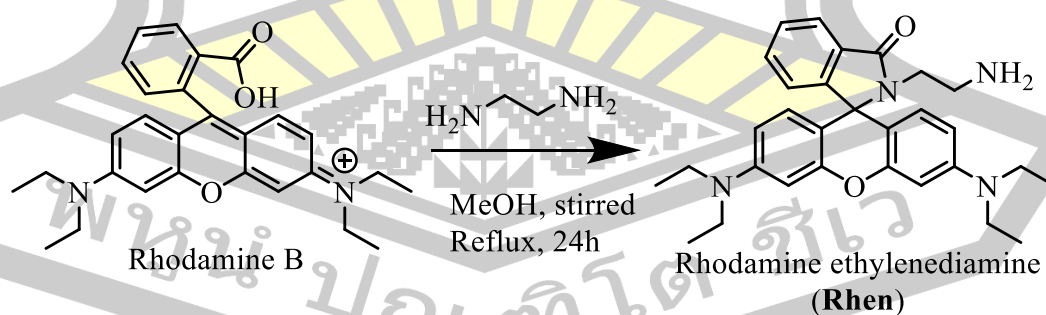
Chemical	Formula	Grade	Company
1,3-cyclohexanedicarboxylic acid	C <sub>8</sub> H <sub>12</sub> O <sub>2</sub>	Reagent	Sigma Aldrich
1,4-cyclohexanedicarboxylic acid	C <sub>8</sub> H <sub>12</sub> O <sub>2</sub>	Reagent	Acros
4-Dimethylaminopyridine	C <sub>7</sub> H <sub>10</sub> N <sub>2</sub>	Reagent	Fluka
Chloroform	CHCl <sub>3</sub>	AR	BDH Prolabo
Dichloromethane	CH <sub>2</sub> Cl <sub>2</sub>	AR	Merck
Dimethyl sulfoxide	C <sub>2</sub> H <sub>6</sub> SO	AR	Merck
Ethanol	C <sub>2</sub> H <sub>5</sub> OH	AR	BDH Prolabo
Ethyl acetate	C <sub>4</sub> H <sub>8</sub> O <sub>2</sub>	Commercial	Zen Point
Ethylenediamine	C <sub>2</sub> H <sub>8</sub> N <sub>2</sub>	Commercial	Carlo Erba
Ethylenediamine	C <sub>2</sub> H <sub>8</sub> N <sub>2</sub>	Commercial	Carlo Erba

**Table 1** list of chemical and reagent used in this work (cont.).

Hexane	$C_6H_{14}$	Commercial	Zen Point
Methanol	$CH_3OH$	AR	BDH Prolabo
<i>N</i> -(3-Dimethylaminopropyl)- <i>N'</i> -ethylcarbodiimide hydrochloride	$C_8H_{17}N_3 \cdot HCl$	Reagent	Fluka
<i>N,N'</i> -Dicyclohexylcarbodiimide	$C_{13}H_{22}N_2$	Reagent	Fluka
Polyethylene glycol (Mn~400)	$(C_2H_4O)_nOH$	-	Fluka
Polyethylene glycol (Mn~4000)	$(C_2H_4O)_nOH$	-	Ajax
Polyethylene glycol (Mn~6000)	$(C_2H_4O)_nOH$	-	Ajax
Rhodamine B	$C_{28}H_{31}ClN_2O_3$	-	Sigma Aldrich
Silica gel	$SiO_2$	-	Merck
Sodium bicarbonate	$NaHCO_3$	-	Riedel-de Haën
Sodium sulphate anhydrous	$Na_2SO_4$	Reagent	Sigma Aldrich
Succinic anhydride	$C_4H_6O_4$	-	Carlo Erba
Tetrahydrofuran	$C_4H_8O$	AR	Fisher
Toluene	$C_7H_8$	AR	Panreac

### 3.2 Methods

#### 3.2.1 Synthesis of Rhodamine ethylenediamine (**Rhen**)

**Scheme 3.1** Synthesis route of **Rhen**.

Rhodamine B ethylenediamine (**Rhen**) was synthesized by a modification of [55]. Rhodamine B (0.40 g, 0.84 mmol) was dissolved in 10 mL of MeOH and ethylenediamine diamine (0.44 mL, excess) added dropwise ethylene diamine (0.44 mL, excess). The mixture was stirred under N<sub>2</sub> gas at reflux temperature. After 24 hr, the reaction was cooled to room temperature and solvent removed by a vacuum evaporator. Crude of **Rhen** was dissolved in DCM, and washed with saturated NaHCO<sub>3</sub> 20 mL (x2), water 20 mL (x2) and saturated NaHCO<sub>3</sub> 20 mL (x2), respectively. The organic phase was dried over anhydrous Na<sub>2</sub>SO<sub>4</sub>, filtered and solvent removed by rotary evaporator under vacuum, then purified by column chromatography using 1:9:0.1 (MeOH: DCM: Triethylamine) to obtain **Rhen** (0.34 g, yield 84%). <sup>1</sup>H-NMR (400 MHz, CDCl<sub>3</sub>)  $\delta$  7.89–7.87 (m, 1H, ArH), 7.46–7.40 (m, 2H, ArH), 7.25–7.10 (m, 1H, ArH), 6.44 (s, 1H, ArH), 6.38 (s, 1H, ArH) 6.37 (s, 2H, ArH), 6.29–6.25 (m, 2H, ArH), 3.32 (q, J = 6.8 Hz, 8H, NCH<sub>2</sub>CH<sub>3</sub>), 3.23 (t, J = 6.8 Hz, 2H, NCH<sub>2</sub>CH<sub>2</sub>), 2.47 (t, J = 6.8 Hz, 2H, NCH<sub>2</sub>CH<sub>2</sub>NH<sub>2</sub>), 1.72 (s, 2H, CH<sub>2</sub>CH<sub>2</sub>NH<sub>2</sub>) and 1.16 (t, J = 7.2 Hz, 12H, NCH<sub>2</sub>CH<sub>3</sub>). ATR-FTIR  $\nu$  2968 cm<sup>-1</sup> (NH stretching), 1671 cm<sup>-1</sup> (C=O stretching) amide, 1611 and 1466 cm<sup>-1</sup> (Ar=CH).

### 3.2.2 Rhodamine-cyclohexane.

#### 3.2.2.1 Synthesis of 1,3-cyclohexane N-(Rhodamine B)-lactam-ethylene diamines (**L1**, **L2**).

The synthesise of Rhodamine-cyclohexane for sensor was optimized by various of solvents, coupling reagents, catalysts and temperatures which show in condition I-V.

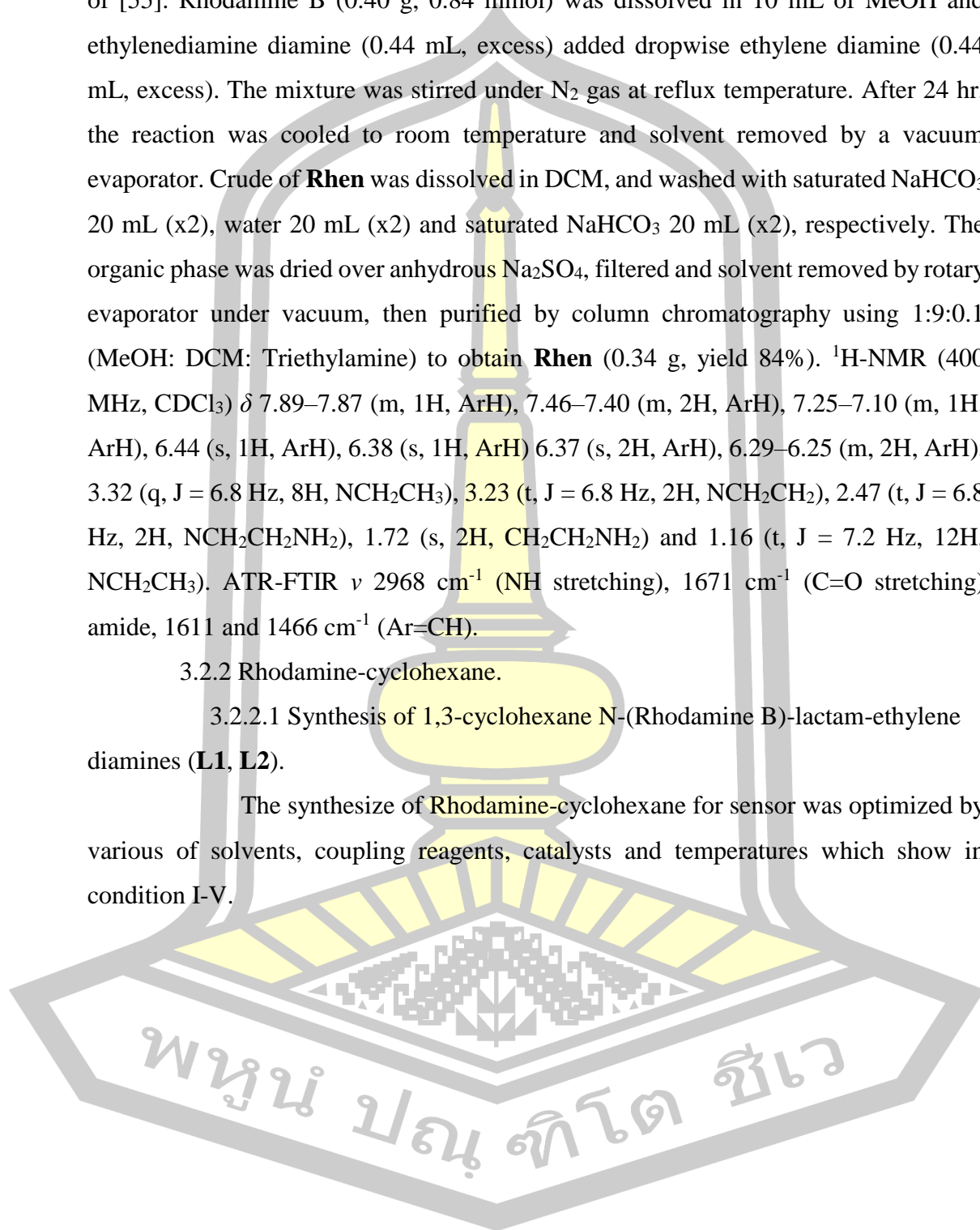


**Table 2** Condition I-V for synthesis of **L1** and **L2**.

Condition	Coupling reagent	Catalyst	Other	Temp (°C)	Time (hr)	Yield (%)
I	DCC	DMAP		rt	36	87.5
II	DCC	DMAP		60	36	86.0
III	DCC	DMAP		120	36	88.5
IV	-	-	SOCl <sub>2</sub>	rt	24	N.D.
V	-	-	SOCl <sub>2</sub> , Et <sub>3</sub> N	rt	24	N.D.
VI	-	-	SOCl <sub>2</sub> , Et <sub>3</sub> N	rt	24	N.D.
VII	-	DMAP		rt	24	N.D.
VIII	-	-	C <sub>2</sub> O <sub>2</sub> Cl <sub>2</sub> , Et <sub>3</sub> N	rt	24	N.D.
IX	DCC	DMAP	-	rt	24	76.3
X	EDC	DMAP	-	rt	24	80.8

Condition I-VIII were used DMF as a solvent.

Condition IX and X were used THF as a solvent.

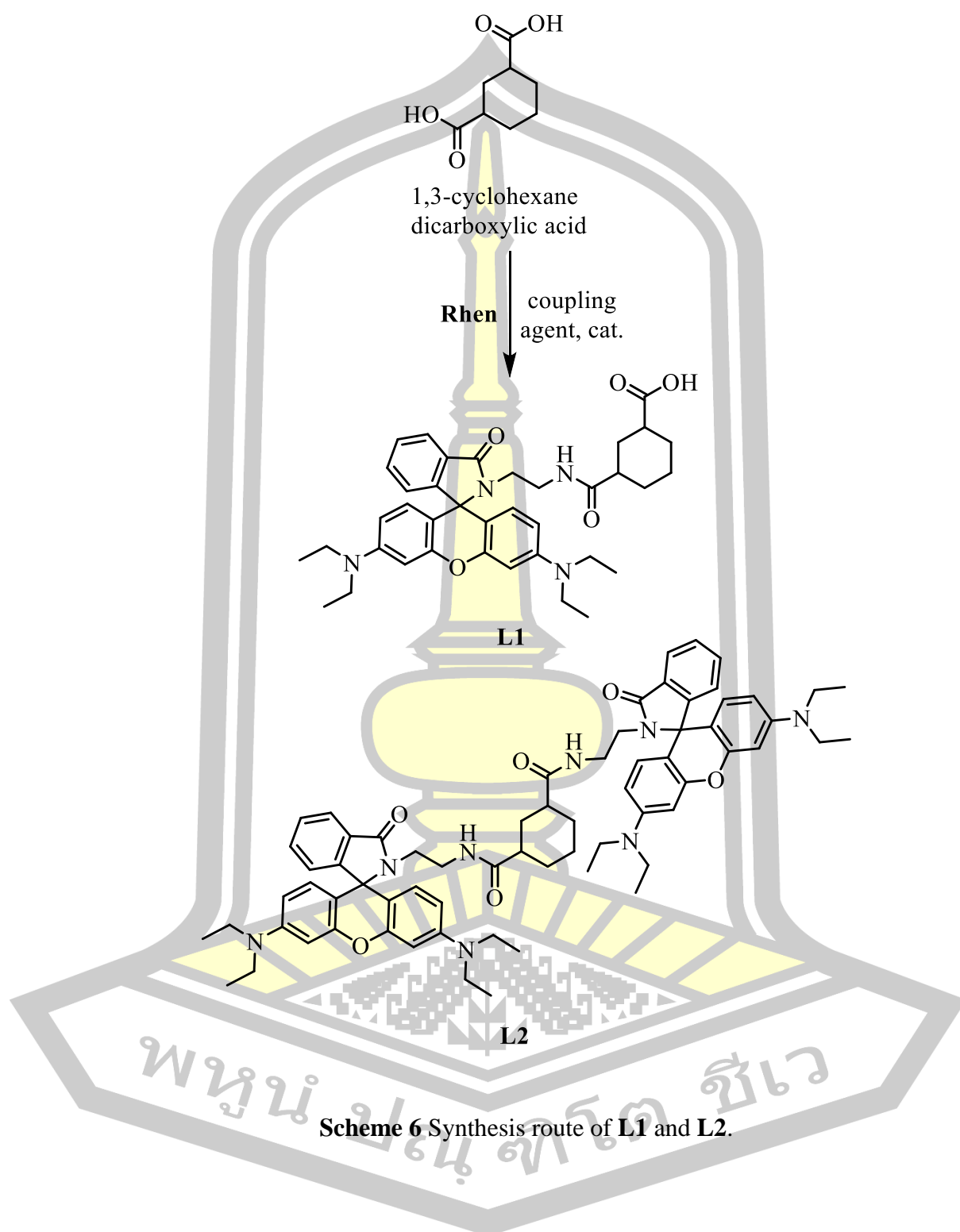
\*N.D.:not define.

**Table 3** Condition I-V for synthesis of **L3** and **L4**.

Condition	Coupling reagent	Catalyst	Other	Temp (°C)	Time (hr)	Yield (%)
I	DCC	DMAP	-	rt	36	85.0
II	DCC	DMAP	-	rt	24	78.0
III	EDC	DMAP	-	rt	24	64.1

Condition I was used DMF as a solvent.

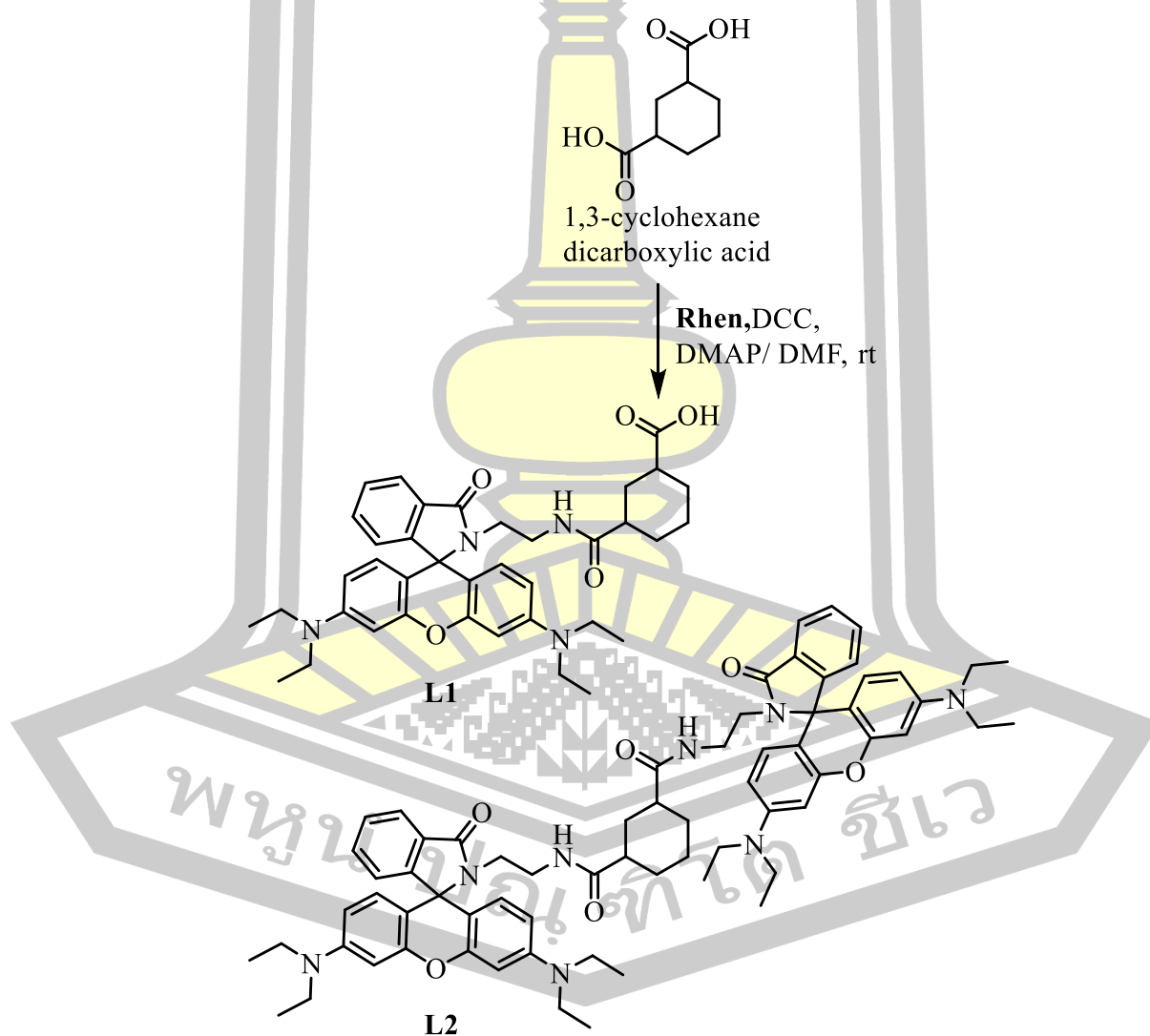
Condition II and III were used THF as a solvent.





## 3.2.2.1.1 Condition I

A **Rhen** (0.22 g, 0.41 mmol), 1,3-cyclohexanedicarboxylic acid (0.04 g, 0.18 mmol), DCC (0.09 g, 0.41 mmol) and DMAP (0.02 g, 0.20 mmol) were dissolved in 10 mL of DMF then vigorously stirred under nitrogen atmosphere at room temperature. The reaction was followed by thin layer chromatography (TLC). The crude was purified by column chromatography 3:1 (hexane:EtOAc) to obtain **L1** (0.1925 g, yield 87.5%).  $^1\text{H-NMR}$  (400 MHz,  $\text{CDCl}_3$ )  $\delta$  7.90 (s, 1H, Ar), 7.50 (s, 2H, Ar), 7.09 (s, 1H, Ar), 6.50 – 6.22 (m, 5H, Ar), 3.40 (d,  $J = 7.1$  Hz, 8H,  $\text{CH}_2$ ), 2.50 (t, 2H,  $\text{CH}_2$ ), 1.19 (s, 12H,  $\text{CH}_3$ ), 1.3–2.1 (m, 10H, cyclohexane).

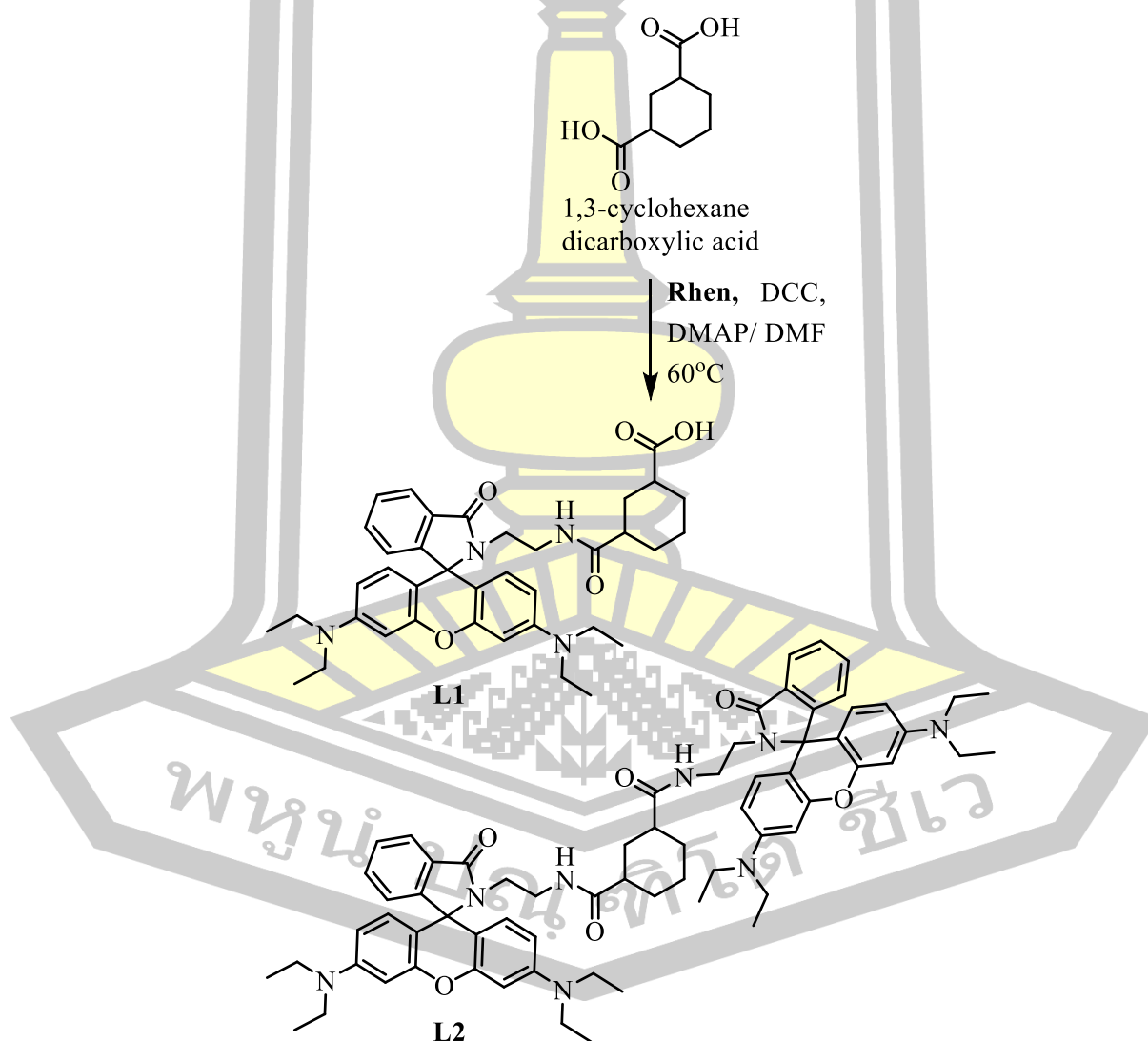


**Scheme 7** The synthesis route of **L1** and **L2** under condition I.



## 3.2.2.1.2 Condition II

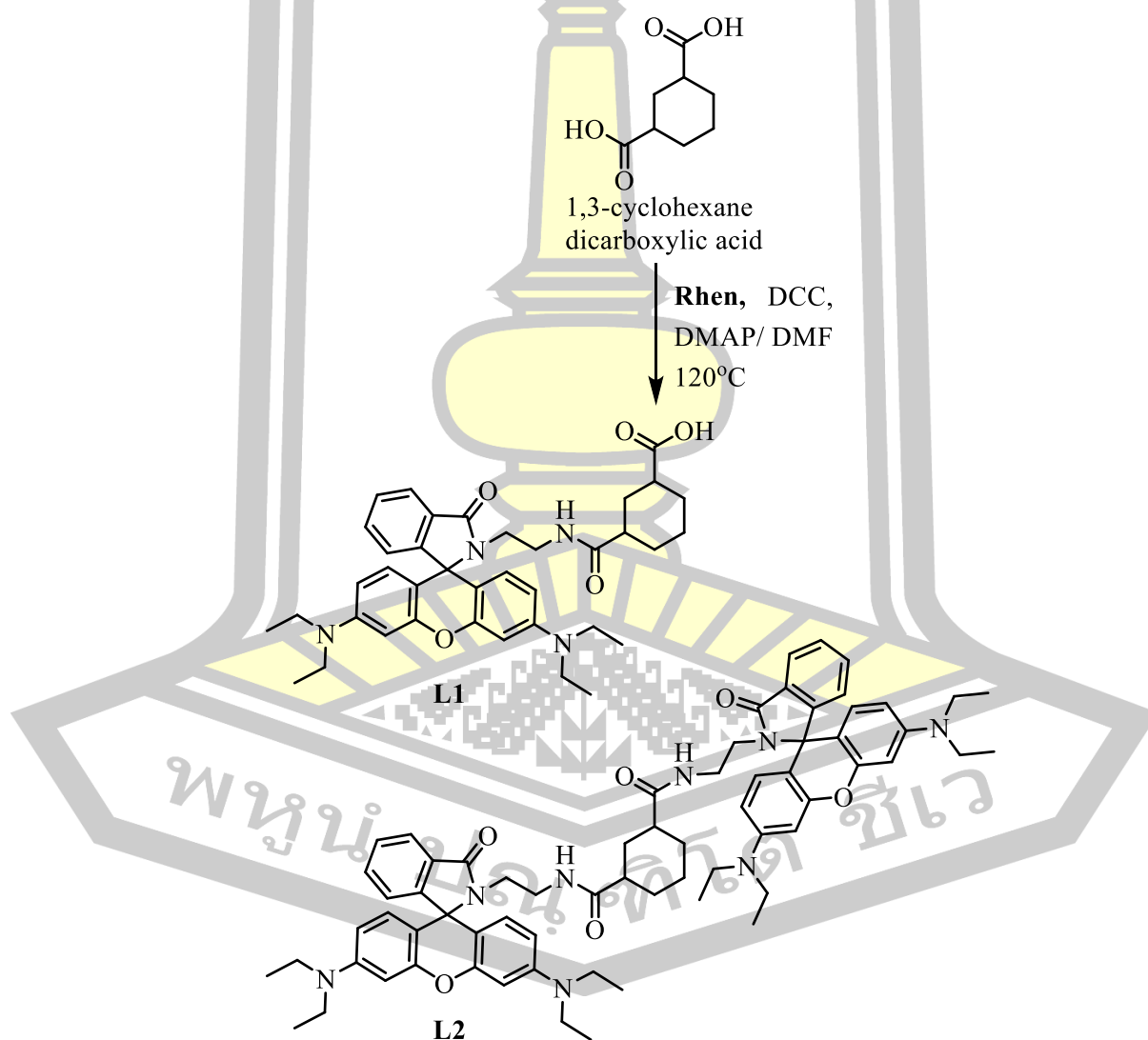
A **Rhen** (0.22 g, 0.41 mmol), 1,3-cyclohexanedicarboxylic acid (0.04 g, 0.18 mmol), DCC (0.09 g, 0.41 mmol) and DMAP (0.02 g, 0.20 mmol) were dissolved in 10 mL of DMF then vigorously stirred under nitrogen atmosphere at 60°C. The reaction was followed by TLC. The crude was purified by column chromatography 3:1 (hexane:EtOAc) to obtain **L1** (0.0344 g, yield 86.0%).  $^1\text{H-NMR}$  (400 MHz,  $\text{CDCl}_3$ )  $\delta$  7.90 (s, 1H, Ar), 7.60 (s, 2H, Ar), 7.12 (s, 1H, Ar), 6.30 – 6.45 (m, 5H, Ar), 3.35 (d,  $J = 7.1$  Hz, 8H,  $\text{CH}_2$ ), 2.50 (t, 2H,  $\text{CH}_2$ ), 1.30 (s, 16H,  $\text{CH}_3$ ), 1.8-2.3 (m, 10H, cyclohexane).



**Scheme 8** The synthesis route of **L1** and **L2** under condition II.

## 3.2.2.1.3 Condition III

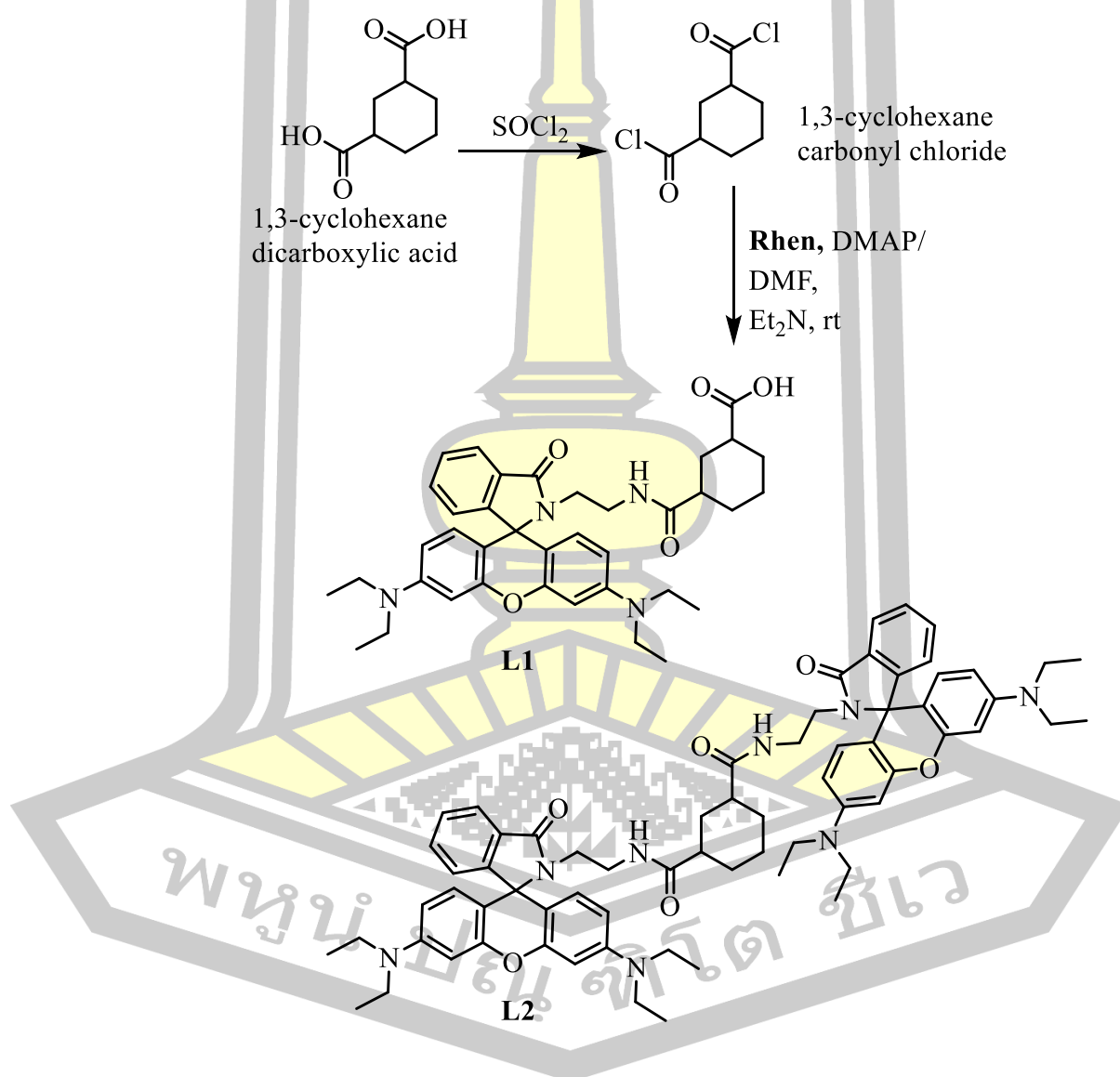
A **Rhen** (0.22 g, 0.41 mmol), 1,3-cyclohexanedicarboxylic acid (0.04 g, 0.18 mmol), DCC (0.09 g, 0.41 mmol) and DMAP (0.02 g, 0.20 mmol) were dissolved in 10 mL of DMF then vigorously stirred under nitrogen atmosphere at 120°C. The reaction was followed by TLC. The crude was purified by column chromatography 3:1 (hexane:EtOAc) to obtain **L2** (0.0354 g, yield 88.5%).  $^1\text{H-NMR}$  (400 MHz,  $\text{CDCl}_3$ )  $\delta$  7.90 (s, 1H, Ar), 7.60 (s, 2H, Ar), 7.02 (s, 1H, Ar), 6.20 – 6.50 (m, 5H, Ar), 3.35 (d,  $J = 7.1$  Hz, 8H,  $\text{CH}_2$ ), 5.5 (s, 1H, NH), 2.30 (t, 2H,  $\text{CH}_2$ ), 1.2 (s, 16H,  $\text{CH}_3$ ), 1.8-2.5 (m, 10H, cyclohexane).



**Scheme 9** The synthesis route of **L1** and **L2** under condition III.

## 3.2.2.1.4 Condition IV

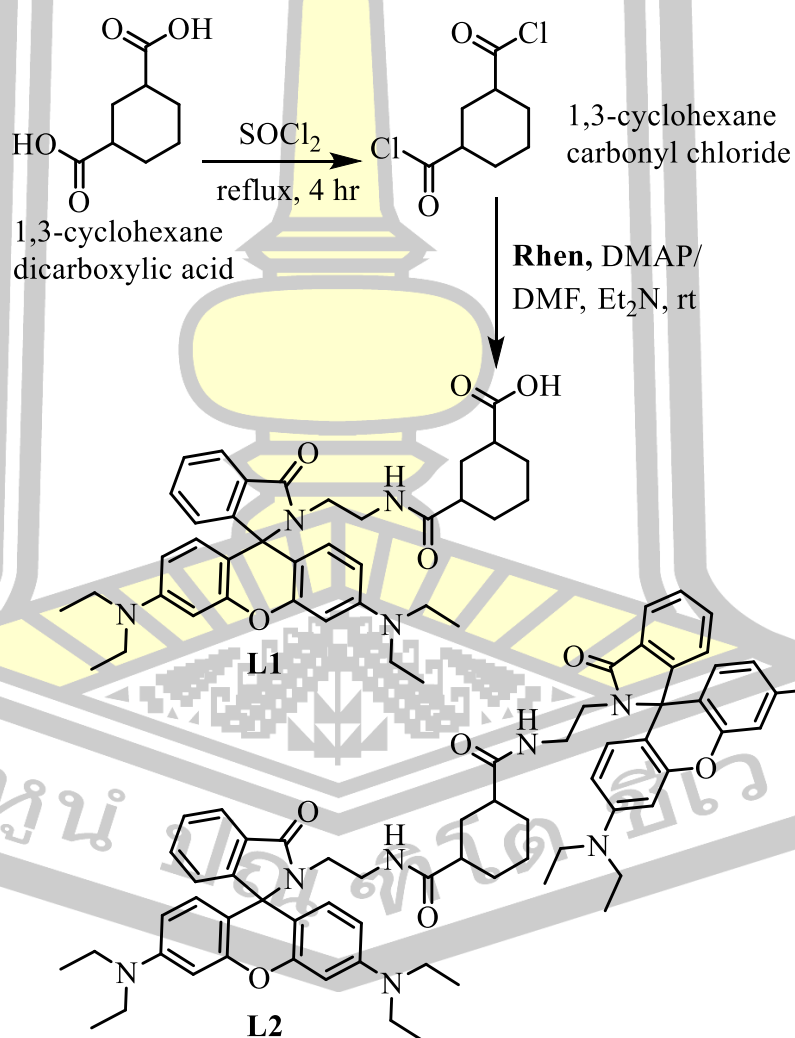
A 1,3-cyclohexanedicarboxylic acid (0.03 g, 0.18 mmol) was dissolved in 10 mL of DMF and vigorously stirred. Then thionyl chloride ( $\text{SOCl}_2$ ) (56.17  $\mu\text{L}$ , 0.75 mmol) was added dropwise into the reaction and vigorously stirred under nitrogen atmosphere at room temperature. After that, the **Rhen** was added into cyclohexane dicarbonyl chloride. The reaction was followed by TLC. The crude was purified by column chromatography 3:1 (hexane:EtOAc).



**Scheme 10** The synthesis route of **L1** and **L2** under condition IV.

## 3.2.2.1.5 Condition V

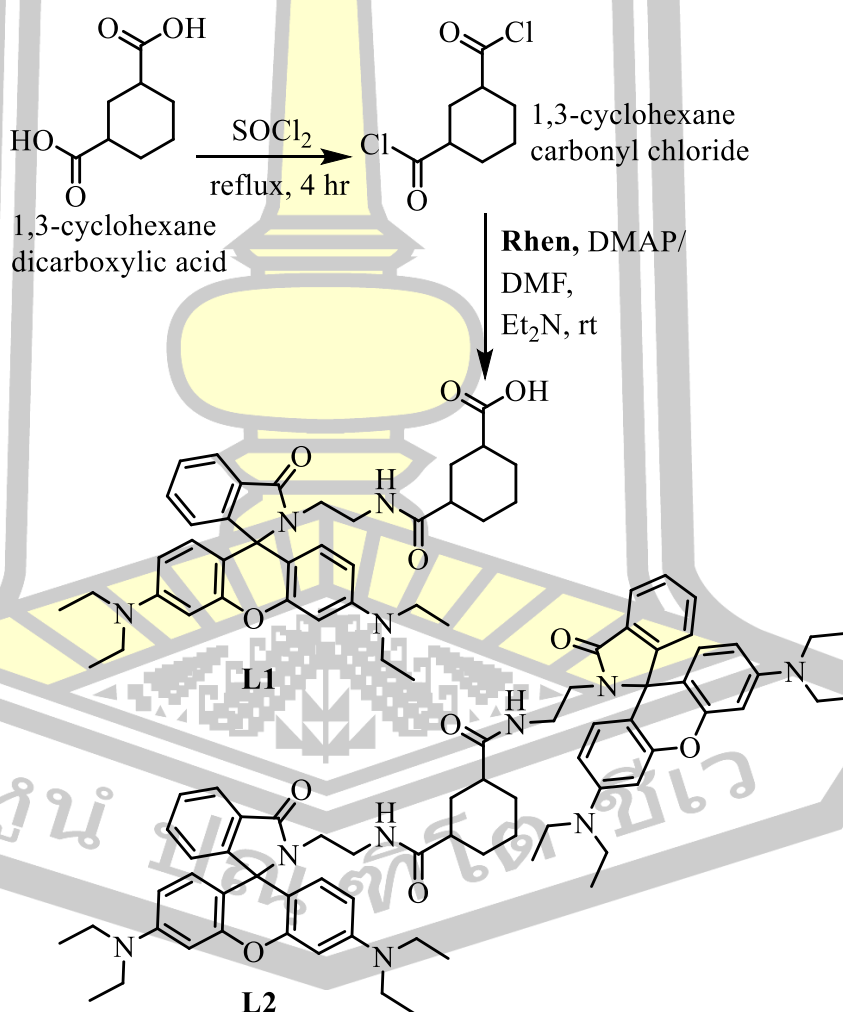
A 1,3-cyclohexanedicarboxylic acid (0.03 g, 0.18 mmol) was dissolved in 10 mL of DMF and vigorously stirred. Then thionyl chloride ( $\text{SOCl}_2$ ) (168.13  $\mu\text{L}$ , 2.25 mmol) was added dropwise into the reaction and vigorously stirred under nitrogen atmosphere at reflux temperature for 4 hr. After that, cyclohexanedicarbonyl chloride was evaporated and redissolved by 5 mL of DCM. Then cyclohexanedicarbonyl chloride was added dropwise into the solution of the **Rhen** (0.20 g, 0.41 mmol),  $\text{Et}_3\text{N}$  (58.85  $\mu\text{L}$ , 0.41 mmol) and vigorously stirred under nitrogen atmosphere at room temperature for 24 hr. The reaction was followed by TLC. The crude was purified by column chromatography 3:1 (hexane:EtOAc).



**Scheme 11** The synthesis route of **L1** and **L2** under condition V.

## 3.2.2.1.6 Condition VI

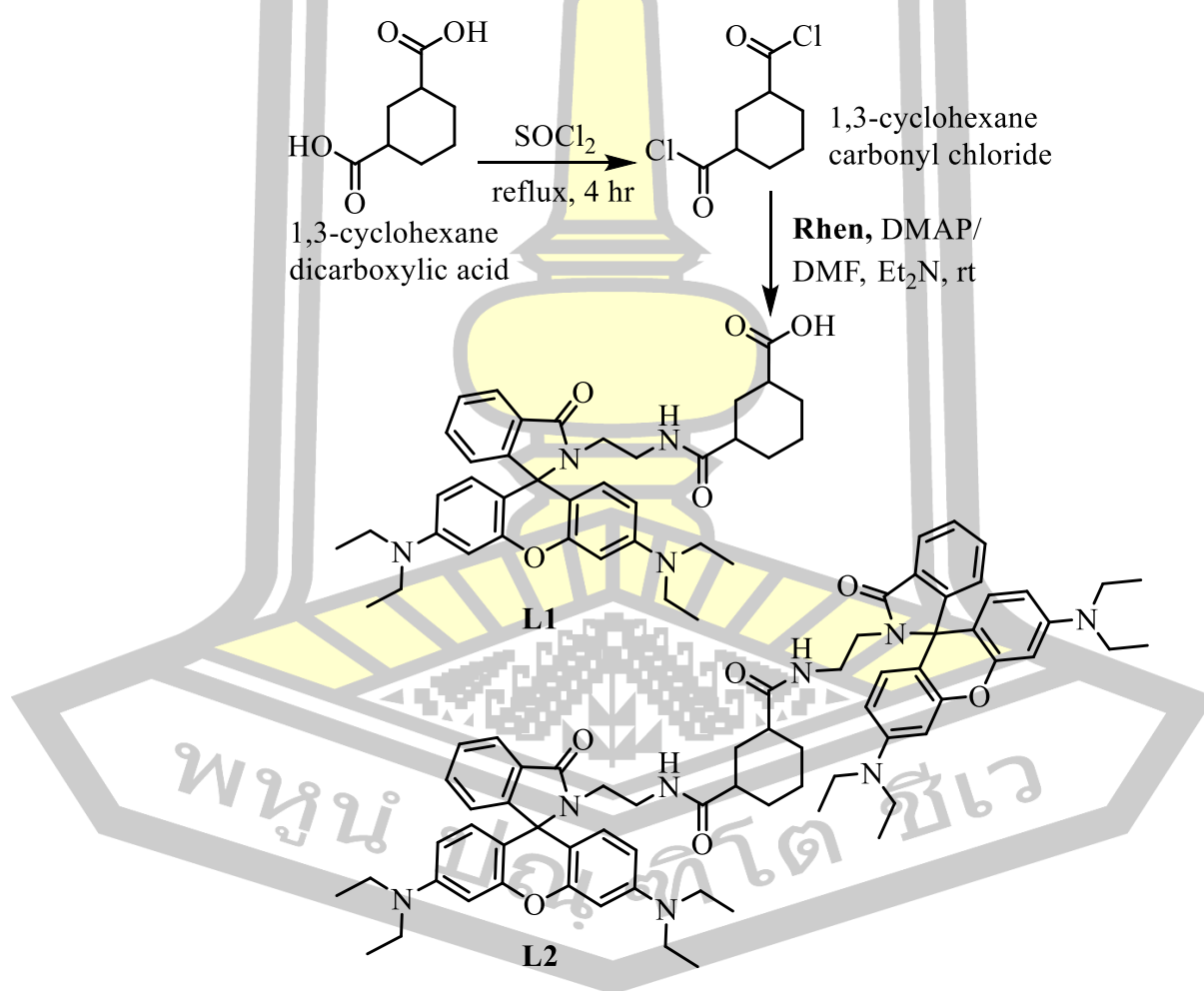
A 1,3-cyclohexanedicarboxylic acid (0.03 g, 0.18 mmol) was dissolved in 10 mL of DMF and vigorously stirred. Then thionyl chloride ( $\text{SOCl}_2$ ) (81.31  $\mu\text{L}$ , 1.12 mmol) was added dropwise into the reaction and vigorously stirred under nitrogen atmosphere at reflux temperature for 4 hr. After that, cyclohexanedicarbonyl chloride was evaporated and redissolved by 5 mL of DCM. Then cyclohexanedicarbonyl chloride was added dropwise into the solution of the **Rhen** (0.20 g, 0.41 mmol),  $\text{Et}_3\text{N}$  (56.99  $\mu\text{L}$ , 0.41 mmol) and vigorously stirred under nitrogen atmosphere at room temperature for 24 hr. The reaction was followed by TLC. The crude was purified by column chromatography 3:1 (hexane:EtOAc).



**Scheme 12** The synthesis route of **L1** and **L2** under condition VI.

## 3.2.2.1.7 Condition VII

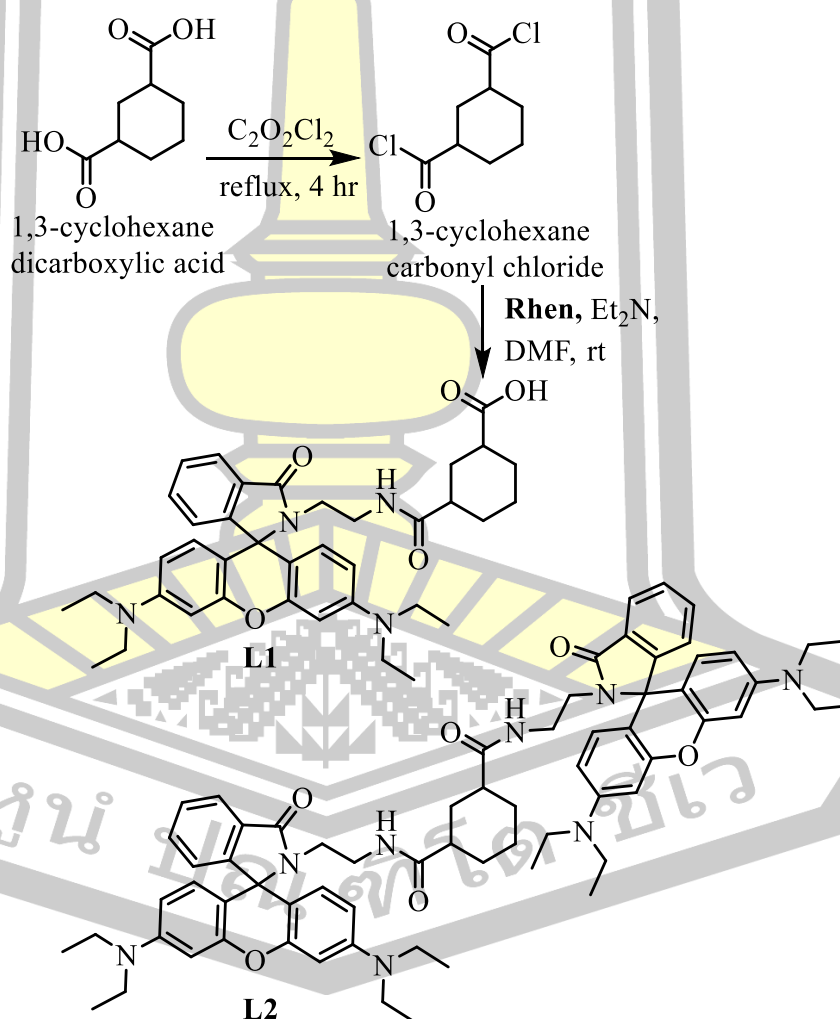
A 1,3-cyclohexanedicarboxylic acid (0.01 g, 0.09 mmol) was dissolved in 10 mL of DMF and vigorously stirred. Then thionyl chloride ( $\text{SOCl}_2$ ) (41.67  $\mu\text{L}$ , 0.56 mmol) was added dropwise into the reaction and vigorously stirred under nitrogen atmosphere at reflux temperature for 4 hr. After that, cyclohexanedicarbonyl chloride was evaporated and redissolved by 5 mL of DMF. Then cyclohexanedicarbonyl chloride was added dropwise into the solution of the **Rhen** (0.10 g, 0.20 mmol),  $\text{Et}_3\text{N}$  (29.12  $\mu\text{L}$ , 0.20 mmol), DMAP (0.03 mmol, 0.56 mmol) and vigorously stirred under nitrogen atmosphere at room temperature for 24 hr. The reaction was followed by TLC. The crude was purified by column chromatography 3:1 (hexane:EtOAc).



**Scheme 13** The synthesis route of **L1** and **L2** under condition VII.

## 3.2.2.1.8 Condition VIII

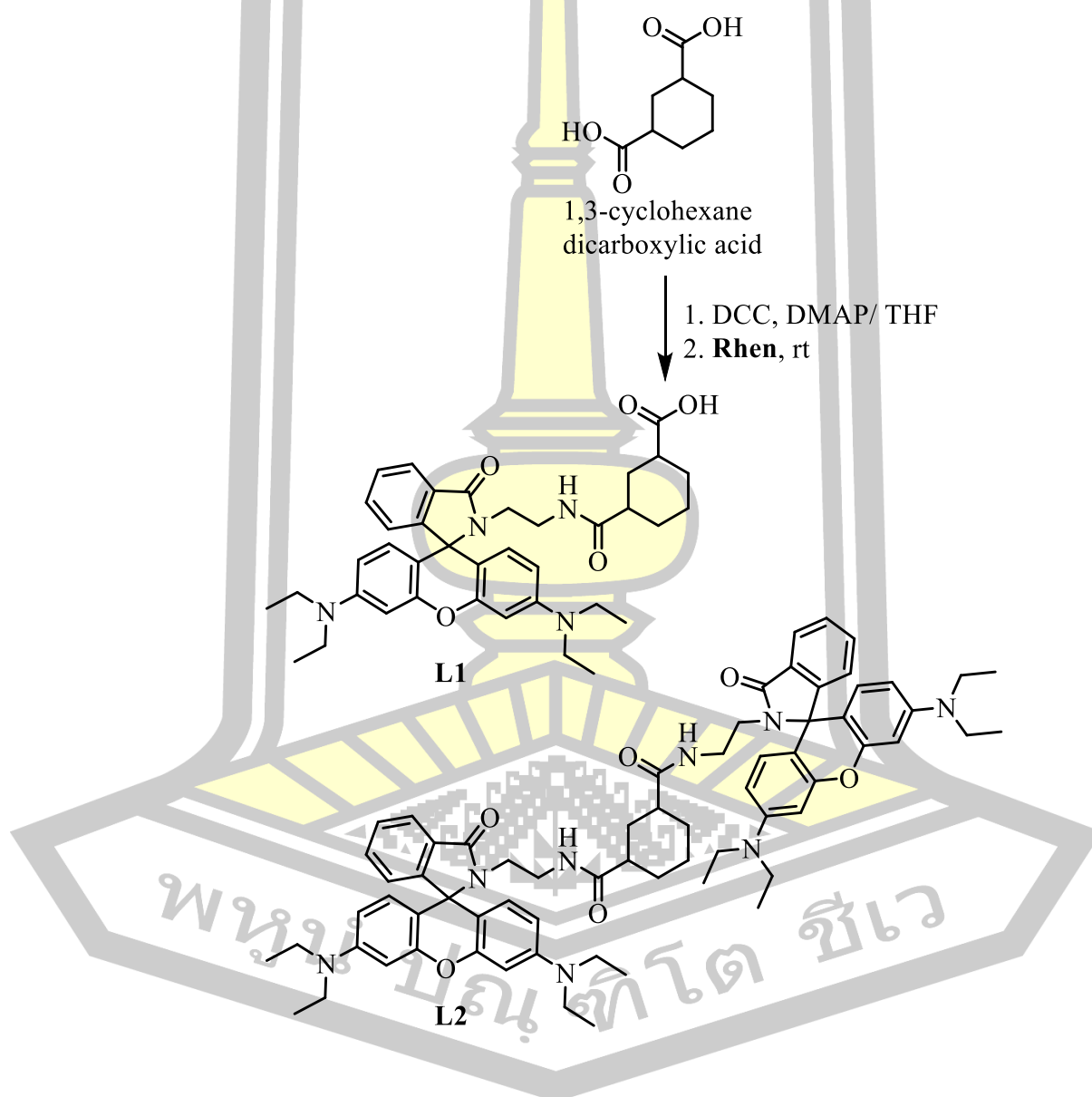
A 1,3-cyclohexanedicarboxylic acid (0.01 g, 0.09 mmol) was dissolved in 10 mL of DMF and vigorously stirred. Then oxalyl chloride ( $\text{C}_2\text{O}_2\text{Cl}_2$ ) (24.85  $\mu\text{L}$ , 0.28 mmol) was added dropwise into the reaction and vigorously stirred under nitrogen atmosphere at reflux temperature for 4 hr. After that, cyclohexanedicarbonyl chloride was evaporated and redissolved by 5 mL of DMF. Then cyclohexanedicarbonyl chloride was added dropwise into the solution of the **Rhen** (0.1 g, 0.09 mmol),  $\text{Et}_3\text{N}$  (30.49  $\mu\text{L}$ , 0.20 mmol) and vigorously stirred under nitrogen atmosphere at room temperature for 24 hr. The reaction was followed by TLC. The crude was purified by column chromatography 3:1 (hexane: EtOAc).



**Scheme 14** The synthesis route of **L1** and **L2** under condition VIII.

## 3.2.2.1.9 Condition IX

A 1,3-cyclohexanedicarboxylic acid (0.03 g, 0.17 mmol), DCC (0.1 g, 0.41 mmol) and DMAP (0.02 g, 0.20 mmol) were dissolved in 10 mL of THF and vigorously stirred for 3 hr. Then added solution of the **Rhen** (0.03 g, 0.17 mmol) and still stirrer. The reaction is followed by TLC. The crude was purified by column chromatography 3:1 (hexane:EtOAc) to obtain **L1** (0.0229 g, yield 76.3%).

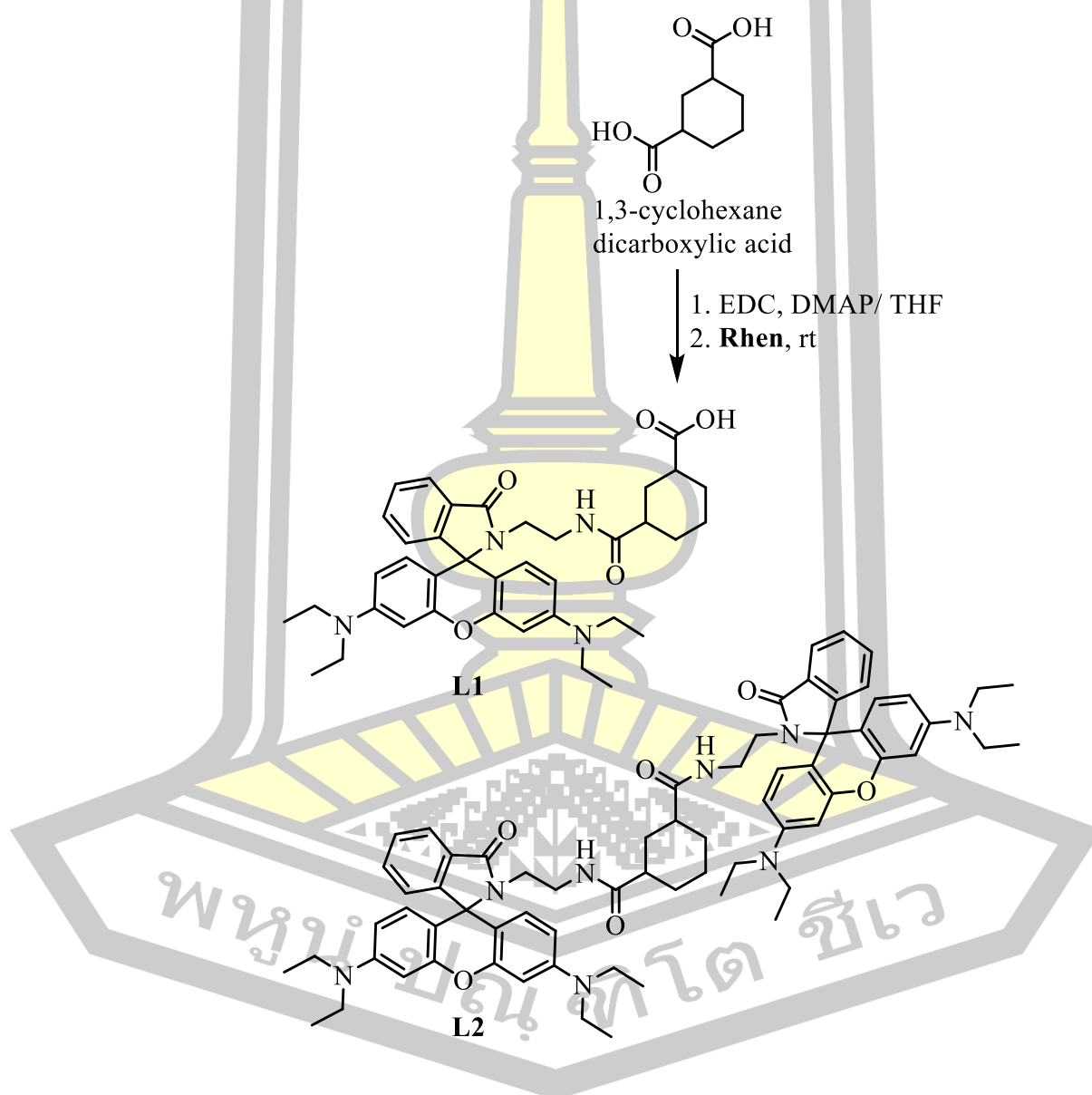


**Scheme 15** The synthesis route of **L1** and **L2** under condition IX.



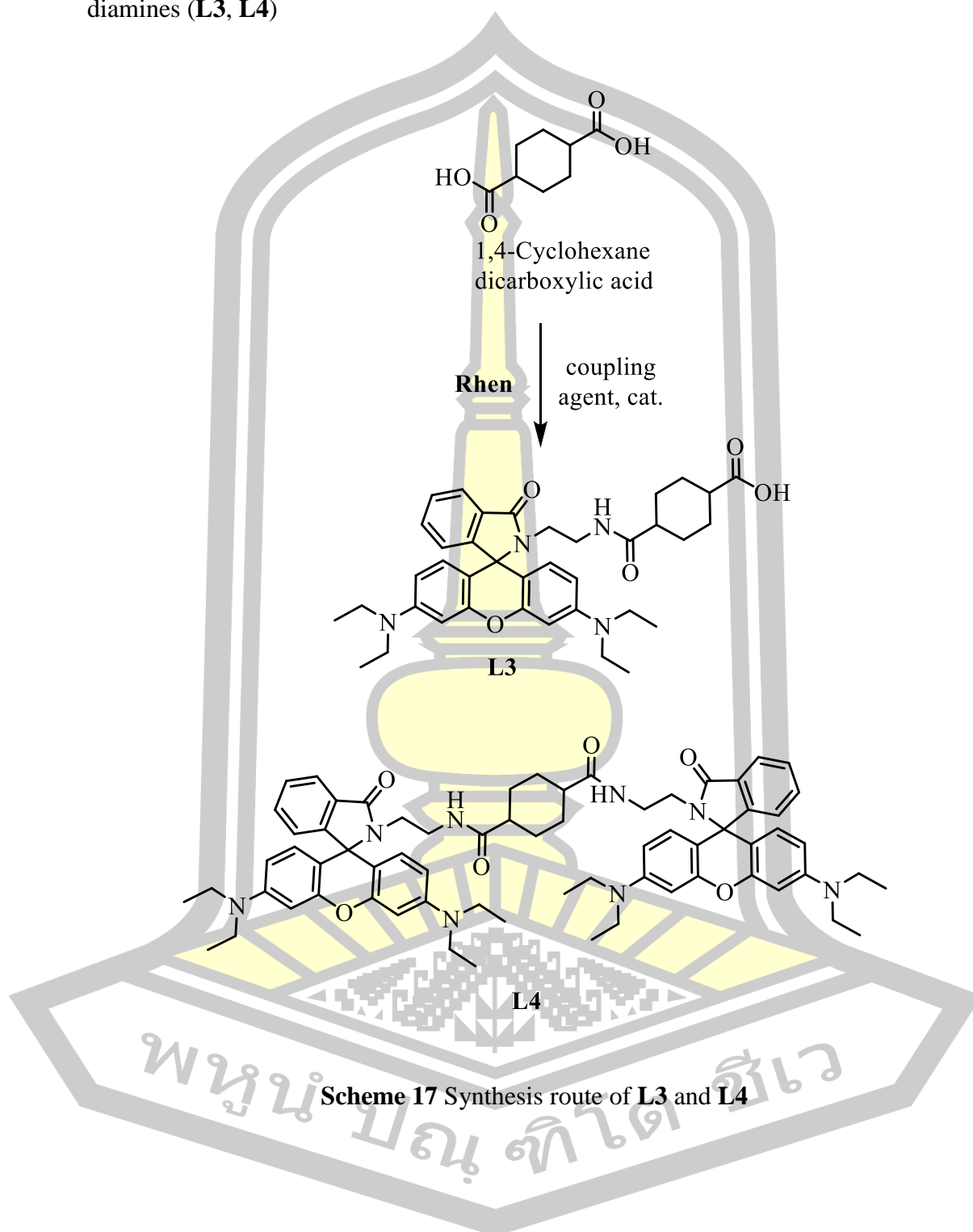
## 3.2.2.1.10 Condition X

A 1,3-cyclohexanedicarboxylic acid (0.08 g, 0.46 mmol), EDC (0.2 g, 1.17 mmol) and DMAP (0.08 g, 0.56 mmol) were dissolved in 10 mL of THF and vigorously stirred for 3 hr. Then added solution of the **Rhen** (0.03 g, 0.17 mmol) and still stirrer. The reaction evaporate followed by TLC. The crude was purified by column chromatography 3:1 (hexane: EtOAc) to obtain **L1** (0.0647 g, yield 80.8%).



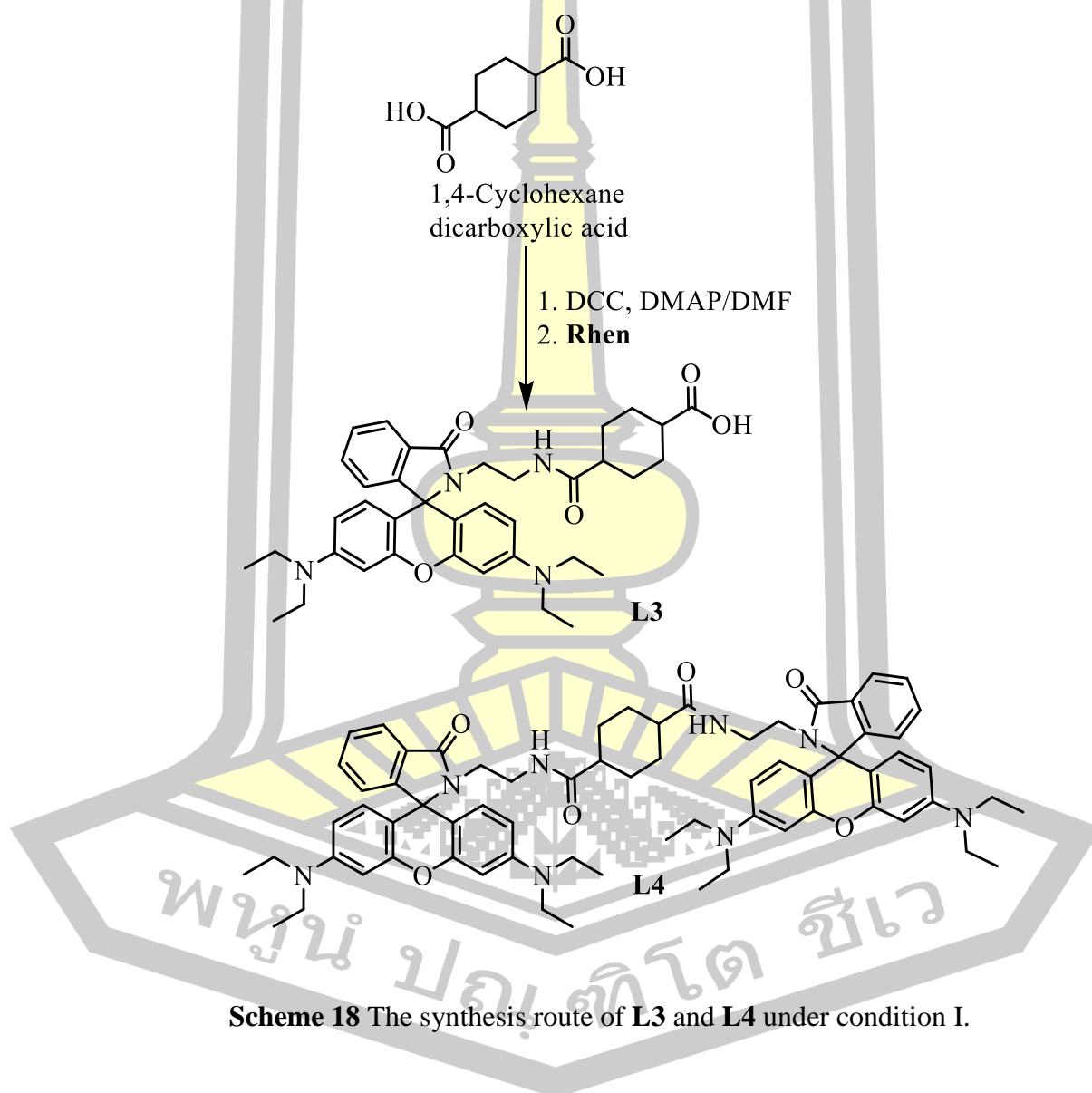
**Scheme 16** The synthesis route of **L1** and **L2** under condition X.

3.2.2.2 Synthesis of 1,4-cyclohexane N-(Rhodamine B)-lactam-ethylene diamines (**L3**, **L4**)



## 3.2.2.2.1 Condition I

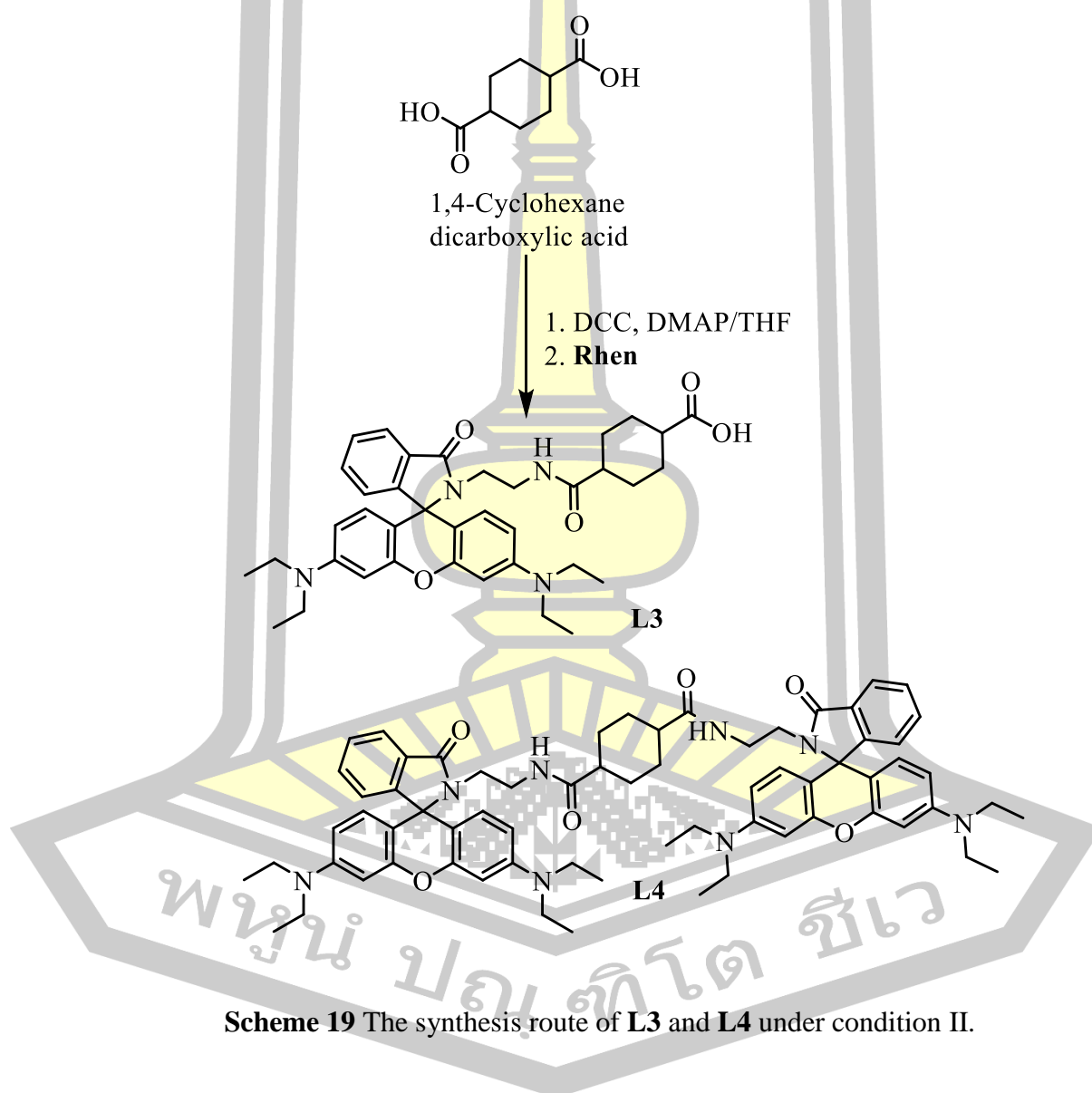
A 1,4-cyclohexanedicarboxylic acid (0.01 g, 0.08 mmol), DCC (0.05 g, 0.20 mmol) and DMAP (0.01 g, 0.01 mmol) were dissolved in 10 mL of DMF and vigorously stirred for 3 hr. Then added solution of the **Rhen** (0.1 g, 0.20 mmol) and still stirrer. The reaction was followed by TLC. The crude was purified by column chromatography 3:1 (hexane:EtOAc) to obtain **L3** (0.0085 g, yield 85.0%).



**Scheme 18** The synthesis route of **L3** and **L4** under condition I.

## 3.2.2.2.2 Condition II

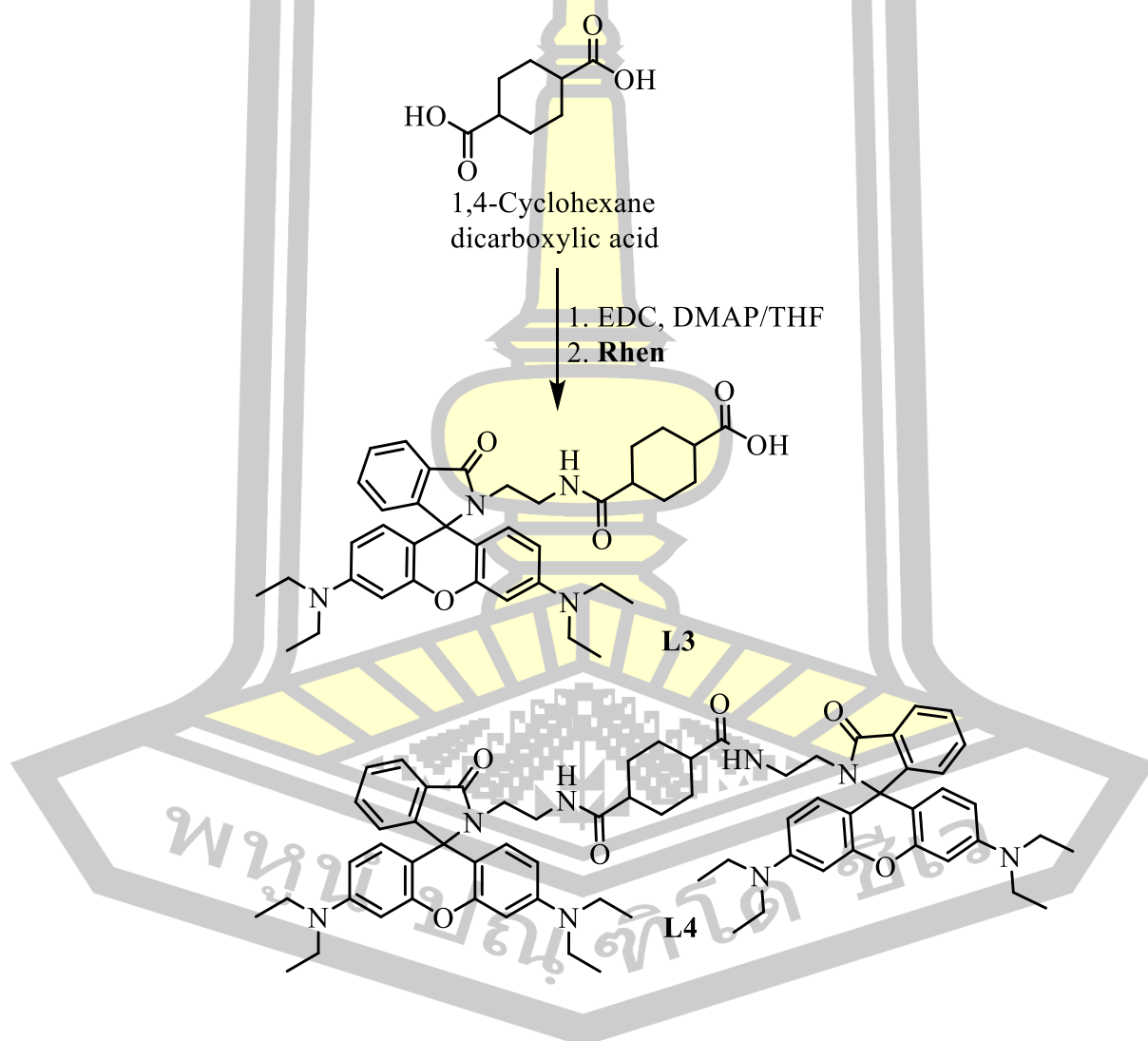
A 1,4-cyclohexanedicarboxylic acid (0.05 g, 0.34 mmol), DCC (0.20 g, 0.82 mmol) and DMAP (0.05g, 0.41 mmol) were dissolved in 10 mL of THF and vigorously stirred for 3 hr. Then added solution of the **Rhen** (0.06 g, 0.34 mmol) and still stirrer. The reaction was followed by TLC. The crude was purified by column chromatography 3:1 (hexane:EtOAc) to obtain **L3**. (0.0390 g, yield 78%).



**Scheme 19** The synthesis route of **L3** and **L4** under condition II.

## 3.2.2.2.3 Condition III

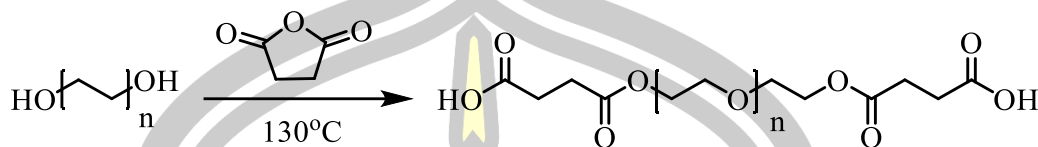
A 1,4-cyclohexanedicarboxylic acid (0.08 g, 0.46 mmol), EDC (0.23 g, 1.17 mmol) and DMAP (0.08 g, 0.56 mmol) were dissolved in 10 mL of THF and vigorously stirred for 3 hr. Then added solution of the **Rhen** (0.5 g, 1.03 mmol) and still stirrer. The reaction was followed by TLC. The crude was purified by column chromatography 3:1 (hexane:EtOAc) to obtain **L3** (0.0513 g, yield 64.1%).  $^1\text{H-NMR}$  (400 MHz,  $\text{DMSO-}d_6$ )  $\delta$  7.89 (s, 1H, Ar), 7.77 (s, 2H, Ar), 7.01 (s, 1H, Ar), 6.61–6.41 (m, 5H, Ar), 3.35 (d,  $J = 7.1$  Hz, 8H,  $\text{CH}_2$ ), 2.26 (t, 2H,  $\text{CH}_2$ ), 1.26 (s, 16H,  $\text{CH}_3$ ).



**Scheme 20** The synthesis route of **L3** and **L4** under condition III.

### 3.2.3 Rhodamine-PEG (L5, L6 and L7)

#### 3.2.3.1 Synthesis of PEG-COOH



**Scheme 21** Synthesis route of **PEG-COOH**.

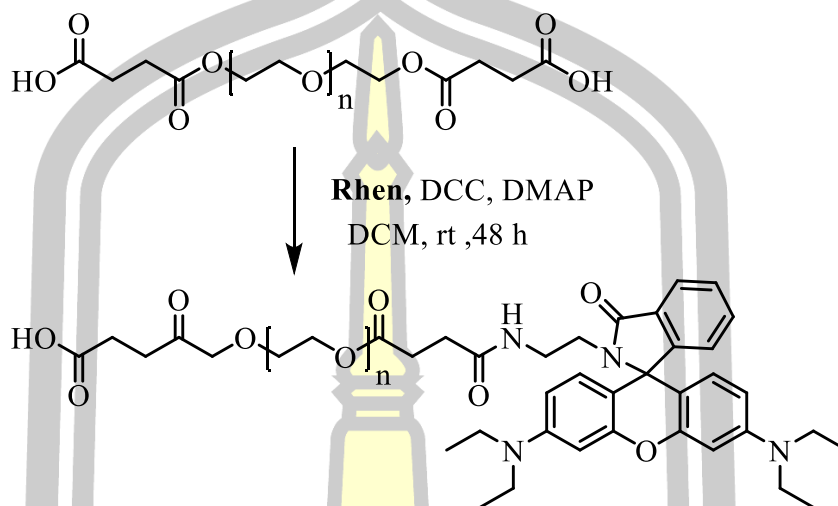
The PEG-400 (5.00 g, 1.25 mmol) was added to round-bottom flask then added 25 mL of toluene and evaporated, the flask was cooled to room temperature and charged with N<sub>2</sub> gas before succinic anhydride (5 g, 5.0 mmol) was added. The reaction mixture was allowed to stir at 130°C for 6 h. The crude product was dissolved in DCM, and the solution was precipitated in cold diethyl ether and precipitation 2 time in DCM/ether. The final product was obtained as white solid (**PEG400-COOH**, 0.4869 g, yield 97.38%). <sup>1</sup>H-NMR (400 MHz, CDCl<sub>3</sub>) δ 12.14 (s, 2H, OH), 3.33 (s, 6H, CH<sub>2</sub>), 2.40 (d, 5H, CH<sub>2</sub>). ATR-FTIR ν 3329 cm<sup>-1</sup> (O-H stretching) carboxylic, 2928 cm<sup>-1</sup> (CH stretching), 1672 cm<sup>-1</sup> (C=O).

The PEG-4000 (2.50 g, 1.25 mmol) was added to round-bottom flask then added 25 mL of toluene and evaporated, the flask was cooled to room temperature and charged with N<sub>2</sub> gas before succinic anhydride (0.02 g, 5.0 mmol) was added. The reaction mixture was allowed to stir at 130°C for 6 h. The crude product was dissolved in DCM, and the solution was precipitated in cold diethyl ether and precipitation 2 time in DCM/ether. The final product was obtained as white solid (**PEG4000-COOH**, 0.2362 g, yield 94.52%).

The PEG-6000 (2.50 g, 1.25 mmol) was added to round-bottom flask then added 25 mL of toluene and evaporated, the flask was cooled to room temperature and charged with N<sub>2</sub> gas before succinic anhydride (0.02 g, 5.0 mmol) was added. The reaction mixture was allowed to stir at 130°C for 6 h. The crude product was dissolved in DCM, and the solution was precipitated in cold diethyl ether and precipitation 2 time in DCM/ether. The final product was obtained as white solid (**PEG6000-COOH**,

0.2281 g, yield 91.24%).

### 3.2.3.2 Synthesis of Rhodamine-PEG (L5)

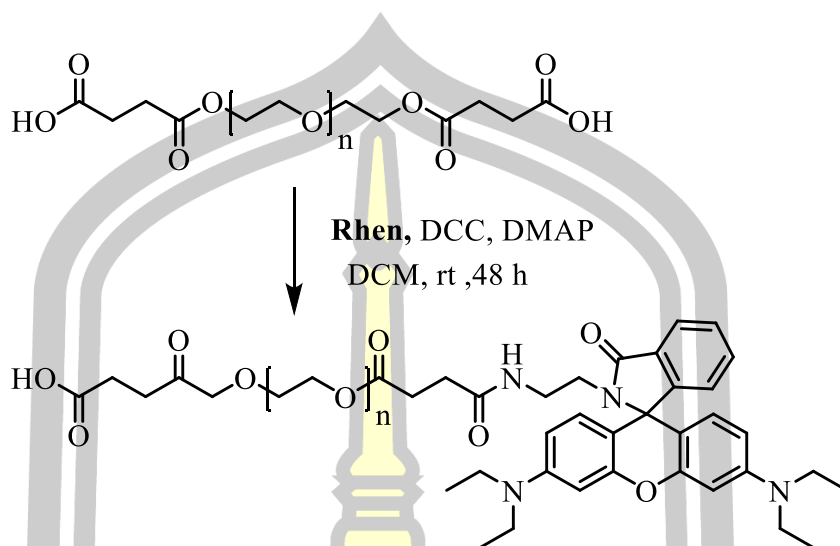


**Scheme 22** Synthesis route of **L5**.

The **PEG400-COOH** (0.99 g, 1.66 mmol) was added to round bottom flask, then added toluene and evaporated. After the flask was then cooled to room temperature and charged with  $\text{N}_2$  gas, dry DCM (25 mL) was added. The DCC (0.51 g, 2.5 mmol), DMAP (0.04 g, 0.7 mmol) were added and stirred until homogenous. Added Rhodamine derivatives (0.8 g, 1.88 mmol) in dry DCM. The reaction mixture was stirred at room temperature for 48 h to obtain **L5** (0.8112 g, 81.93%)  $^1\text{H-NMR}$  (400 MHz,  $\text{CDCl}_3$ )  $\delta$  7.87 (s, 1H, Ar), 7.36 (s, 2H, Ar), 7.01 (s, 1H, Ar), 6.23–6.34 (m, 5H, Ar), 3.28 (d,  $J = 7.1$  Hz, 8H,  $\text{CH}_2$ ), 3.01 (s, 8H,  $\text{CH}_2$ ), 2.26 (t, 2H,  $\text{CH}_2$ ), 2.07 (d, 56H,  $\text{CH}_2$ ), 1.26 (s, 16H,  $\text{CH}_3$ ). ATR-FTIR  $\nu$  3351  $\text{cm}^{-1}$  (O-H stretching) carboxylic, 3010  $\text{cm}^{-1}$  (NH stretching), 1727  $\text{cm}^{-1}$  (C=O) amide, 1687 and 1419  $\text{cm}^{-1}$  (Ar=CH).



## 3.2.3.3 Synthesis of Rhodamine-PEG (L6)

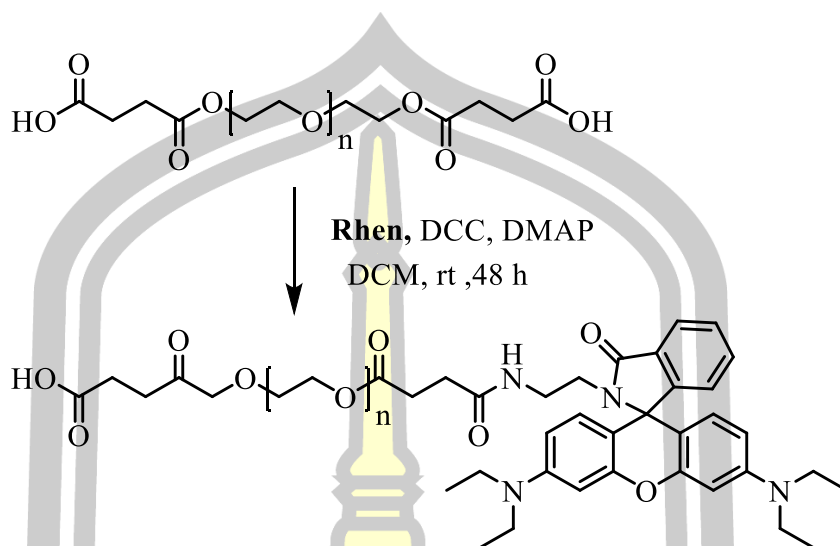


Scheme 23 Synthesis route of L6.

The **PEG4000-COOH** (0.25 g, 0.09 mmol) was added round bottom flask, then added toluene and evaporated. After the flask was then cooled to room temperature and charged with N<sub>2</sub> gas, dry DCM (25 mL) was added. The DCC (0.02 g, 0.19 mmol), DMAP (29.0 mg, 0.02 mmol) were added and stirred until homogenous. Added **Rhen** (0.02 g, 0.07 mmol) in dry DCM. The reaction mixture was stirred at room temperature for 48 h to obtain **L6** (0.2161 g, 86.44%).

พหุ ประทีป ชีวะ

### 3.2.3.4 Synthesis of Rhodamine-PEG (L7)

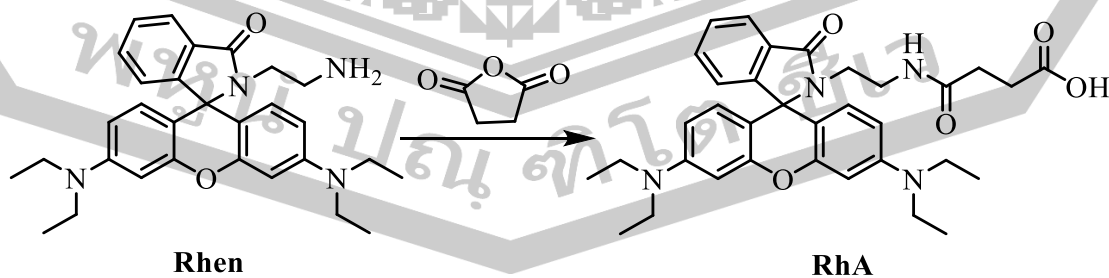


**Scheme 24** Synthesis route of **L7**.

The **PEG6000-COOH** (1 g, 1.96 mmol) was added round bottom flask, then added toluene and evaporated. After the flask was then cooled to room temperature and charged with N<sub>2</sub> gas, dry DCM (25 mL) was added. The DCC (0.062 g, 0.30 mmol), DMAP (0.04 g, 0.7 mmol) were added and stirred until homogenous. Added Rhodamine derivatives (0.01 g, 0.08 mmol) in dry DCM. The reaction mixture was stirred at room temperature for 48 h.

### 3.2.4 Rhodamine anhydride (L8)

#### 3.2.4.1 Synthesis of Rhodamine anhydride (L8)



**Scheme 25** Synthesis route of **L8**.

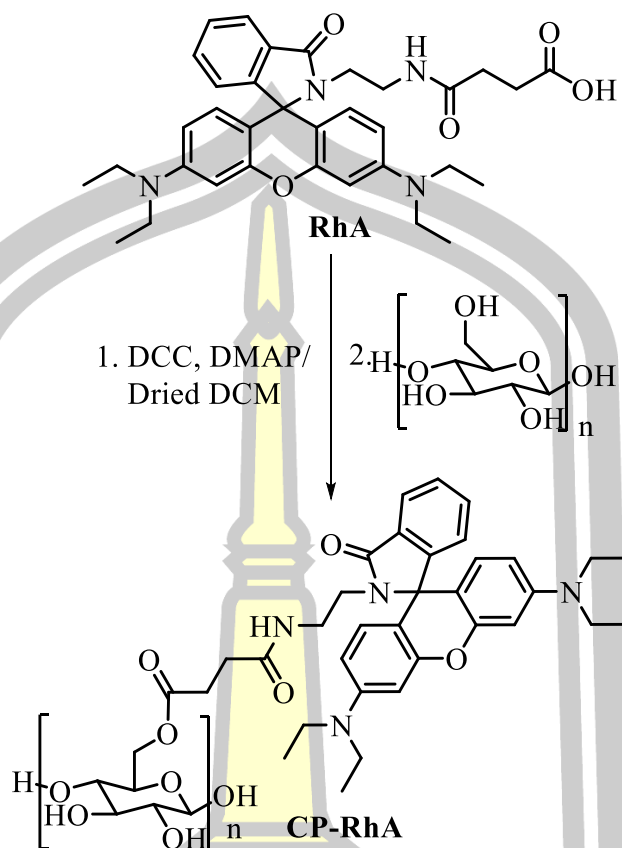
Rhodamine ethylenediamine anhydride (**L8**) was synthesized by a modification of the method in [56]. The **Rhen** (0.25 g, 0.50 mmol) was dissolved in dry DCM and succinic anhydride (0.04 g, 0.05 mmol) added and then stirred under N<sub>2</sub> gas at room temp. After 2 hr, solvent was removed from the mixture by vacuum evaporator and the product purified by column chromatography using 1:9:0.1 (MeOH:DCM: Triethylamine) to obtain **L8** (0.23 g, yield 80 %) <sup>1</sup>H-NMR (400 MHz, CDCl<sub>3</sub>)  $\delta$  11.92 (br s, 1H, COOH), 7.92–7.80 (m, 1H, ArH), 7.50–7.47 (m, 2H, ArH), 7.10–7.04 (m, 1H, ArH), 6.47–6.24 (s, 6H, ArH), 5.58(s, 1H, NH), 3.60 (q, J = 8 Hz, 2H, CH<sub>2</sub>NH), 3.34 (br s, 2H, NCH<sub>2</sub>), 3.09 (m, J = 12 Hz, 8H, NCH<sub>2</sub>CH<sub>3</sub>), 2.55(br s, 2H, CH<sub>2</sub>COOH), 2.44(br s, 2H, CH<sub>2</sub>CONH), 1.40 (s, 12H, NCH<sub>2</sub>CH<sub>3</sub>) and 1.16 (t, J = 16 Hz, 12H, NCH<sub>2</sub>CH<sub>3</sub>). ATR-FTIR  $\nu$  3351 cm<sup>-1</sup> (O-H stretching) carboxylic, 2971 cm<sup>-1</sup> (NH stretching), 1725 cm<sup>-1</sup> (C=O) amide, 1632 and 1467 cm<sup>-1</sup> (Ar=CH).

#### 3.2.4.2 Preparation of paper based sensor (**CP-L8**)

Modified cellulose paper was prepared by a method adapted from [57]. Sheets of cellulose paper (0.2x1 cm) were soaked in 0.1 M of NaOH for 10 min and then washed with THF, DCM and dry DCM, respectively. **L8** (0.25 g, 0.42 mmol), DCC (0.10 g, 0.51 mmol) and DMAP (2.61 mg, 0.02 mmol) were mixed in 10 ml of dry DCM. Dried sheets of cellulose paper were put into the mixture solution and shaken for 10 h. Modification of cellulose paper was taken out of solution then washed with THF, DCM and dry DCM, respectively.

### 3.3 Characterization

<sup>1</sup>H-NMR spectrometer was used for proven of **L1, L2, L3, L5, L6, L8, PEG-COOH, PEG400-COOH, PEG4000-COOH, Rhen**. ATR-FTIR was used for proven of **Rhen, L6, PEG-COOH, PEG400-COOH** and **CP-L8**. The surface morphology of **CP-L8** was perform by scanning electron microscopy.



**Scheme 26** Synthesis route of **CP-L8**.

### 3.4 Complexation studies of ligand and metal ions

The complexation study of ligand and metal ions were performed by mixed 2 mL of ligand with 1.5 ml of metal ions ( $\text{Na}^+$ ,  $\text{K}^+$ ,  $\text{Ag}^+$ ,  $\text{Mg}^{2+}$ ,  $\text{Ca}^{2+}$ ,  $\text{Pb}^{2+}$ ,  $\text{Co}^{2+}$ ,  $\text{Ni}^{2+}$ ,  $\text{Cu}^{2+}$ ,  $\text{Zn}^{2+}$ ,  $\text{Cd}^{2+}$ ,  $\text{Hg}^{2+}$ ,  $\text{Al}^{3+}$ ,  $\text{Cr}^{3+}$ ,  $\text{Fe}^{3+}$ ,  $\text{Au}^{3+}$ ,  $\text{Pt}^{2+}$ ,  $\text{Ru}^{2+}$ ). The mixtures were measure by UV-Vis spectrometer (scan mode 250-700 nm) and fluorescence spectrometer (excitation at 520 nm, emission at 540 nm (slit 10/10)).

### 3.5 The estimated pH of ligand

The solution of ligand was adjusted pH value by 0.1 M of NaOH and HCl. The result was measured by UV-Vis (scan mode 250-700 nm) and fluorescent spectrometer (excitation at 520 nm, emission at 540 nm (slit 10/10)).

### 3.6 The estimated pH of ligand

Theoretical calculations were performed with density functional theory by using Gaussian 05 software package. The chemical structures and electronic distributions of **L8** were optimized at the B3LYP/LanL2DZ level.



## CHAPTER 4

### RESULTS AND DISCUSSION

#### 4.1 Synthesis of Rhodamine ethylenediamine (Rhen)

The precursor (**Rhen**) were easily synthesized in good yields by a condensation reaction of Rhodamine B and ethylenediamine under N<sub>2</sub> atmosphere at reflux temperature for 3 days. Then workup and purification to give **Rhen** in 84%. Chemical position of **Rhen** were proven by <sup>1</sup>H-NMR, FTIR and mass spectrometer. The <sup>1</sup>H-NMR spectrum showed characteristic signals of –CH<sub>2</sub> and –CH groups in the region of 1.0–2.1 and 2.2–2.6 ppm, aromatic protons at 7.8–5.5 ppm. FTIR spectrum appear 3336 (NH), 2962 (C–H), 2935, 2852 (–C–H), 1682 (C=O), 1620, 1517 (C]C), 1227 (C–O). MS (MALDI-TOF) calcd. for [C<sub>30</sub>H<sub>36</sub>N<sub>4</sub>O<sub>2</sub>]<sup>+</sup>: *m/z* 484.28. Found: *m/z* 485.91 [M+H]<sup>+</sup>

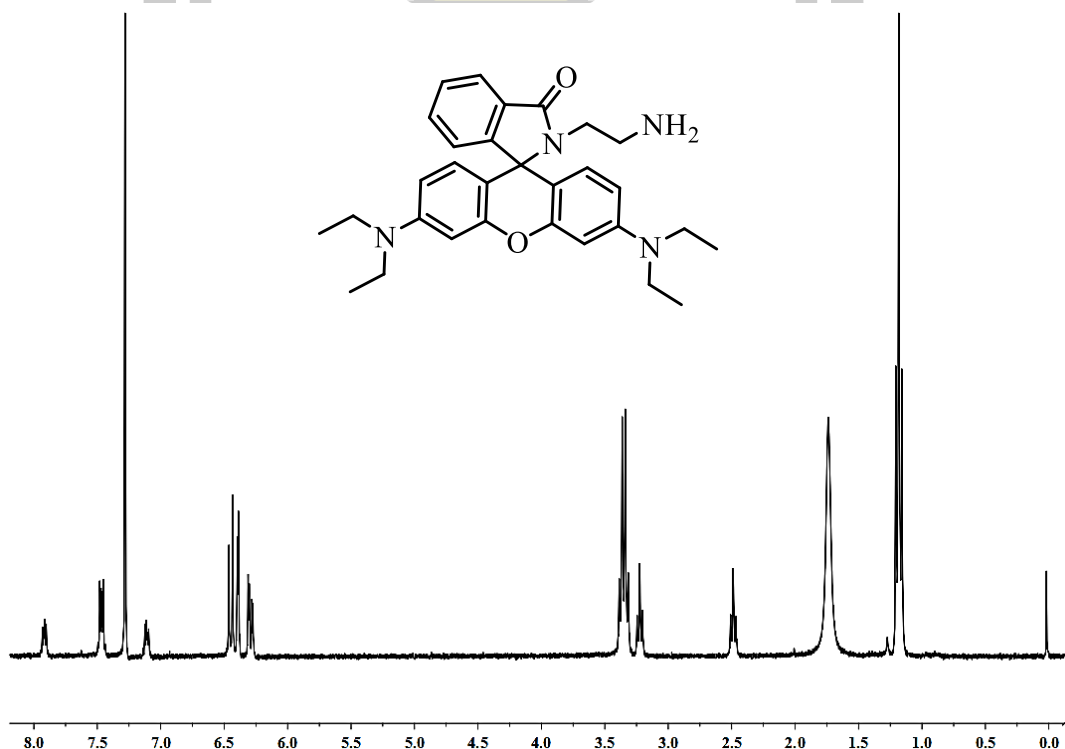
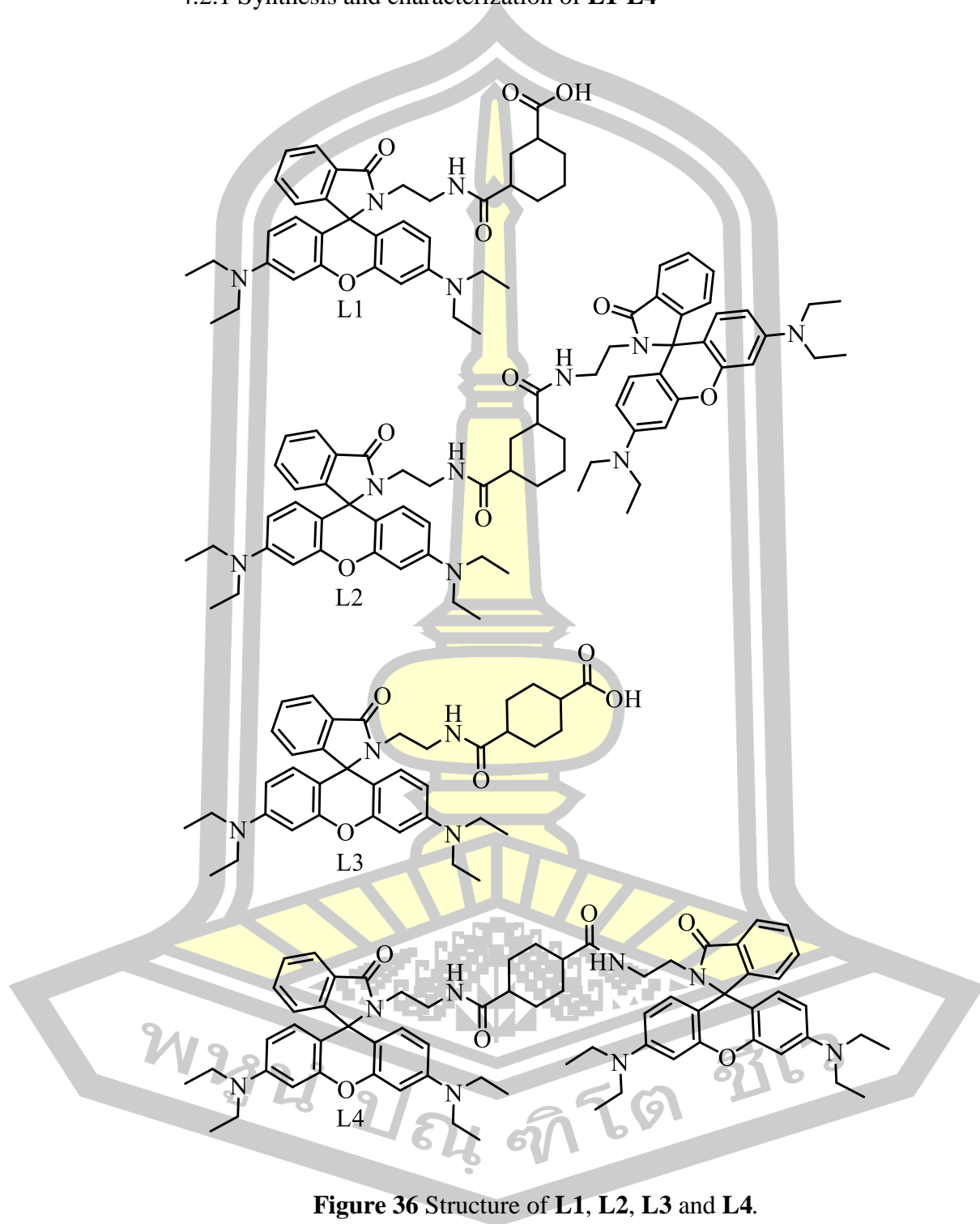


Figure 35 <sup>1</sup>H-NMR spectrum of **Rhen**.

## 4.2 Rhodamine-cyclohexane (L1-L4)

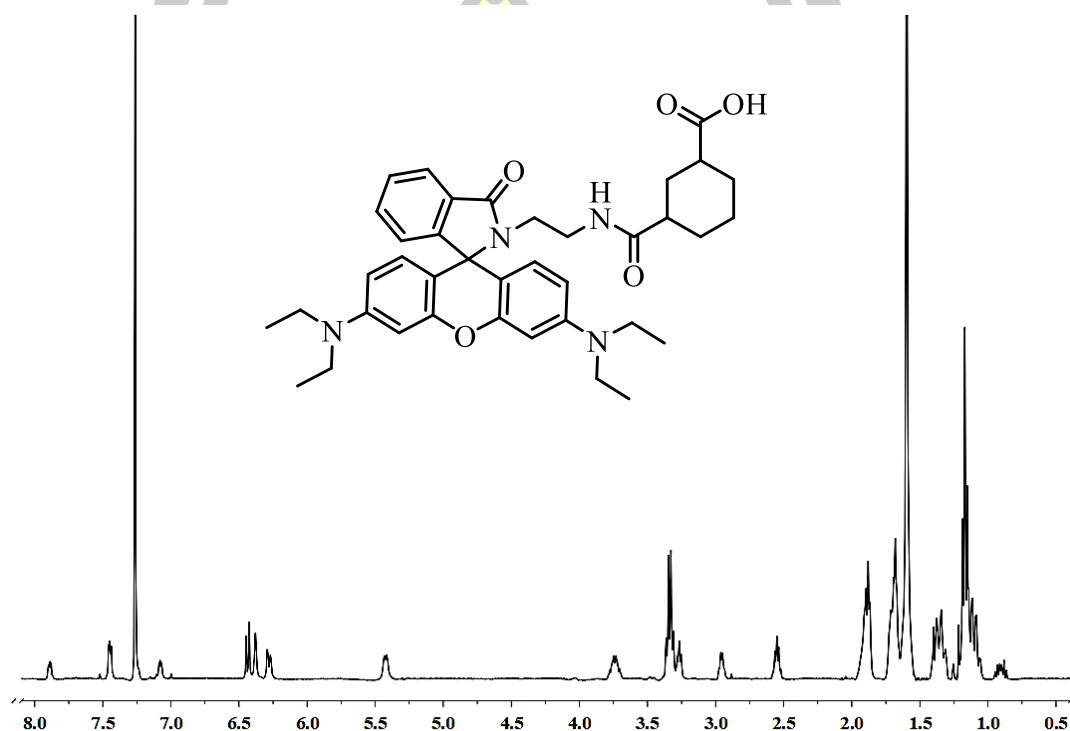
### 4.2.1 Synthesis and characterization of L1-L4





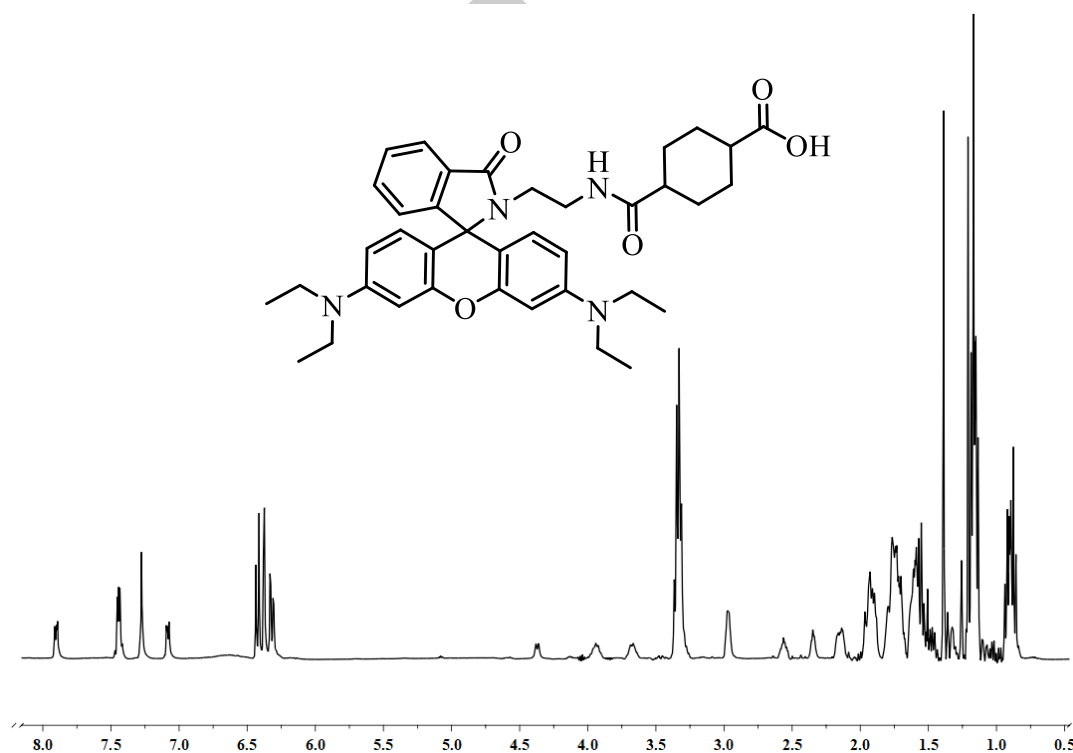
The **L1-L4** were synthesized by a amidation reaction of **Rhen** and 1,3 or 1,4-cyclohexane dicarboxylic acid. DCC and DMAP were used coupling reagent and catalyst in reaction. The reaction was proceeded under N<sub>2</sub> atmosphere at room temperature for 36 hr in DMAF or THF. The product had yield about 52.07-76.19%.

#### 4.2.1.1 Synthesis and characterization of **L1**



**Figure 37** <sup>1</sup>H-NMR spectrum of **L1**.

The **L1** was completely synthesized in condition II, which DCC, DMAP as a coupling reagent and catalyst, respectively. The reaction was set at 60°C in DMF about 3 days. The purification was proceeded by column chromatography 3:1 (hexane:EtOAc) to obtain **L1** (0.0344 g) with 86% yield. The <sup>1</sup>H-NMR spectrum showed characteristic signals of -CH<sub>2</sub> and -CH groups in the region of 1.0-2.1 and 3.5-2.3 ppm, aromatic protons at 7.9-6.2 ppm and amide proton at 5.5 ppm.

4.2.1.2 Synthesis and characterization of **L2****Figure 38**  $^1\text{H}$ -NMR spectrum of **L2**.

The **L2** was completely synthesized in condition III, which DCC, DMAP as a coupling reagent and catalyst, respectively. The reaction was set at 120°C in DMF about 3 days. The purification was proceeded by column chromatography 3:1 (hexane:EtOAc) to obtain **L1** (0.0354 g) with 88.5% yield. The  $^1\text{H}$ -NMR spectrum showed characteristic signals of  $-\text{CH}_2$  and  $-\text{CH}$  groups in the region of 1.0–2.1 and 3.5–2.3 ppm, aromatic protons at 7.9–6.2 ppm and amide proton at 5.5 ppm.

### 4.3 Rhodamine-PEG (L5, L6 and L7)

#### 4.3.1 Synthesis and characterization of PEG-COOH, L5-L7

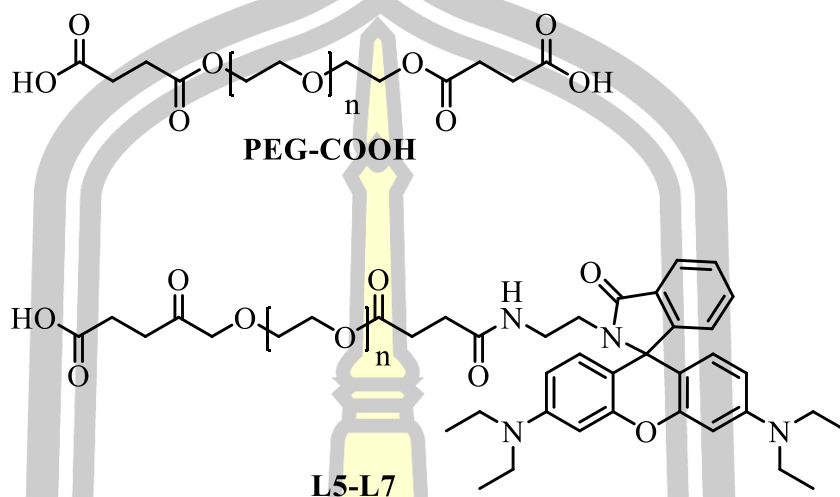


**Figure 39** Structure of **PEG-COOH** and **L5-L7**.

##### 4.3.1.1 Synthesis and characterization of **PEG-COOH**

The **PEG-COOH** was synthesized by coupling reaction of PEG (various molecular weight; 400, 4000 and 6000) and succinic anhydride without solution at high temperature about 6 h. The **PEG-COOH** has a white solid after recrystallization by DCM/Ether. The products given high yield; 97.38, 94.52 and 91.24 % for **PEG400-COOH**, **PEG4000-COOH** and **PEG6000-COOH**, respectively.

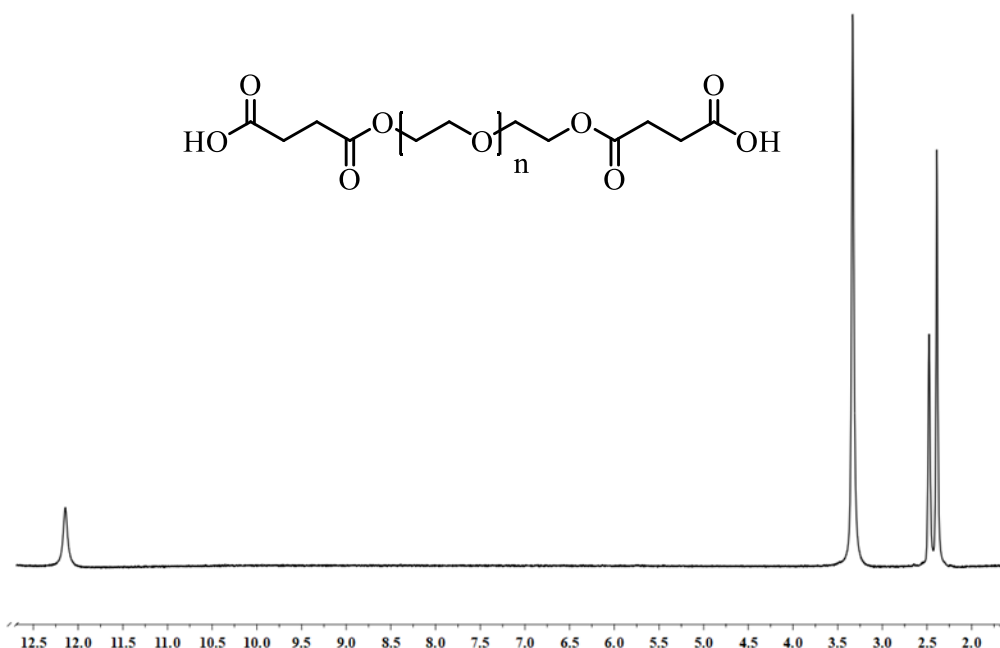


**Figure 40**  $^1\text{H}$ -NMR spectrum of **PEG-COOH**

#### 4.3.1.2 Synthesis and characterization of **L5-L7**

The Rhodamine-PEG (**L5**, **L6**) was synthesized by coupling reaction of **Rhen** and **PEG-COOH**. First step, polyethylene glycol was modified at end by succinic anhydride under  $\text{N}_2$  atmosphere at high temperature without solvent. After 6 hr, polyethylene glycol carboxylic acid was linked with **Rhen** via DCC, DMAP as coupling reagent and catalyst, respectively. After workup give yield about 97.38% of **L5** (pink solid) and 94.52% for **L6** (white film). However, we cannot synthesize the **L7** by use the **L5** and **L6** synthesis method.

พหุ ประทีป ชีวะ

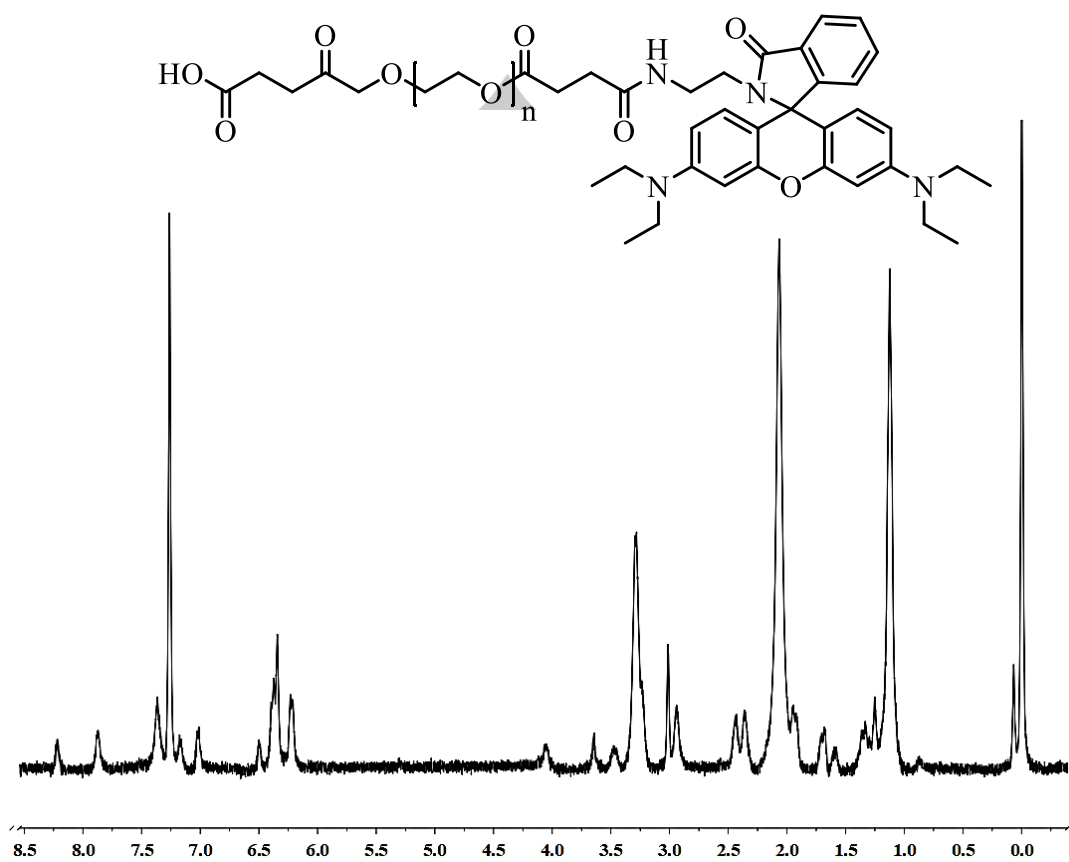
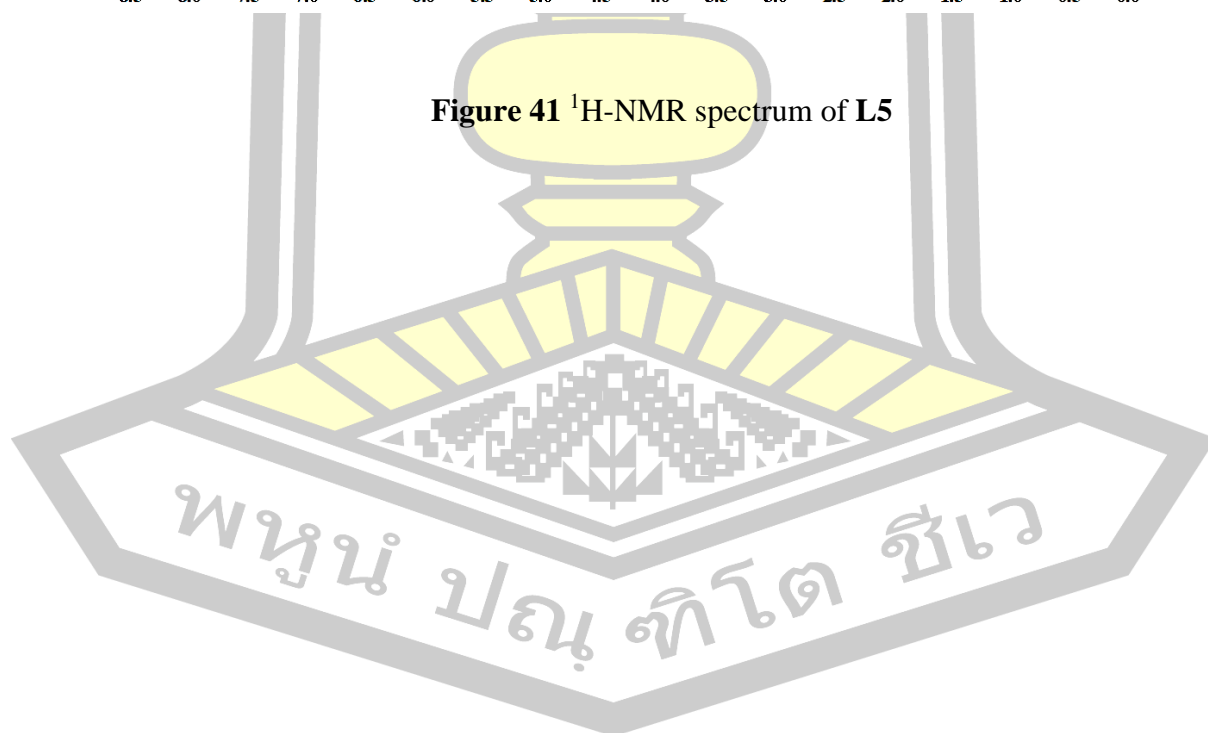
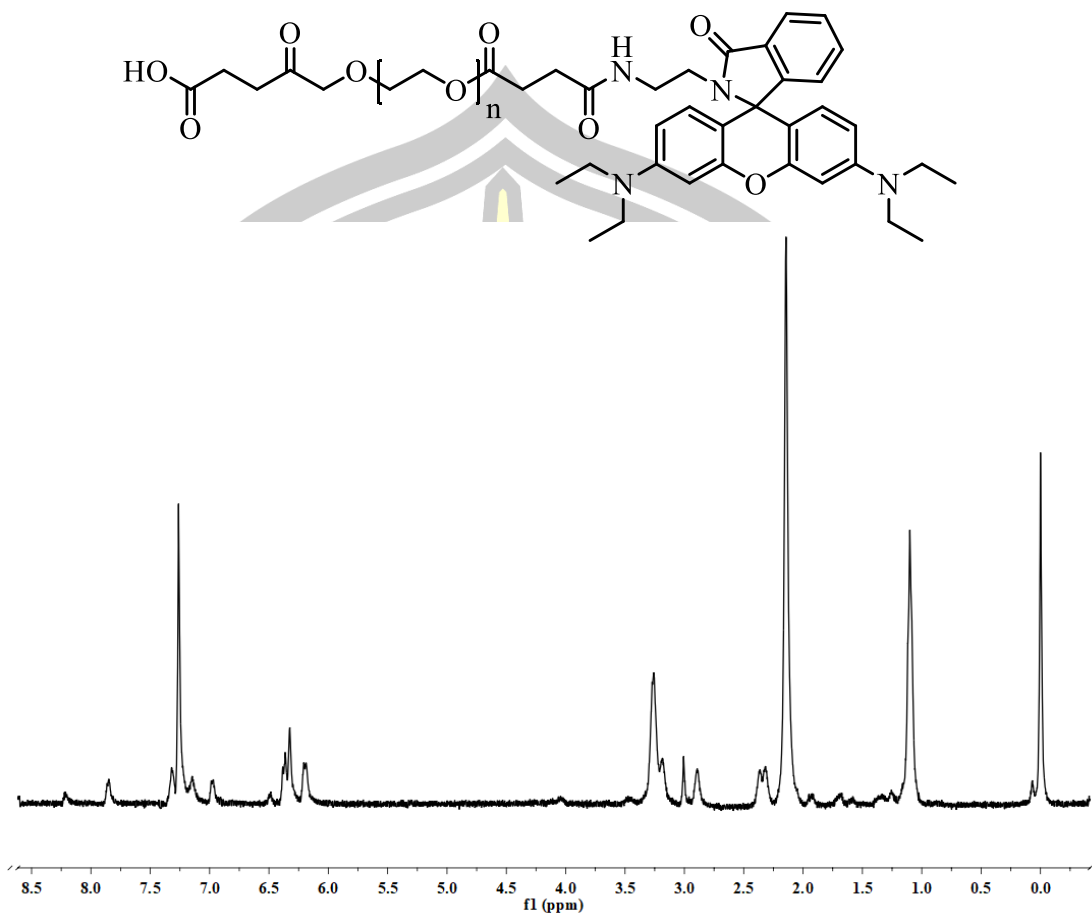


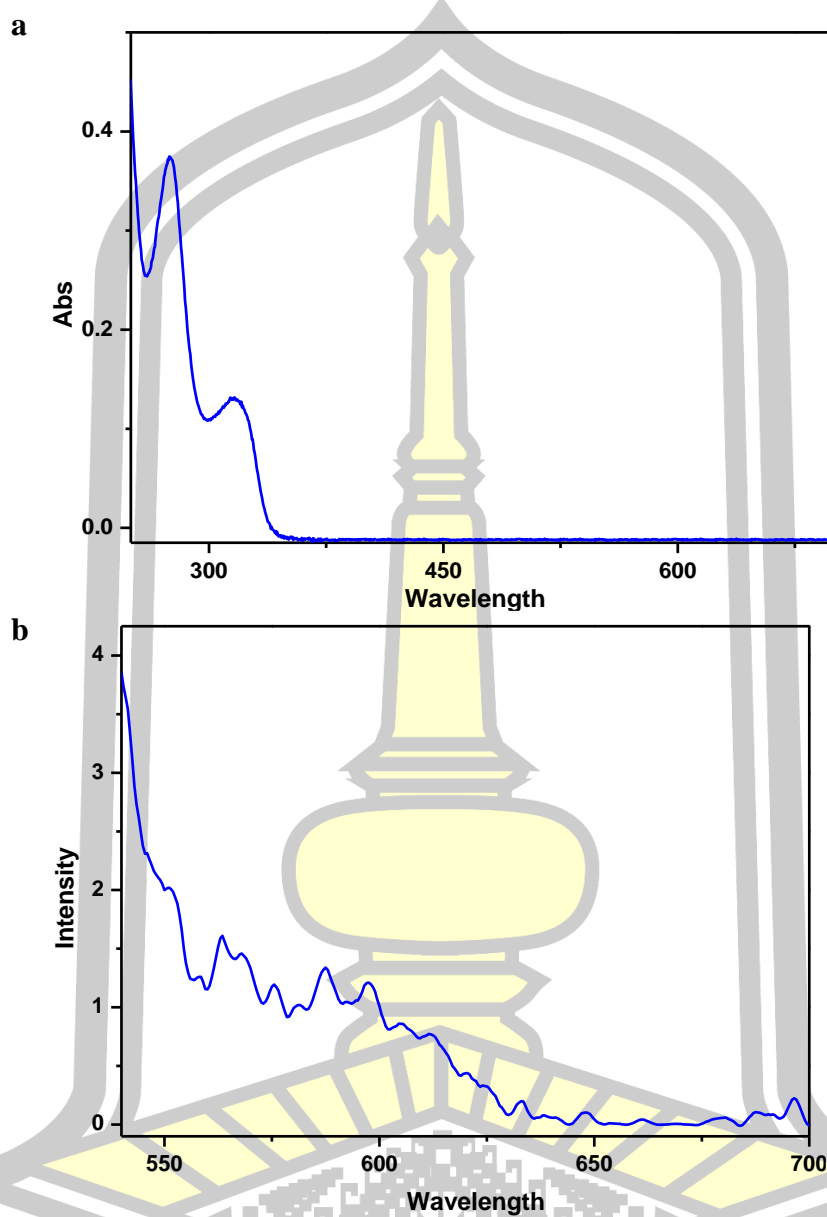
Figure 41 <sup>1</sup>H-NMR spectrum of L5





**Figure 42**  $^1\text{H}$ -NMR spectrum of **L6**.

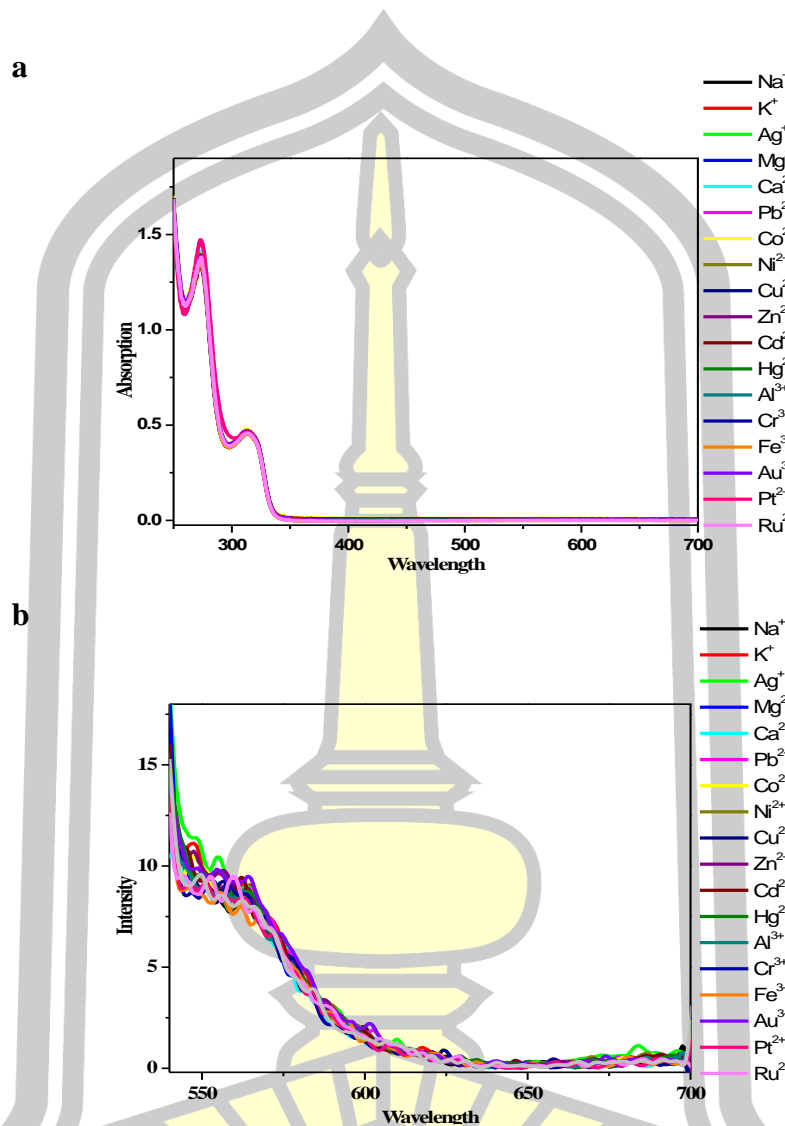
The  $^1\text{H}$ -NMR spectrum of **PEG-COOH** showed characteristic signals of  $-\text{OCH}_2$  and  $=\text{OCH}$  groups at 2.3 and 3.3 ppm and carboxylic acid proton at 12.0 ppm. IR spectrum show  $-\text{OH}$  ( $3830\text{ cm}^{-1}$ ),  $\text{C}=\text{O}$  ( $1631\text{ cm}^{-1}$ ) and  $-\text{CH}$  ( $2928\text{ cm}^{-1}$ ) peak. The  $^1\text{H}$ -NMR spectrum of **L5** showed characteristic signals of  $-\text{CH}_2$  and  $-\text{CH}$  groups in the region of 1.0–2.1 and 2.5–3.0 ppm,  $-\text{OCH}_2$  at 3.28 ppm,  $\text{NH}$  of amide at 4.0 ppm and aromatic protons at 7.0–7.8 ppm. IR spectrum show  $\text{OH}$  ( $3100\text{ cm}^{-1}$ ),  $-\text{NH}$  ( $2931\text{ cm}^{-1}$ ), amide ( $1727\text{ cm}^{-1}$ ) and aromatic ( $1687$  and  $1419\text{ cm}^{-1}$ ) peak. UV-Vis absorption spectrum of **L5** appeared at 270 and 315 nm due to ligand localized  $n-\pi^*$  and  $\pi-\pi^*$  transitions. Moreover, the UV-Vis and fluorescent spectra of **L5** disappeared absorption and emission transition at 400–600 nm region (Figure 43) and the solution has colorless which confirmed that the Rhodamine ring-closed spirolactam form was present in these compounds [58].



**Figure 43** (a) UV-Vis spectrum of **L5** and (b) fluorescence spectrum of **L5**  
 $\lambda_{\text{ex}}=520\text{ nm}$ ,  $\lambda_{\text{em}}=540\text{ nm}$ .

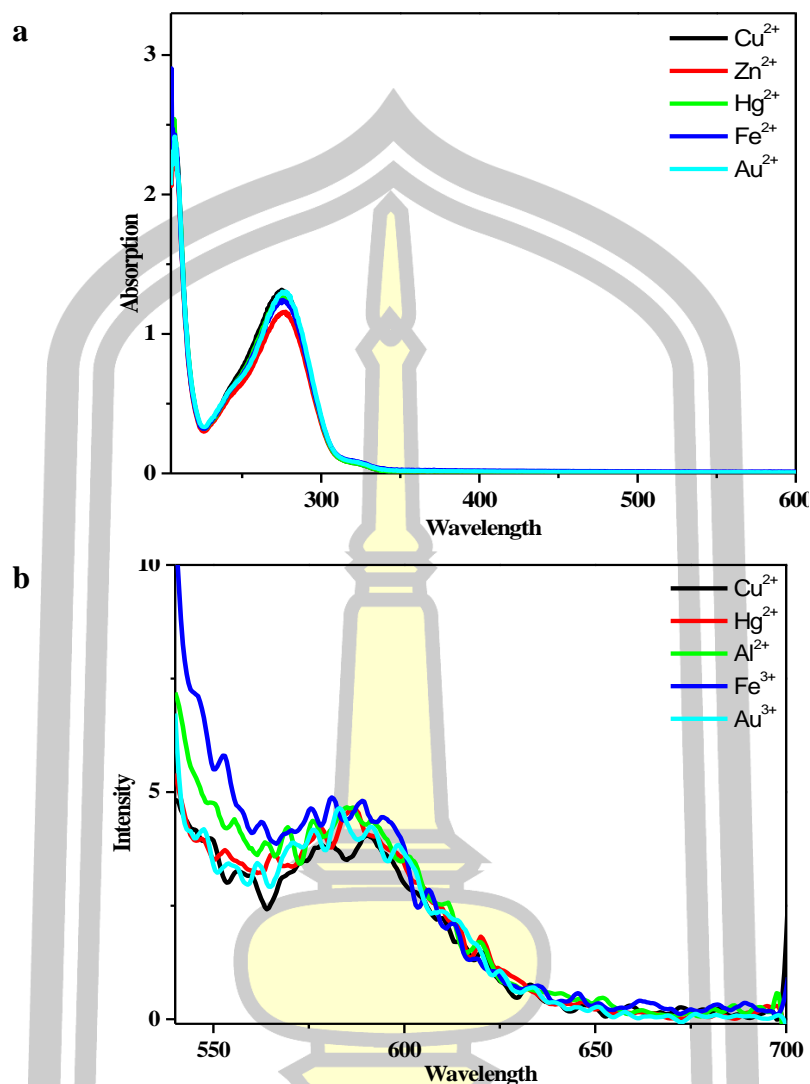


## 4.3.2 Complexation study with metal ions



**Figure 44** (a) UV-Vis spectra (b) fluorescence spectra of **L5** ( $10^{-5}$  M) added various metal ion ( $10^{-5}$  M) in EtOH.

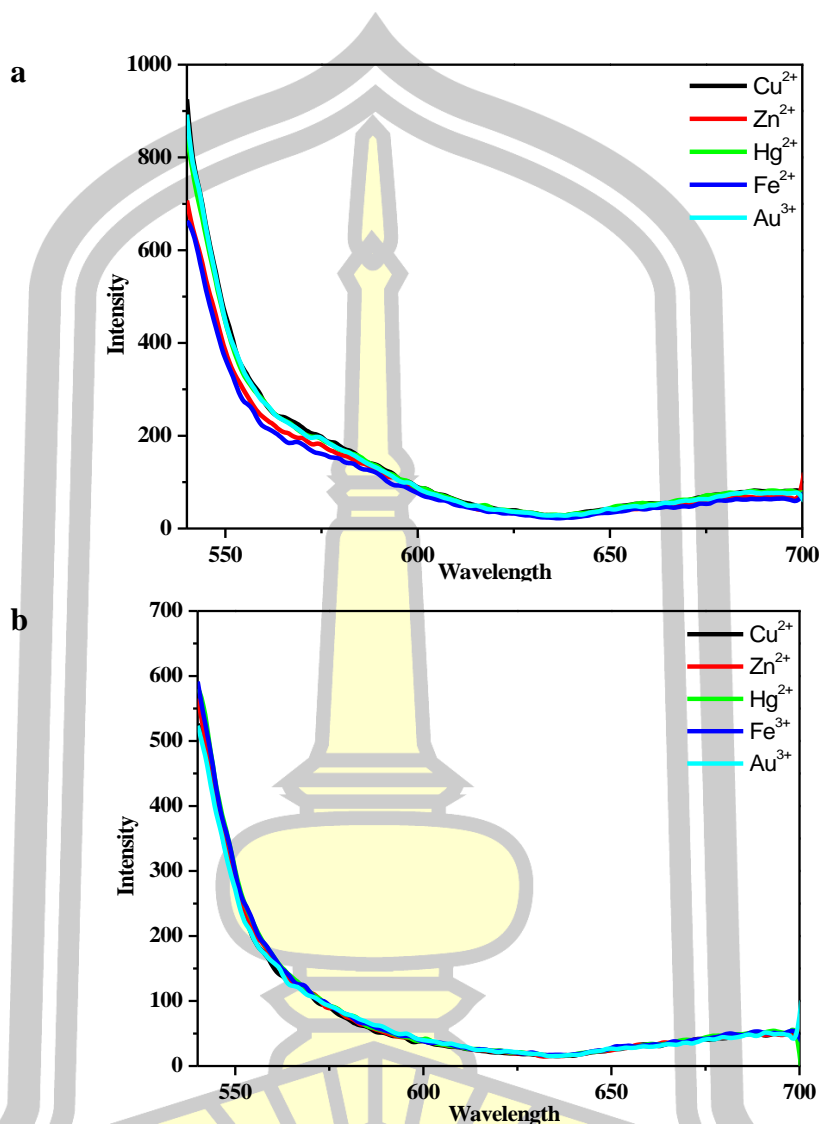
We studied the UV-Vis and fluorescent selectivity of **L5** ( $10^{-5}$  M) with  $10^{-5}$  M of Na<sup>+</sup>, K<sup>+</sup>, Ag<sup>+</sup>, Mg<sup>2+</sup>, Ca<sup>2+</sup>, Pb<sup>2+</sup>, Co<sup>2+</sup>, Ni<sup>2+</sup>, Cu<sup>2+</sup>, Zn<sup>2+</sup>, Cd<sup>2+</sup>, Hg<sup>2+</sup>, Al<sup>3+</sup>, Cr<sup>3+</sup>, Fe<sup>3+</sup>, Au<sup>3+</sup>, Pt<sup>2+</sup> and Ru<sup>2+</sup>. The result is absorption and emission not appeared at 400–600 nm and solution has colorless. Therefore, metal ions cannot induce a spirolactam ring opening.



**Figure 45** (a) UV-Vis (b) fluorescence spectra of **L5** ( $10^{-5}$  M) added various metal ions ( $10^{-3}$  M) in EtOH.

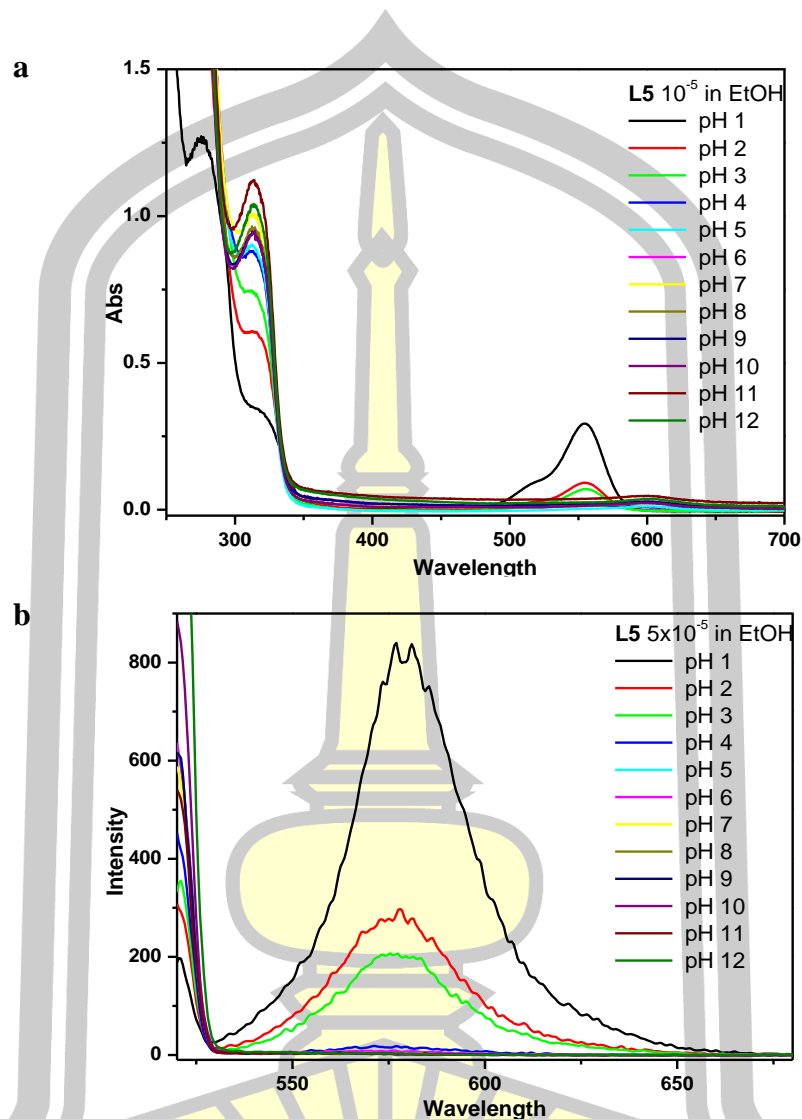
In Figure 45, we studied complexation of **L5** ( $10^{-5}$  M) with high concentration only 5 metal ions such as  $\text{Cu}^{2+}$ ,  $\text{Hg}^{2+}$ ,  $\text{Al}^{3+}$ ,  $\text{Fe}^{3+}$  and  $\text{Au}^{3+}$  ( $10^{-3}$  M). The UV-Vis and fluorescence spectra not changed that confirmed a **L5** not respond with a high concentration of metal ions.

## 4.3.3 Micellar sensor study



**Figure 46** Fluorescence spectra of (a) **L5** ( $5 \times 10^{-5}$  M)+SDS and (b) **L5** ( $5 \times 10^{-5}$  M) +TX-100 added 5 metal ion ( $10^{-3}$  M) in EtOH.

Micellar sensor study, we use SDS and Triton X-100 as a surfactant at critical micelle concentration (CMC). Only 5 metal ions were used in this study such as  $\text{Cu}^{2+}$ ,  $\text{Hg}^{2+}$ ,  $\text{Al}^{3+}$ ,  $\text{Fe}^{3+}$  and  $\text{Au}^{3+}$  ( $10^{-3}$  M). Fluorescence spectra not appear emission at region 550-600 nm. The result indicated that the micellar sensor cannot ring-opened spirolactam.

4.3.4 pH study of **L5**

**Figure 47** (a) UV-Vis spectra (b) fluorescence spectra of **L5** ( $10^{-5}$  M) various pH (1-12).

The pH estimated was studied with different pH in the range of 1.0-12.0 by adjusting the solution of **L5** ( $5 \times 10^{-5}$  M) with various amounts of 0.1 M HCl or NaOH aqueous solution. The solution of **L5** changed from colorless to pink color at low pH (1-4). The UV-Vis and fluorescence spectra of **L5** in pH 1-3 showed a significant increase at 580-600 nm due to  $H^+$ -induced spirolactam ring-opening. Therefore, **L5** can operate effectively at low pH.

#### 4.4 Rhodamine Anhydride (L8)

##### 4.4.1 Synthesis and characterization of L8

The **L8** was readily synthesized in two steps. First, Rhodamine B was converted to Rhodamine ethylenediamine (**Rhen**) using a condensation reaction of Rhodamine B and ethylenediamine under N<sub>2</sub> refluxed for 3 days in small amount of MeOH. Then, amidation reaction between **Rhen** and succinic anhydride was prepared in dry DCM at room temperature for 2 hr to give **L8** in 80% yield. Chemical structure and purity of chemosensor were proven by UV-Vis, fluorescence, ATR-FTIR and SEM techniques.

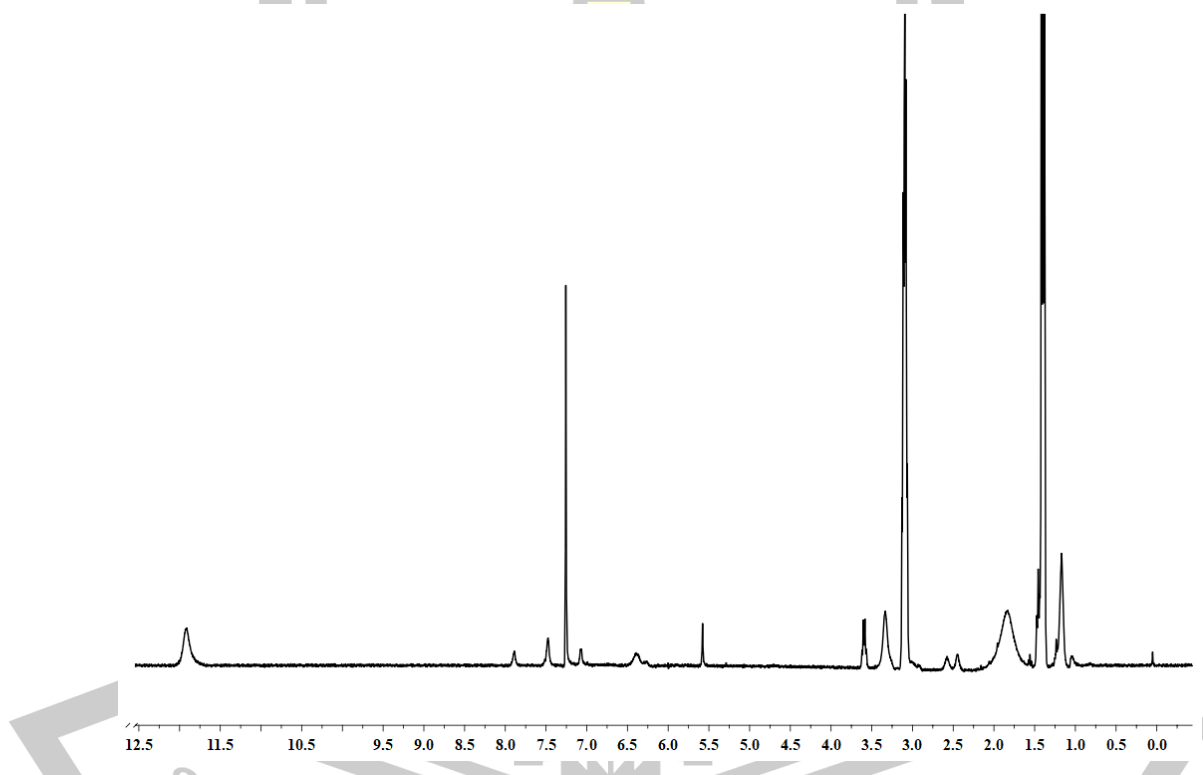


**Figure 48** <sup>1</sup>H-NMR spectrum of **L8**.

From Figure 48, the <sup>1</sup>H-NMR spectrum showed characteristic signals of -CH<sup>2</sup> and -CH groups in the region of 1.0-2.1 and 2.2-2.6 ppm, aromatic protons at 7.8-5.5 ppm and a carboxylic proton in 11-12 ppm, respectively. UV-Vis spectrum of **L8** appeared absorption peaks at 270 and 315 nm due to ligand localized n-π\* and

$\pi$ - $\pi^*$  transitions. Moreover, the UV-Vis absorption and fluorescence emission spectrum of **L8** in the 400-600 nm were not found (Figure 49) and the solution was colorless which confirmed that the Rhodamine ring-closed spirolactam form was presented in these compound [58].

#### 4.4.2 Selectivity of **L8**

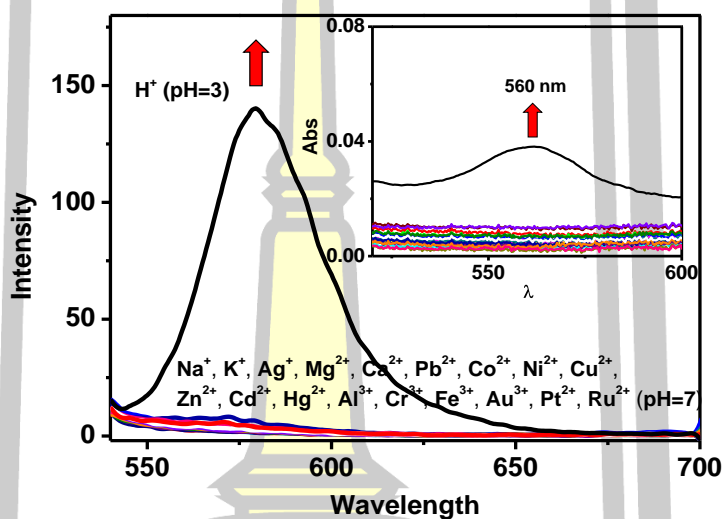


**Figure 49** Fluorescence spectra of **L8** in the present various metal ions (10  $\mu$ M) and proton in MeOH:H<sub>2</sub>O (Ratio 1:1).

Considering that oxygen and nitrogen atoms can bind with various metal ions in solution, it is very important to determine whether other ions have potential to interfere. Upon addition of Na<sup>+</sup>, K<sup>+</sup>, Ag<sup>+</sup>, Mg<sup>2+</sup>, Ca<sup>2+</sup>, Pb<sup>2+</sup>, Co<sup>2+</sup>, Ni<sup>2+</sup>, Cu<sup>2+</sup>, Zn<sup>2+</sup>, Cd<sup>2+</sup>, Hg<sup>2+</sup>, Al<sup>3+</sup>, Cr<sup>3+</sup>, Fe<sup>3+</sup>, Au<sup>3+</sup>, Pt<sup>2+</sup>, Ru<sup>2+</sup> at 10  $\mu$ M to **L8** solutions at neutral pH, no significant changes were observed in the fluorescence spectra as shown in Figure 49. It might be that there are not sufficient coordination sites between various metal ions and **L8**, which cannot induce the spirolactam ring-opening and fluorescence emission from Rhodamine B. However, lower pH (higher concentrations of H<sup>+</sup>) can induce spirolactam ring-opening and fluorescence emission. The results demonstrated that **L8** can selectively detect pH changes in the presence of various metal ions [59].

#### 4.4.3 Characterization of **L8** and application.

To further apply the **L8** as a portable pH sensor, the Rhodamine ethylene diamine anhydride (**L8**) was grafted into activated cellulose papers. In this strategy, the Rhodamine moiety supplied the pH sensitive component via acid induced ring-opening reaction. The successive chemical modification of **L8** on cellulose paper (**CP-L8**) was proven using ATR-FTIR, SEM and solid stated fluorescent. The FTIR spectrum of **CP-L8** exhibited characteristic absorption bands of cellulose material in the region of 3500 (O-H), 2900 (C-H) and 1100 (C-O)  $\text{cm}^{-1}$  and showed absorption bands of Rhodamine at 1648 and 1626 (C=O)  $\text{cm}^{-1}$ . Moreover, the NH amide linked peak at 3450  $\text{cm}^{-1}$  was confirmed the chemical modification of **L8** on cellulose papers. In addition, ATR-FTIR was also used to confirm the binding of the carbonyl group on Rhodamine moieties of **CP-L8** with  $\text{H}^+$ . This was clearly observed that upon addition of  $\text{H}^+$  as shown in Figure 50, the carbonyl stretching band of **CP-L8** at 1647  $\text{cm}^{-1}$  was changed to the lower number (1626  $\text{cm}^{-1}$ ) [60].

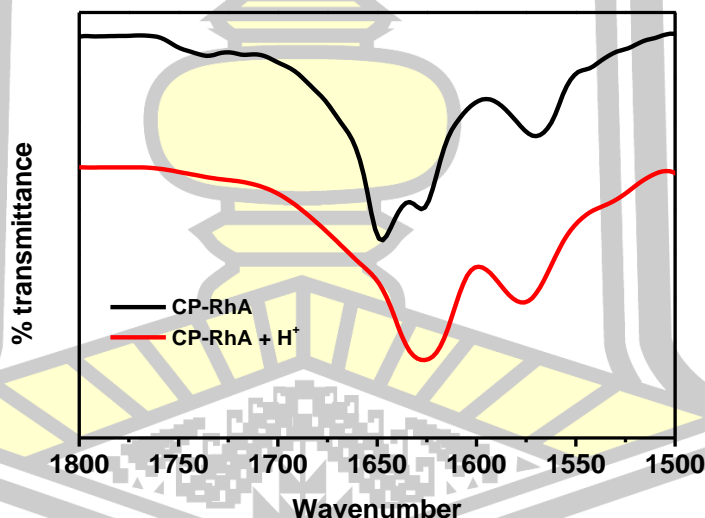


**Figure 50** FT-IR spectra of **CP-L8** and **CP-L8·H<sup>+</sup>**

From the SEM images (Figure 51) of **CP-L8**, the integrity of the cellulose fiber was not degraded by modification. The SEM images showed that the diameter of fibers in original and grafted-papers were in the range of 6-20  $\mu\text{M}$ . The fiber structure



of grafted-paper after treatment with  $H^+$  showed the smooth and dark areas due to the increasing of hydrogen bond networks of **CP-L8** by proton protonation [61,62].

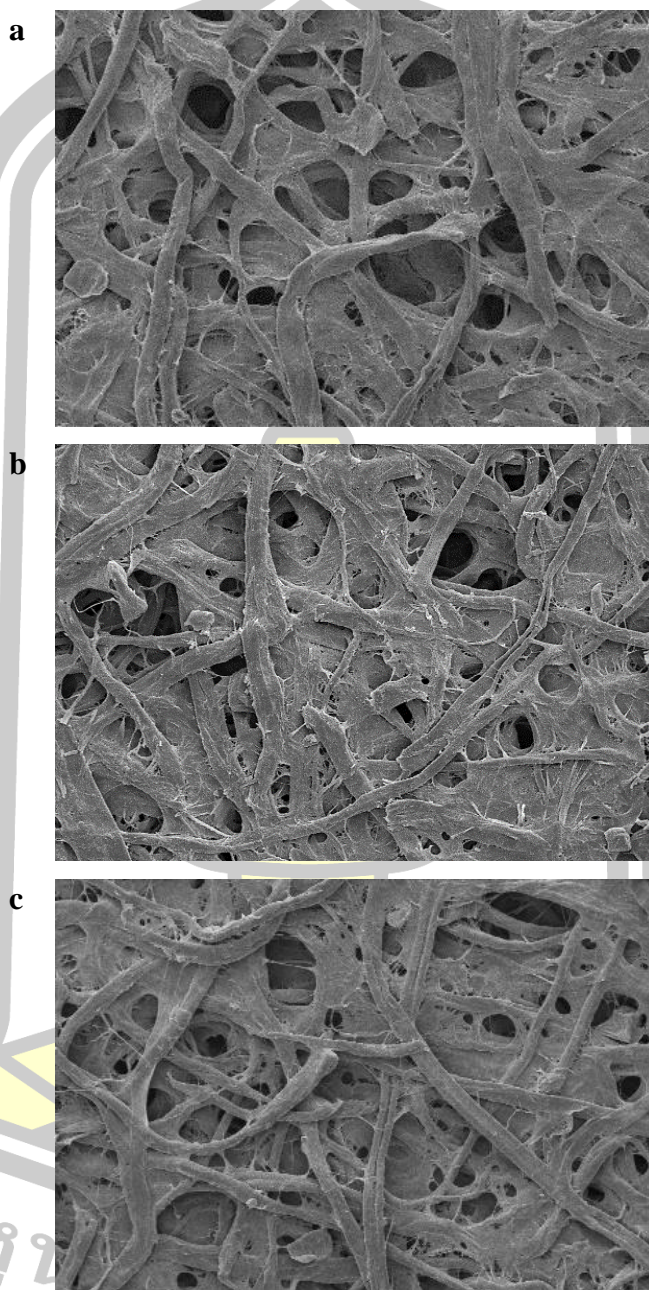


**Figure 51** SEM images of (a) original cellulose paper, (b) paper-grafted **L6** and (c) paper-grafted **L8** treated with  $H^+$ .

In order to evaluate the **CP-L8** for pH detection, a series of visible color changes experiments were carried out with different pH in the range of 1.0-12.0 by adjusting various amount of HCl or NaOH aqueous solution [63]. The fluorescence images of **CP-L8** proceeded under UV light at 365 nm are shown in Figure 52. It was observed that the **CP-L8** displayed an enhanced orange fluorescence at low pH (1-5) due to  $H^+$ -induced spirolactam ring-opening and decreased fluorescence when pH increases. Meanwhile, the fluorescence spectra also showed a significant decrease at 580-600 nm with increasing pH as demonstrated in Figure 53a, similar results were observed under visible-light irradiation, the **CP-L8** showed deep pink color for low pH values and turning to colorless at high pH.

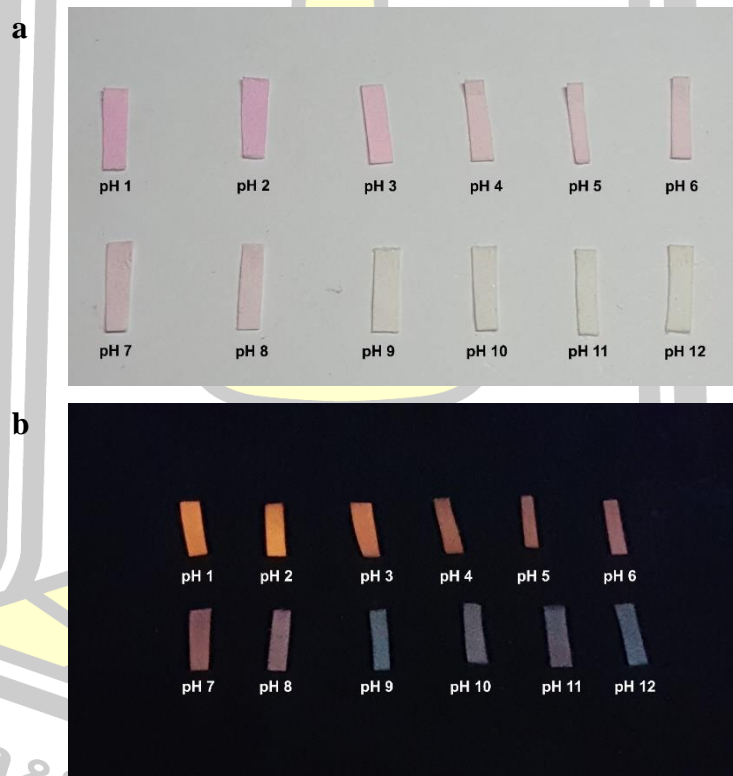


**Figure 52** Colorimetric (a) and fluorescence (b) photographs of **CP-L8** with different pH.

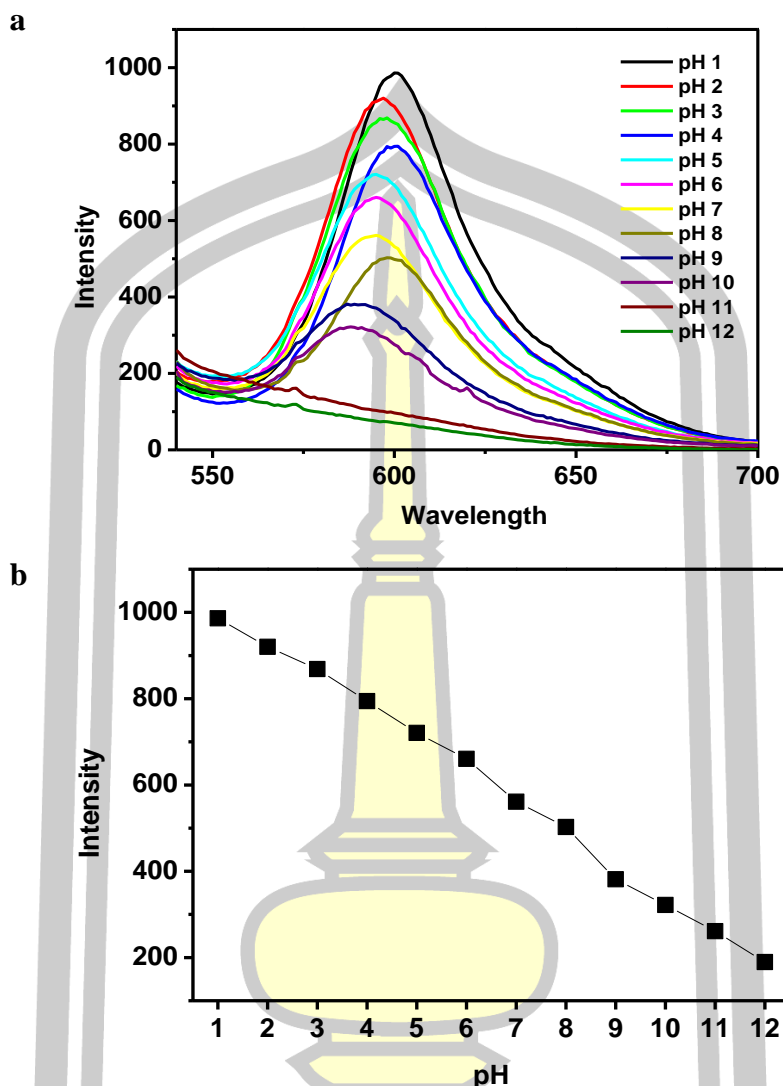


**Figure 53** The solid-state fluorescence spectra of **CP-L8** (a) upon soak in vary pH (1-12) from 540-700 nm, (b) The plot of maximum fluorescence intensities versus pH 1-12 ;  $\lambda_{\text{ex}} = 520$  nm.

#### 4.4.4 Computational calculations of **L8**

Theoretical calculations were performed with density functional theory using the Gaussian 09 software package [64]. The chemical structures, electronic distributions and transitions of **L8** are optimized at the B3LYP/ LanL2DZ level [65]. The electron distributions and orbital energies of the highest occupied molecular orbital (HOMO) and the lowest unoccupied molecular orbital (LUMO) of **L8** in neutral form and protonated form are shown in Figure 53. The HOMO of neutral **L8** was localized

on the xanthenes moiety, while LUMO was mainly contributed by the spirolactam units. However, both HOMO and LUMO of protonated **L8** were changed from neutral one. In addition, a decreased energy band-gap from 0.146 eV to 0.086 eV after protonation was discovered which was in well accordance with the blue-shift spectra [66].

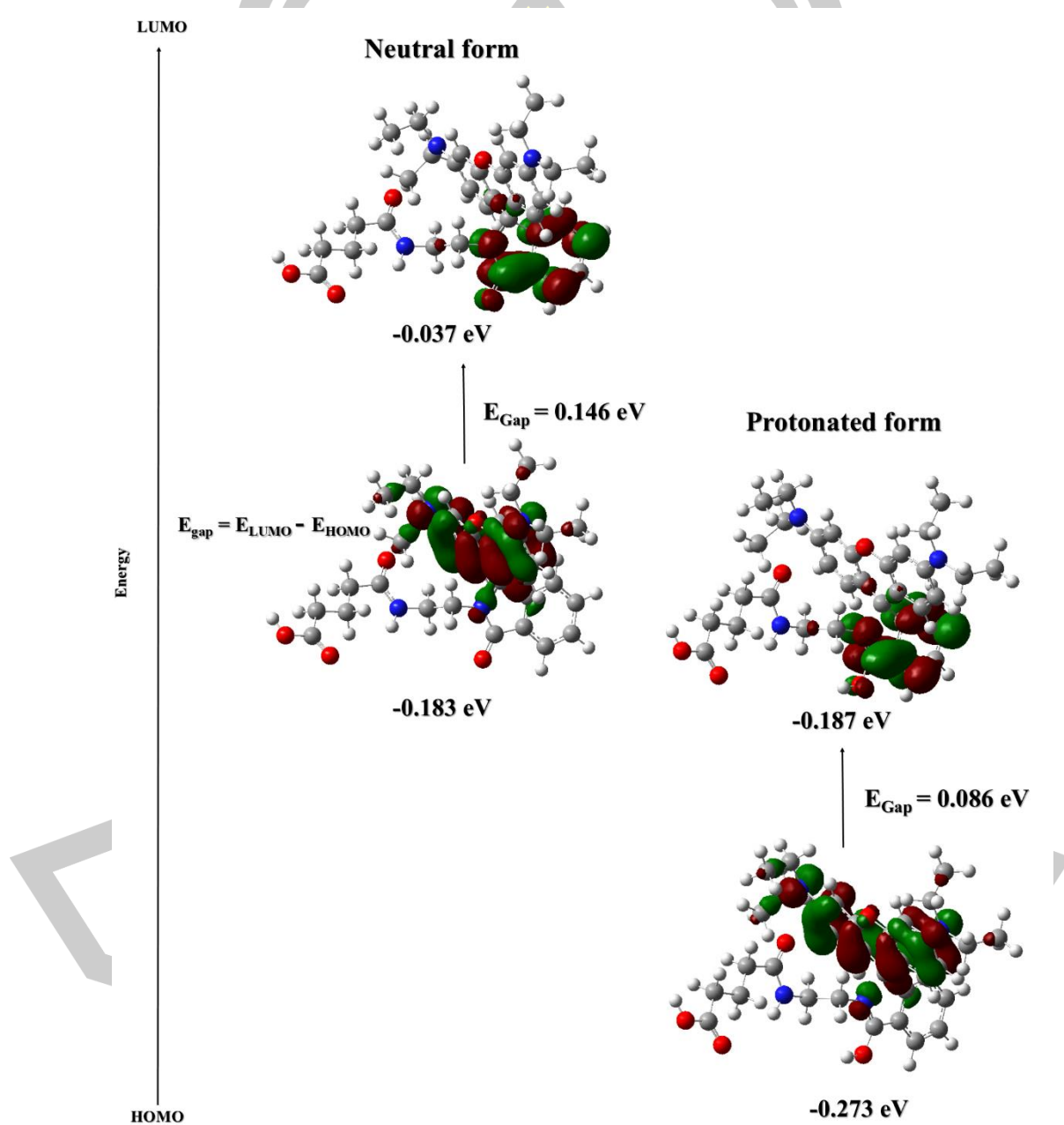


**Figure 54** Molecular orbital energy level of **L8** in natural and protonated form.

## CHAPTER 5

### CONCLUSION

#### 5.1 Rhodamine-cyclohexane (L1-L4)

We have successfully synthesized a Rhodamine cyclohexane (**L1**, **L3**). Chemical structures and purity of **L1** and **L3** were proven by NMR, MS and IR spectroscopies. The **L1** and **L3** will use for further experiment.

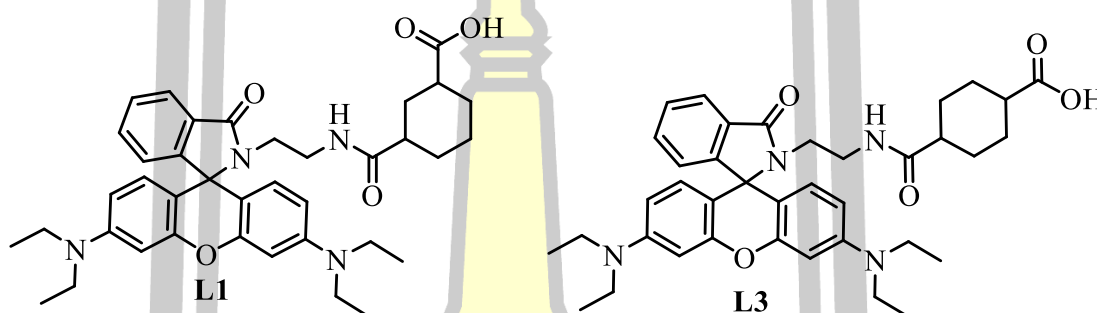
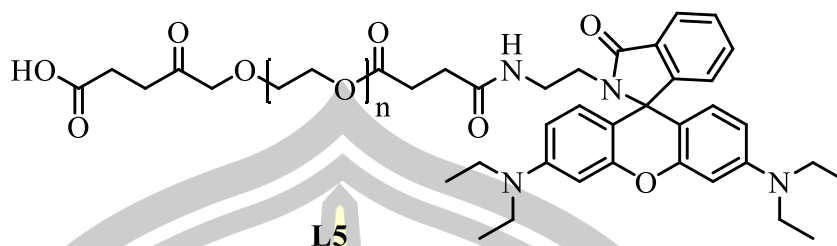


Figure 55 Structure of **L1** and **L3**.

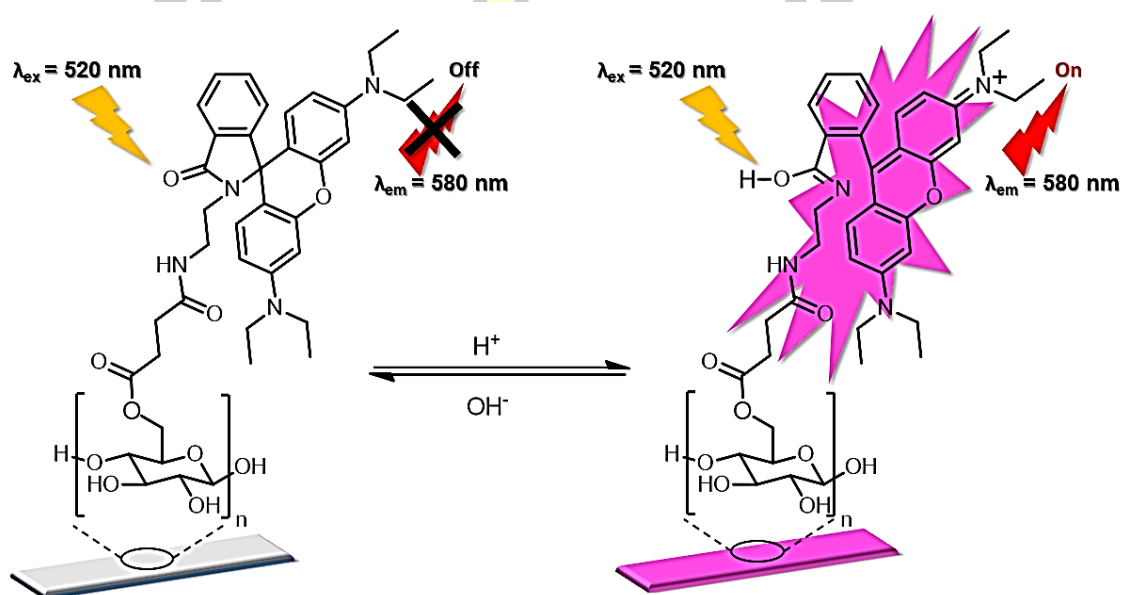
#### 5.2 Rhodamine-PEG (L5)

We have successfully synthesized Rhodamine-PEG (**L5** and **L6**). The chemical position was characterized by UV-Vis, Fluorescence, NMR and IR spectroscopies. **L5** showed absorption spectrum and fluorescence enhancement at 580 nm at low pH (1-3). Moreover, **L5** not respond with various metal ions such as  $\text{Na}^+$ ,  $\text{K}^+$ ,  $\text{Ag}^+$ ,  $\text{Mg}^{2+}$ ,  $\text{Ca}^{2+}$ ,  $\text{Pb}^{2+}$ ,  $\text{Co}^{2+}$ ,  $\text{Ni}^{2+}$ ,  $\text{Cu}^{2+}$ ,  $\text{Zn}^{2+}$ ,  $\text{Cd}^{2+}$ ,  $\text{Hg}^{2+}$ ,  $\text{Al}^{3+}$ ,  $\text{Cr}^{3+}$ ,  $\text{Fe}^{3+}$ ,  $\text{Au}^{3+}$ ,  $\text{Pt}^{2+}$ ,  $\text{Ru}^{2+}$ . However, **L5** will develop for high selectivity and high sensitivity in future.



**Figure 56** Structure of **L5**.

### 5.3 Rhodamine anhydride (**L8**)



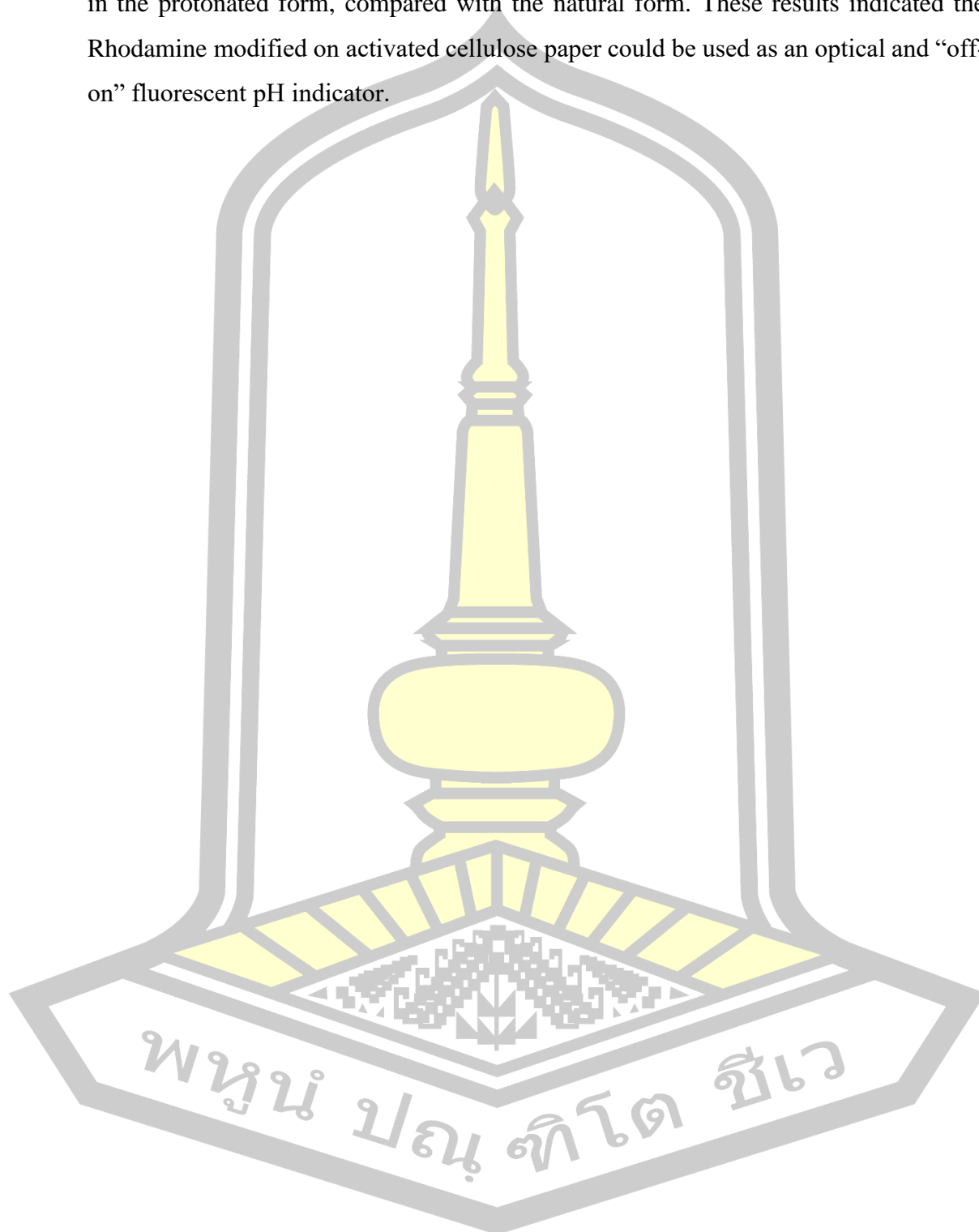
**Scheme 27** Proposed selective detection mechanism of pH optical and fluorescent sensor based on Rhodamine modified on activated cellulose paper (**CP-L8**).

We have successfully synthesized a Rhodamine ethylenediamine anhydride (**L8**) and functionalized it on activated cellulose paper (**CP-L8**) for use as a pH sensor.

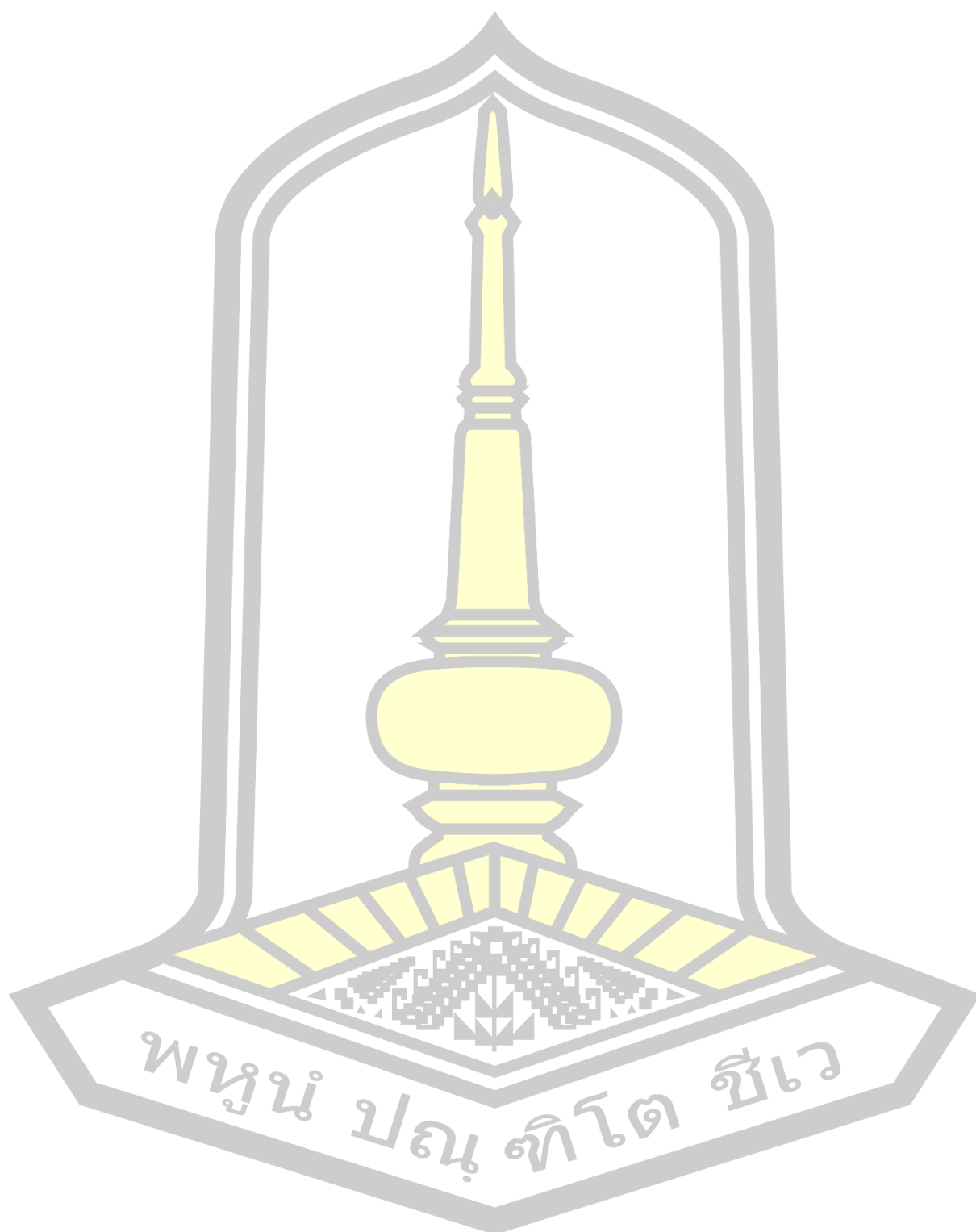
In aqueous solution, **L8** showed fluorescence enhancement at 580 nm upon addition of  $H^+$ . No interference with the pH sensor was observed from various metal ions such as  $Na^+$ ,  $K^+$ ,  $Ag^+$ ,  $Mg^{2+}$ ,  $Ca^{2+}$ ,  $Pb^{2+}$ ,  $Co^{2+}$ ,  $Ni^{2+}$ ,  $Cu^{2+}$ ,  $Zn^{2+}$ ,  $Cd^{2+}$ ,  $Hg^{2+}$ ,  $Al^{3+}$ ,  $Cr^{3+}$ ,  $Fe^{3+}$ ,  $Au^{3+}$ ,  $Pt^{2+}$ ,  $Ru^{2+}$ . To further study its potential as a portable pH sensor, **L8** was immobilized on activated cellulose paper to obtain the composites pH sensor (**CP-L8**). In modified paper (**CP-L8**), the fluorescence image showed high orange fluorescence



and a deep pink color visible at low pH. The DFT calculations showed blue-shift spectra in the protonated form, compared with the natural form. These results indicated the Rhodamine modified on activated cellulose paper could be used as an optical and “off-on” fluorescent pH indicator.



## REFERENCES





## REFERENCES

- [1] Lehn J. M. (1988). Supramolecular chemistry-scope and perspectives molecules, supermolecules, and molecular devices. *Angew. Chemie Int. Ed. Engl.*, 27, 89–112. doi: 10.1002/anie.198800891.
- [2] Dugas, H., & Penney, C. (1981). *Bioorganic chemistry: a chemical approach to enzyme action*. New York, USA: Springer US.
- [3] Lewis J. E. M., Beer P. D., Loeb S. J., & Goldup S. M., (2017). Metal ions in the synthesis of interlocked molecules and materials. *Chem. Soc. Rev.*, 46, 2577–2591. doi: 10.1039/C7CS00199A.
- [4] Atwood J. L., Steed J. W. (2004). *Encyclopedia of Supramolecular Chemistry*. New York, USA: Taylor & Francis publishing
- [5] Lehn, J. (2006). *Molecular Recognition*. In *Supramolecular Chemistry*, New York, USA: Springer US. doi:10.1002/3527607439.ch2
- [6] Wang W. *Introductory Chapter: What is Chemical Sensor?* Retrived from <https://www.intechopen.com/books/progresses-in-chemical-sensor/introductory-chapter-what-is-chemical-sensor->.
- [7] Hou, C., Xiong, Fu, Y. N., Jacquot, C. C., Squier, T. C., & Cao. (2011). H. Turn-on ratiometric fluorescent sensor for Pb<sup>2+</sup> detection. *Tetrahedron Lett.*, 52, 692–2696. doi: 10.1016/j.tetlet.2011.03.075.
- [8] Demchenko, A. P. (2009). *Introduction to fluorescence sensing*, Switzerland: Springer International Publishing.
- [9] Valeur, B. (2001). *Molecular fluorescence: principles and applications*. Weinheim, Germany: Wiley-VCH Verlag GmbH.
- [10] Arden, J., Deltau, G., Huth, V., Kringel, U., Peros, D., & Drexhage, K. H. (1991). Fluorescence and lasing properties of Rhodamine dyes. *J. Lumin.*, 48-49, 352–358. doi: 10.1016/0022-2313(91)90137-K.
- [11] Beija, M., Afonso, C. A. M., & Martinho, J. M. G. (2009). Synthesis and applications of Rhodamine derivatives as fluorescent probes. *Chem. Soc. Rev.*, 38, 2410–2433. doi: 10.1039/B901612K

- [12] Li, H., Guan, H., Duan, X., Hu, Wang, J. G., & Wang, Q. (2013) An acid catalyzed reversible ring-opening/ring-closure reaction involving a cyano-Rhodamine spirolactam. *Org. Biomol. Chem.*, *11*, 1805-1809.  
doi: 10.1039/C3OB27356C.s
- [13] Kim, H. N., Lee, M. H., Kim, H. J., Kim, J. S., & J., Yoon. (2008). A new trend in Rhodamine-based chemosensors: Application of spirolactam ring-opening to sensing ions. *Chem. Soc. Rev.*, *37*,  
doi: 1465-1472.10.1039/B802497A
- [14] Tchounwou, P. B., Yedjou, C. G., Patlolla, A. K., & Sutton, D. J. (2012). Molecular, Clinical and Environmental Toxicology. Luch, A (Eds.), *Heavy Metal Toxicity and the Environment* (pp. 133–164). Berlin, Germany: Springer.
- [15] Agency for Toxic Substances and Disease Registry (ATSDR). (1999). Toxicological profile for Mercury. Atlanta, GA: U.S. Department of Health and Human Services, Public Health Service.
- [16] De Jesus, R. M., , Silva, L. O. B., Castro, J. T., De Azevedo Neto, A. D., De Jesus, R. M., & Ferreira, S. L. C. (2013). Determination of mercury in phosphate fertilizers by cold vapor atomic absorption spectrometry. *Talanta*, *106*, 293-297,  
doi: 10.1016/j.talanta.2012.11.001
- [17] Chai, X., Chang, X., Hu, Z., He, Q., Z., & Li, Z. (2010). Solid phase extraction of trace Hg(II) on silica gel modified with 2-(2-oxoethyl)hydrazine carbothioamide and determination by ICP-AES. *Talanta*, *82*, 1791-1796,  
doi: 10.1016/j.talanta.2010.07.076
- [18] Aldroobi, K. S. A., Shukri, A., Bauk, S., Munem, E. M. A., & Abuarra, A. M. A. (2013). Determination of arsenic and mercury level in scalp hair from a selected population in Penang, Malaysia using XRF technique. *Radiat. Phys. Chem.*, *91*, 9-14. doi: 10.1016/j.radphyschem.2013.06.004
- [19] Srineetha, U & Venkata Reddy, M & Bhaskar, Matcha. (2014). Effect of Environmental acidic pH on Oxygen Consumption in Different stages of Fish, *Cyprinus carpio*(L). *8*. 2319-2399.

- [20] Copatti, C., Garcia, L., Kochhann, D., Cunha, M., Becker, A., & Baldisserotto, B. (2011). Low water hardness and pH affect growth and survival of silver catfish juveniles. *Ciência Rural*, 41, 1482-1487.  
doi: 10.1590/S0103-84782011005000101.
- [21] Mihajlović, R. P., Jakšić, L. N., & Džudović, R. M. (2006). Coulometric generation of acids and bases for acid-base titrations in non-aqueous solvents. *Anal. Chim. Acta*, 557, 37-44. doi: 10.1016/j.aca.2005.10.015
- [22] Maskula, S., Nyman, J., & Ivaska, A. (2000). Titration of strong and weak acids by sequential injection analysis technique. *Talanta*, 52, 91-9.  
doi: 10.1016/S0039-9140(00)00323-4.
- [23] Zuliani, C., Matzeu, G., & Diamond, D. (2014). A potentiometric disposable sensor strip for measuring pH in saliva. *Electrochim. Acta*, 132, 292-296.  
doi: 10.1016/j.electacta.2014.03.140.
- [24] Ke, J., Dou, H., Zhang, X., Uhagaze, D. S., Ding, X., & Dong, Y. (2016). Determination of pKa values of alendronate sodium in aqueous solution by piecewise linear regression based on acid-base potentiometric titration. *J. Pharm. Anal.*, 6, 404-409. doi: 10.1016/j.jpha.2016.07.001.
- [25] Georgiev, N. I., Dimitrova, M. D., Krasteva, P. V., & Bojinov, V. B., (2017). A novel water-soluble 1,8-naphthalimide as a fluorescent pH-probe and a molecular logic circuit. *J. Lumin.*, 187, 383-391.  
doi: 10.1016/j.jlumin.2017.03.049.
- [26] Chen, H. X., Wang, X. D., Song, X. H., Zhou, T. Y., Jiang, Y. Q., & Chen, X. (2010). Colorimetric optical pH sensor production using a dual-color system. *Sens. Actuators, B.*, doi: 10.1016/j.snb.2010.01.068.
- [27] Wang, X. Y., Huang, D. W., Niu C. G., Guo, L. J., Cui, J. J., Hu, L. Y., Zeng, G. M. (2016). An internal reference fluorescent pH sensor with two pH-sensitive fluorophores carrier. *Sens. Actuators, B.*, 234, 593-601,  
doi: 10.1016/j.snb.2016.05.036.
- [28] Shiraishi, T., Saito, T., Kagechika, H., & Hirano, T., (2014). Development of a novel fluorescent sensor to detect a specific range of pH. *Tetrahedron Lett.*, 55, 6784-6786. doi: 10.1016/j.tetlet.2014.10.037.

- [29] Tian, M., Peng, X., Fan, J., Wang, J., & Sun, S. (2012). A fluorescent sensor for pH based on Rhodamine fluorophore. *Dye. Pigment.*, 95, 112-115. doi: 10.1016/j.dyepig.2012.03.008.
- [30] Monahan, C., Bien, J. T., Smith, B. D. (1998). Fluorescence sensing due to allosteric switching of pyrene functionalized functionalized cis-cyclohexane-1, 3-dicarboxylate decreases. *Chem. Commun.*, 0, 431-432. doi: 10.1039/A705445I.
- [31] Li, Z. B., Lin, J., Sabat, M., Hyacinth, M., & Pu, L. (2007). Enantioselective fluorescent recognition of chiral acids by cyclohexane-1,2-diamine-based bisbinaphthyl molecules. *J. Org. Chem.*, 72, 4905–4916. doi: 10.1021/jo0704715.
- [32] Costero, A. M., Colera, M., Gaviña, P., Gil, S., & Llaosa, Ú. (2008). Fluorescent chemosensors based on cyclohexane: selective sensing of succinate and malonate versus their longer or shorter homologues. *Tetrahedron.*, 64, 7252-7257. doi:10.1016/j.tet.2008.05.064.
- [33] Costero, A. M., Colera, M., Gavina, P., Gil, S., Kubinyi, M., Pal, K., & Kallay, M. (2008). Chiral cyclohexane based fluorescent chemosensors for enantiomeric discrimination of aspartate. *Tetrahedron*, 64, 3217–3224. doi:10.1016/j.tet.2008.01.085.
- [34] Sahana, S., Mishra, G., Sivakumar, S., & Bharadwaj, P. K. (2018). Rhodamine - cyclohexane diamine based 'turn-on' fluorescence chemosensor for Cr<sup>3+</sup>: Photophysical & confocal cell imaging studies. *J. Photochem. Photobiol. A Chem.*, 351, 42–49. doi: 10.1016/j.jphotochem.2017.10.004.
- [35] Liu, T., & Liu, S. (2011). Responsive polymers-based dual fluorescent chemo sensors for Zn<sup>2+</sup> ions and temperatures working in purely aqueous media. *Anal. Chem.*, 83, 2775–2785. doi: 10.1021/ac200095f.
- [36] Joshi, B. P., Park, J. Y., & Lee, K. H. (2014). Recyclable sensitive fluorimetric detection of specific metal ions using a functionalized PEG-PS resin with a fluorescent peptide sensor, *Sens. Actuators, B. Chem.*, 191, 122–129. doi: 10.1016/j.snb.2013.09.075

- [37] Xu, Z., Li, J., Guan, S., Zhang, L., & Dong, C., (2015). Highly selective and sensitive fluorescence chemosensor for the detection of palladium species based on Tsuji-Trost reaction. *Spectrochim. Acta Part a Mol. Biomol. Spectrosc.*, 148, 7-11, doi: 10.1016/j.saa.2015.03.130.
- [38] Li, G., Tao, F., Liu, Q., Wang, L., Wei, Z., Zhu, F., Chen, W., Sun, H., & Zhou, Y. (2016). A highly selective and reversible water-soluble polymer based-colorimetric chemosensor for rapid detection of  $\text{Cu}^{2+}$  in pure aqueous solution. *New J. Chem.*, 40, 4513–4518. doi: 10.1039/c5nj03526k.
- [39] Du, W., Cheng, Y., Shu, W., & Qi, Z. (2017). A novel Rhodamine-based fluorescence chemosensor containing polyether for mercury (ii) ions in aqueous solution. *Quim. Nova*, 40, 733-738. doi: 10.21577/0100-4042.20170060.
- [40] Best, Q. A., Xu, R., McCarroll, M. E., Wang, L., & Dyer, D. J. (2010). Design and Investigation of a Series of Rhodamine-based fluorescent probes for optical measurements of pH. *Org. Lett*, 12, 3219-3221. doi: 10.1021/ol1011967.
- [41] Hu, Z. Q., Li, M., Liu, M. D., Zhuang, W. M., & Li, G. K. (2013). A highly sensitive fluorescent acidic pH probe based on Rhodamine B diethyl-2-aminobutenedioate conjugate and its application in living cells. *Dye. Pigment.*, 96, 71-75. doi: 10.1016/j.dyepig.2012.07.012.
- [42] Lv, H. S., Huang, S. Y., Zhao, B. X., & Miao, J. Y. (2013). A new Rhodamine B-based lysosomal pH fluorescent indicator. *Anal. Chim. Acta.*, 788, 177-182. doi: 10.1016/j.aca.2013.06.038.
- [43] Tan, J. L., Zhang, M. X., Zhang, F., Yang, T. T., Liu, Y., Li, Z. B., & Zuo, H. (2015). A novel 'off-on' colorimetric and fluorescent Rhodamine-based pH chemosensor for extreme acidity. *Spectrochim. Acta - Part A Mol. Biomol. Spectrosc.*, 140, 489-494. doi: 10.1016/j.saa.2014.12.110.

- [44] Lee, D., Swamy, K. M. K., Hong, J., Lee, S., & Yoon, J. (2018). A Rhodamine-based fluorescent probe for the detection of lysosomal pH changes in living cells. *Sensors Actuators, B Chem.*, 266, 416-421. doi: 10.1016/j.snb.2018.03.133.
- [45] Ghosh, K., Sarkar, T., & Samadder, A. (2012). A Rhodamine appended tripodal receptor as a ratiometric probe for  $\text{Hg}^{2+}$  ions. *Org. Biomol. Chem.*, 10, 3236-3243. doi: 10.1039/c2ob00009a.
- [46] Zhanga, D., Li, M., Wang, M., Wang, J., Yanga, X., Ye, Y., & Zhao, Y. (2013). A Rhodamine-phosphonate off-on fluorescent sensor for  $\text{Hg}^{2+}$  in natural water and its application in live cell imaging. *Sensors Actuators, B Chem.*, 177, 997-1002. doi: 10.1016/j.snb.2012.11.080.
- [47] Ghosh, K., Sarkar, T., & Majumdar, A. (2013). Rhodamine-labeled sensor bead as a colorimetric and fluorometric dual assay for  $\text{Hg}^{2+}$  ions in water. *Asian J. Org. Chem.*, 2, 157-163. doi: 10.1002/ajoc.201200134.
- [48] Yan, F., Wang, M., Cao, D., Yang, N., Ma, B., & Chen, L. (2013). Recognition preference of Rhodamine derivative bearing phthalimido Gly for  $\text{Hg}^{2+}$  by UV-Vis and fluorescence spectroscopy. *J. Spectrosc.*, 1, 1-7. doi: 10.1155/2013/878234.
- [49] Ghosh, K., Sarkar, T., & Majumdar, A. (2013). Rhodamine-labelled new architecture for dual sensing of  $\text{Co}^{2+}$  and  $\text{Hg}^{2+}$  ions. *Tetrahedron Lett.*, 54, 6464-6468. doi: 10.1016/j.tetlet.2013.09.062.
- [50] Bordini, J., Calandrelli, I., Silva, G. O., Ferreira, K. Q., Leitão-Mazzi, D. P. S., Espreafico, E. M., & Tfouni, E. (2013). A Rhodamine-B-based turn-on fluorescent sensor for biological iron(III). *Inorg. Chem. Commun.*, 35, 255-259. doi: 10.1016/j.inoche.2013.06.017.
- [51] Zhang, D., Li, M., Jiang, Wang, Y. C., Wang, Z., Ye, Y., & Zhao, Y. (2013). A new sensitive and selective chromogenic and fluorescent chemodosimeter for  $\text{Hg}(\text{II})$  in aqueous media and its application in live cell imaging. *Dye. Pigment.*, 99, 607-612. doi: 10.1016/j.dyepig.2013.06.021.



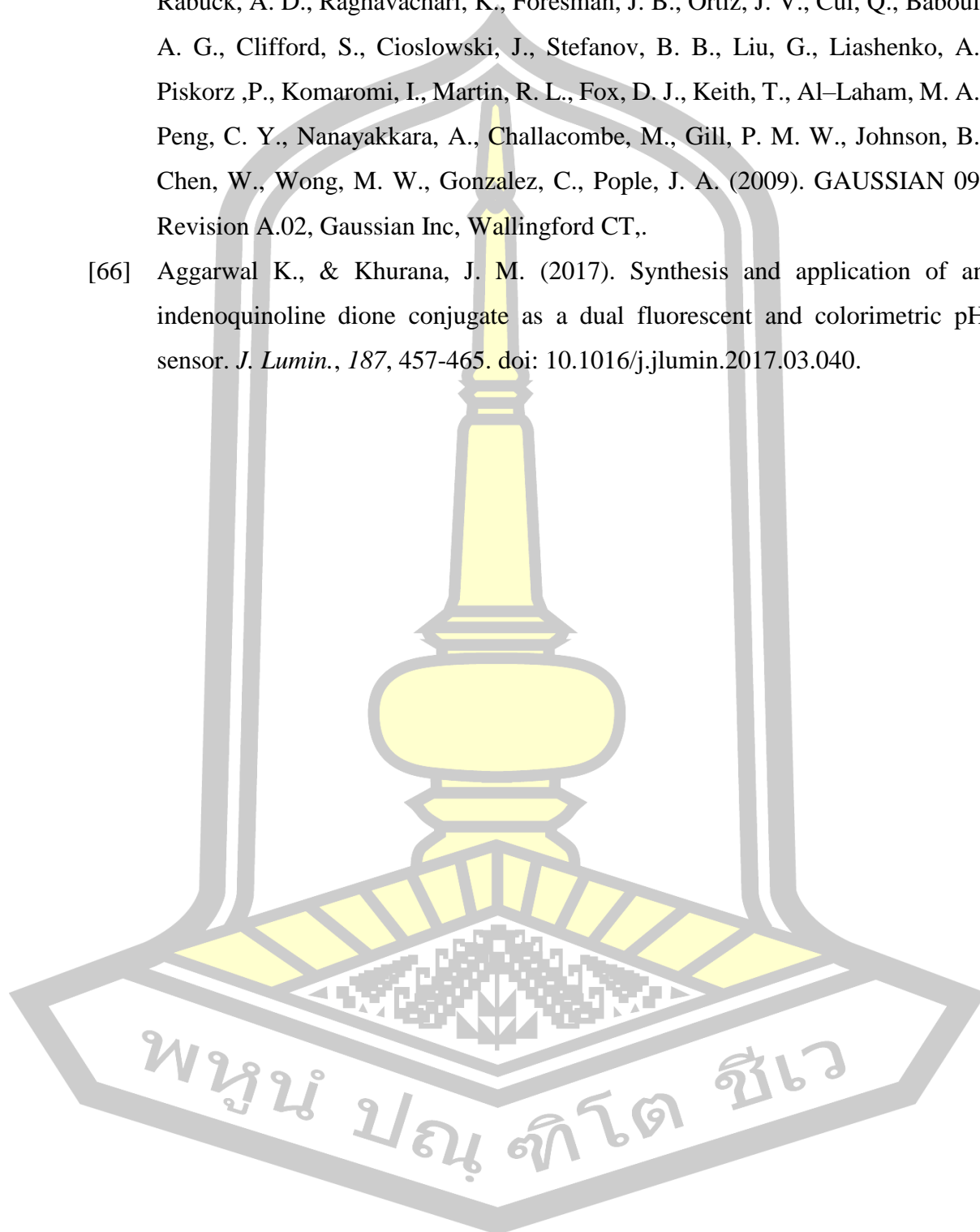
- [52] Liu, Y., Liu, Y., Xu Z., Yang, L., Wang, Z., Zhang, D., & Ye, Y. (2016). A Rhodamine-based 'turn-on' fluorescent probe for  $\text{Fe}^{3+}$  in aqueous solution and its application in bioimaging. *Monatsh. Chem.*, 147, 311-317. doi: 10.1007/s00706-015-1521-9.
- [53] Jiang, C., Wang, M., Wang, Y., Tang, X., Zhang, Y., Zhang, H., Ma, L., & Wang, J., (2017). Synthesis and evaluation of two novel Rhodamine-based fluorescence probes for specific recognition of  $\text{Fe}^{3+}$  ion. *Tetrahedron Lett.*, 58, 2560-2565. doi: 10.1016/j.tetlet.2017.05.052.
- [54] Srisuratsiri, P., Kanjanasirirat, P., Chairongdua, A., & Kongsaree, P. (2017). Reversible Rhodamine-alkyne  $\text{Au}^{3+}$ -selective chemosensor and its bioimaging application. *Tetrahedron Lett.*, 58, 3194-3199. doi: 10.1016/j.tetlet.2017.07.014.
- [55] Kaewtong, C., Niamsa, N., Wannoo, B., Morakot, N., Pulpoka, B., & Tuntulani, T. (2014). Optical chemosensors for  $\text{Hg}^{2+}$  from terthiophene appended Rhodamine derivatives: FRET based molecular and in situ hybrid gold nanoparticle sensors. *New J. Chem.*, 38, 3831-3839. doi: 10.1039/c4nj00412d.
- [56] Bao, X., Cao, Q., Xu, Y., Gao, Y., Xu, Y., Nie, X., Zhou, B., Pang, T., & Zhu, J. (2015). Synthesis and evaluation of a new Rhodamine B and Di(2-picoly)amine conjugate as a highly sensitive and selective chemosensor for  $\text{Al}^{3+}$  and its application in living-cell imaging. *Bioorganic Med. Chem.*, 23, 694-702. doi: 10.1016/j.bmc.2014.12.070.
- [57] Dietrich, M., Delaittre, G., Blinco, J. P., Inglis, A. J., Bruns, M., & Barner-Kowollik, C. (2012). Photoclickable surfaces for profluorescent covalent polymer coatings. *Adv. Funct. Mater.*, 22, 304-312. doi: 10.1002/adfm.201102068.
- [58] Bag, B., & Pal, A. (2011). Rhodamine-based probes for metal ion-induced chromo-/fluorogenic dual signaling and their selectivity towards  $\text{Hg(II)}$  ion. *Org. Biomol. Chem.*, 9, 4467-4480. doi: 10.1039/c0ob01179g.

- [59] Tian, M., Peng, X., Fan, J., Wang, J., & Sun, S. (2012). A fluorescent sensor for pH based on Rhodamine fluorophore. *Dye. Pigment.*, 95, 112-115.  
doi: 10.1016/j.dyepig.2012.03.008.
- [60] Kaewtong, C., Niamsa, N., Pulpoka, B. & Tuntulani, T. (2014). Reversible sensing of aqueous mercury using a Rhodamine-appended polyterthiophene network on indium tin oxide substrates. *RSC Adv.*, 4, 52235-52240.  
doi: 10.1039/c4ra11353e.
- [61] Rull-Barrull, J., D'Halluin, M., Le Grogne, E., & Felpin, F. X. (2016). Chemically-modified cellulose paper as smart sensor device for colorimetric and optical detection of hydrogen sulfate in water. *Chem. Commun.*, 52, 2525-2528.  
doi: 10.1039/c5cc09889k.
- [62] D'Halluin, M., Rull-Barrull, J., Bretel, G., Labrugère, C., Le Grogne, E., & F., Felpin, X. (2017). Chemically modified cellulose filter paper for heavy metal remediation in water. *ACS Sustain. Chem. Eng.*, 5, 1965-1973.  
doi: 10.1021/acssuschemeng.6b02768.
- [63] Yan, Z., Zhang, X., Bao, C., H., Tang, Zhao, Q., Hu, L., & You, J. (2018). A novel luminol derivative and its functionalized filter-paper for reversible double-wavelength colorimetric pH detection in fruit juice. *Sens. Actuators, B. Chem.*, 262, 869-875. doi: 10.1016/j.snb.2018.02.100.
- [64] Li, Z., Li, L. J., Sun, T., Liu, L., & Xie, Z. (2016). Benzimidazole-BODIPY as optical and fluorometric pH sensor. *Dye. Pigment.*, 128, 165-169.  
doi: 10.1016/j.dyepig.2016.01.029.
- [65] Frisch, M. J., Trucks, G. W., Schlegel, H. B., Scuseria, G. E., Robb, M.A., Cheeseman, J. R., Montgomery, J. A. Jr., Vreven, T., Kudin, K. N., Burant, J. C., Millam, J. M., Iyengar, S. S., omasi, J., Barone, TV., Mennucci, B., Cossi, M., Scalmani, G., Rega, N., Petersson, G. A., Nakatsuji, H., Hada, M., Ehara, Toyota, M., Fukuda, K. R., Hasegawa, J., Ishida, M., Nakajima, T., Honda, Kitao, Y. O., Nakai, H., Klene, M., Li, X., Knox, J. E., Hratchian, H. P., Cross, J. B., Bakken, V., Adamo, C., Jaramillo, J., Gomperts, R., Stratmann, R. E., Yazyev, O., Austin, A. J., Cammi, R., Pomelli, C., Ochterski, J. W., Ayala, P. Y., Morokuma, K., Voth, G. A., Salvador, P., Dannenberg, J. J., Zakrzewski, V.



G., Dapprich, S., Daniels, A. D., Strain, M. C., Farkas, O., Malick, D. K., Rabuck, A. D., Raghavachari, K., Foresman, J. B., Ortiz, J. V., Cui, Q., Baboul, A. G., Clifford, S., Cioslowski, J., Stefanov, B. B., Liu, G., Liashenko, A., Piskorz, P., Komaromi, I., Martin, R. L., Fox, D. J., Keith, T., Al-Laham, M. A., Peng, C. Y., Nanayakkara, A., Challacombe, M., Gill, P. M. W., Johnson, B., Chen, W., Wong, M. W., Gonzalez, C., Pople, J. A. (2009). GAUSSIAN 09, Revision A.02, Gaussian Inc, Wallingford CT,.

- [66] Aggarwal K., & Khurana, J. M. (2017). Synthesis and application of an indenoquinoline dione conjugate as a dual fluorescent and colorimetric pH sensor. *J. Lumin.*, 187, 457-465. doi: 10.1016/j.jlumin.2017.03.040.



## BIOGRAPHY

<b>NAME</b>	Mr.Thianthan Taweetanavanich
<b>DATE OF BIRTH</b>	7 December 1993
<b>PLACE OF BIRTH</b>	Surin, Thailand
<b>ADDRESS</b>	311 Village No.11, Yha Plong Sub-district, Muang District, Sisaket, 33000
<b>EDUCATION</b>	2006 Junior School, Sisaket wittayalai School 2012 Senior High School, Sisaket wittayalai School 2016 Bachelor's Degree (Chemistry), Maharakham University 2018 Master's Degree (Chemistry), Maharakham University
<b>Research grants &amp; awards</b>	Center of Excellence for Innovation in Chemistry (PERCH-CIC) Outstanding presentation in 2018 International Congress for Innovation in Chemistry (PERCH-CIC Congress X)
<b>Research output</b>	Taweetanavanich, T., & Kaewtong, C. (2018). Sci&Tech RMUTT J., 8, 1-12

